Universidade de Aveiro
2013

Departamento de Física

Ana Sofia Sebastião Bartolomeu

Validação do nível do mar no modelo MSYM para o Mar do Sul da China

Sea level validation in MSYM model for the South China Sea

Universidade de Aveiro Departamento de Física
2013

Ana Sofia Sebastião Bartolomeu

Validação do nível do mar no modelo MSYM para o Mar do Sul da China

Sea level validation in MSYM model for the South China Sea

Dissertação apresentada à Universidade de Aveiro para cumprimento dos requisitos necessários à obtenção do grau de Mestre em Meteorologia e Oceanografia Física, realizada sob a orientação científica do Doutor João Miguel Sequeira Silva Dias, Professor Auxiliar do Departamento de Física da Universidade de Aveiro e co-orientação do Doutor Paulo Chambel Leitão, Investigador na Empresa Hidromod.

o júri / the jury

presidente /
president

Prof. Doutor Paulo Manuel Cruz Alves da Silva,
Professor auxiliar da Universidade de Aveiro

vogais /
examiners committee

Doutor Marcos Duarte Mateus,
Investigador auxiliar do Instituto Superior Técnico

Prof. João Miguel Sequeira Silva Dias,
Professor auxiliar da Universidade de Aveiro

agradecimentos / acknowledgements

Gostaria de agradecer a todos os que possibilitaram a realização desta dissertação. Um especial agradecimento ao Professor Doutor João Miguel Sequeira Silva Dias e ao Doutor Paulo Chambel Leitão, pela orientação, dedicação, disponibilidade, colaboração, tempo despendido e partilha de conhecimentos, à Madalena Malhadas pela disponibilidade e conselhos ao longo do trabalho, ao João Ribeiro pelas sugestões e apoio informático prestado, ao Nuno Vaz pelo primeiros conhecimentos e aplicações do modelo utilizado, ao Eduardo Aires e Hélio Santos pelas trocas de ideias e convívio, a todos os meus amigos e à minha turma, pelo apoio, parceria, cooperação, amizade, ajuda, dedicação e preocupação.

À empresa Hidromod e a todos os seus colaboradores o meu "Muito Obrigado!" pela recetividade, confiança, apoio, colaboração, simpatia durante o estágio, que foram essenciais para a realização deste trabalho.

Mais ainda, agradeço muito à minha família e a quem esteve sempre comigo, pois sem eles nada era possível, pelo constante apoio, confiança, compreensão, acompanhamento, motivação, conforto e carinho dado ao longo desde processo.

A todos, o meu sincero "Bem-haja"!

palavras-chave

Mar do Sul da China, Estreito de Malaca, Estreito de Singapura, análise harmónica, maré astronómica, maré meteorológica, monções, vento.

resumo

A região do Mar do Sul da China, e os Estreitos da Malásia e Singapura são caracterizados por um comportamento complexo da maré sob a influência dos Oceanos Pacífico e Índico, mas também devido à batimetria e geografia da região. Enquanto a maré é semidiurna no Estreito da Malásia, esta apresenta um carácter misto e diurno entre o Estreito de Singapura e o Mar do Sul da China. Para além da complexidade da região, esta é também economicamente importante e a sua navegabilidade deve ser garantida. Neste sentido, a Hidromod desenvolveu uma aplicação numérica hidrodinâmica para o Estreito da Malásia (modelo MSYM), a partir do modelo MOHID. O modelo MSYM permite, entre outos parâmetros, reproduzir o nível do mar, que necessitam de ser validados. Para a validação do modelo, as previsões são comparadas com observados (disponíveis), sendo este o principal objetivo deste trabalho. Numa primeira parte, foi feita a validação do nível do mar para seis marégrafos do GLOSS incluídos na região do Mar do Sul da China e Estreitos da Malásia e Singapura. A comparação entre observações e previsões numéricas revelou um coeficiente de correlação superior a 0.95 (considerando todas as estações) e um *RMSE* centrado próximo dos 10 cm nas estações localizadas no Estreito da Malásia (utilizando o domínio de maior resolução horizontal) e de 15 – 20 cm na costa Este da Malásia. Por outro lado, a região é fortemente influenciada por monções de Nordeste (entre Novembro e Março) e de Sudoeste (entre Maio e Setembro) que, atuando sobre o Mar do Sul da China tendem a gerar anomalias positivas ou negativas da maré no Estreito de Singapura, respetivamente. Para estudar este fenómeno, foi analisado o nível do mar em Tanjong Pagar (no Estreito de Singapura), identificando-se anomalias do nível do mar positivas e negativas. São exemplos o dia 25 de Dezembro, associado a uma forte intensidade do vento de Nordeste (anomalia positiva) e o dia 7 de Fevereiro relacionado com uma variação da direção do vento (anomalia negativa). Ambas as anomalias são da ordem de 30 cm e as discrepâncias entre o nível do mar observado e simulados pelo MSYM correspondem principalmente à maré residual (meteorológica). Por fim, a análise da maré em duas estações localizadas no Estreito da Malásia revelou diferenças significativas entre dados observados e previsões numéricas em maré morta, que estão associadas essencialmente à reprodução da maré astronómica pelo modelo MSYM.

keywords

South China Sea, Malacca Strait, Singapore Strait, harmonic analysis, astronomic tide, storm surge, monsoons, wind.

abstract

The South China Sea region, and the Malacca and Singapore Straits are known for the complex behavior of their tides, which are under the influence of the Pacific and Indian Oceans, and are modified by the bathymetry and geography of the region. While the tide is semidiurnal in the Malacca Strait, in the Singapore Strait and the South China Sea the tides are mixed and diurnal. In spite of the region's dynamic complexity, it is an economically important region, and its navigability needs to be assured. As such, Hidromod has developed a hydrodynamical numerical application for the Malacca Strait (the MSYM model) from the MOHID model. The MSYM model calculates, among other parameters, the sea level that needs to be validated. In order to validate the model, the predictions are compared with (available) observations, which is the main goal of this work. In a first part, a validation of the sea level for six GLOSS tide-gauges in the South China Sea region and the Straits of Malacca and Singapore was done. This analysis revealed a correlation coefficient between observations and predictions of over 0.95 (taking every station into account) and a *RMSE* centered around 10 cm in the stations in the Malacca Strait (using the domain with higher horizontal resolution), and of 15-20 cm in the East coast of Malacca. On the other hand, the region is deeply influenced by Northeast monsoons (between November and March) and by Southwest monsoons (between May and September). These act over the South China Sea and tend to induce positive or negative sea level anomalies in the Singapore Strait. In order to study this phenomenon, the sea level in Tanjong Pagar (in the Singapore Strait) was studied, and the positive and negative anomalies were identified. For example, the 25th of December is linked with a strong northeasterly wind (positive) while in the 7th of February with a shift in the wind direction there is a negative anomaly. Both anomalies are in the order of 30 cm and the differences between the observed and predictions sea levels are mainly due to the residual tide (meteorological). Finally, the tidal analysis in two stations located in the Malacca Strait has revealed significant differences between observed data and simulations, during neap tide, which are mostly associated with the reproduction of the astronomical tide by the MSYM model.

Table of Contents

List of Figures

List of Tables

List of Acronyms

CISL - Computational and Information Systems Laboratory at the National Center for Atmospheric Research in Boulder

FES - Finite Element Solution

GFS - Global Forecast System

NOOA - National Oceanic and Atmospheric Administration

GLOSS - Global Sea Level Observing System

GMT – Greenwich Mean Time

HC - Mean complex amplitude error

IST - Instituto Superior Técnico

HYDEC - Hydraulics-Environmental-Civil Engineering Company

MARETEC - Marine and Environmental Technology Research Center

MEH Project - Marine Electronic Highway Project

MLS - Mean Sea Level

MOHID – MOdelo HIDrodinâmico

Monthly SLAs - Monthly mean Sea Level Anomalies

MSYM - Malacca Strait Hydrodynamic Model

NE – North-East

OBCs - Open Boundary Conditions

R – Correlation Coefficient

Relative HC – Relative Mean complex amplitude error

RMSE – Root Mean Square Error

RMSE' – Centred Root Mean Square Error

SCS - South China Sea

SL – Sea Level

SLA – Sea Level Anomalies

SMSL - Seasonal Mean Sea Level

STD - Standard Deviations

SW – South-West

Yearly SLAs - Yearly mean Sea Level Anomalies

List of Symbols of the harmonic constituents

K_1 – Lunar diurnal

K_2 – Lunisolar semidiurnal

M_2 – Principal lunar semidiurnal

M_4 – Shallow water overtides of principal lunar

N_2 – Larger lunar elliptic semidiurnal

O_1 – Lunar diurnal

P_1 – Solar Diurnal

Q_1 – Larger lunar elliptic diurnal

S_2 – Principal solar semidiurnal

S_A - Solar annual

S_{SA} - Solar semianual

Chapter 1 | Introduction

The regions of the South China Sea (SCS), Malacca Strait and Singapore Strait are characterized by a complex tidal behavior (Akdag, 1996), entangled with the co-oscillating nature of the tide from the Pacific and Indian Ocean, mainly in response to the geographical configuration of the area. The combination of these elements with the existence of many islands and small passages, could give an estimate/ overview of the complexity of the tides in the study area and the coastal waters response to various forcing mechanisms that provide the energy and momentum to drive the coastal processes. The South China Sea is one of the broad marginal seas surrounded by the Asian mainland and consists of three main parts (the deep basin, the mainland shelf and the Sunda Shelf) where diurnal and mixed tides predominate. The Singapore Strait is enclosed by the South China Sea and Malacca Strait and is influenced by the interactions between the Indian (mainly semidiurnal) and Pacific Oceans (mainly diurnal) and also presents a complicated coastline geometry, with small islands and sharply varying bottom topography. The Malacca Strait is a channel that links the Indian Ocean and Andaman Sea to the South China Sea and is characterized mainly by a semidiurnal tidal pattern. The South China Sea region is under the strong influence of the Asian monsoons: northeast (NE) monsoons and southeast (SW) monsoons. They dominate the large-scale sea level dynamics of the South China Sea. Due to the depth of the South China Sea, the sea level anomalies generated by the wind over the sea are easily amplified, particularly in the Singapore Strait (Tkalich *et al.*, 2012a).

During the past decade, numerical ocean models have become able to predict the ocean state with the necessary resolution to reproduce the small-scale processes not captured by the observations, which are sparse in space and limited in time. Ocean models have also been widely used in process oriented studies to diagnose ocean problems (Wei *et al.*, 2010). The understanding of the processes reveals itself useful for several areas such as coastal engineering, fisheries, marine environment, oceanography or astronomy.

Moreover, the Malacca and Singapore Straits are important economic regions. The Malacca Strait, for instance, is one of the most important shipping routes in the world. The Malacca Strait is a canal shipping route between the Indian and Pacific Oceans that connects three different countries with the largest number of people in the world: India, Indonesia and China. Thus, the circulation flow through the Malacca Strait is very important, and needs to be investigated (Rizal *et al.*, 2010). On the other hand, there has been an expansion of the oil exploration activity in this region, which is likely to increase in the next few years, as new oil deposits are discovered. As a consequence, oil spills might become more frequent in the Malacca Strait (Camerlengo and Demmler, 1997). Therefore, the different aspects of removal and containment of oil spills under adverse meteorological conditions (NE monsoon, in particular) will necessarily have to undergo an accelerated expansion in the foreseeable future. Near the Malacca Strait, Singapore presents a very variable coastline due to berths, jetties and breakwaters. Because of the geographical location of Singapore (between the Strait of Malacca and the South China Sea), it is of significant importance within global shipping routes. Furthermore, with the increase in shipping and port activities, the marine environmental protection of the Singapore Strait has become more and more critical (Chen *et al.*, 2010a).

Hidromod implemented a hydrodynamic model for this important region, called the Malacca Strait Hydrodynamic Model (MSYM), with the Hydrodynamic Model (MOHID – www.mohid.com). The MOHID modelling system was developed by MARETEC (Marine and Environmental Technology Research Center) at Instituto Superior Técnico (IST) with the collaboration of several partners being

Hidromod one of them. MOHID allows for an integrated modelling of physical and biogeochemical processes at different scales and for different systems (estuaries and watersheds), due to the adoption of an object oriented programming philosophy. The MOHID model encompasses three different tools: MOHID Water, MOHID Land and MOHID Soil. These tools can be used to study the water cycle in an integrated approach. Specifically, the MOHID Water Modelling System is a three-dimensional numerical program to simulate surface water bodies (oceans, estuaries, reservoirs). Over the past years MOHID Water has been used to simulate a variety of physical, chemical and ecological processes at different scales in marine systems. A continuous development effort of new features has been maintained. Model updates and improvements have been made available on a regular basis and used in the framework of many research and engineering projects (mohid.wordpress.com/2012/10/24/ recent-updates-in-mohid-lagrangian-module/). This model has been applied to several coastal and estuarine areas worldwide and has showed its ability to simulate complex features of the flows. MOHID has been applied to the Portuguese coast (including the main estuaries and coastal lagoons), most of the Galician Rías, other European estuaries, as well as some Brazilian estuaries. In this work, the model's application to the Malacca Strait was validated.

The MSYM adopts a downscaling approach using four levels of grid nesting with different dimensions and horizontal resolutions. The first domain (with a horizontal resolution of about 10 km) includes the West Indian Ocean and part of the South China Sea; the second domain (with a horizontal resolution of about 5 km) includes the Andaman Sea and part of the South China Sea; the third domain (with a horizontal resolution of about 1 km) includes the Malacca Strait and finally the fourth domain (with a horizontal resolution of about 200 m) includes the Singapore Strait. This model application simulates the sea level and the currents for all domains with a time step of 240 s for the first domain, 120 s for the second and third domains and 30 s for the fourth domain.

The validation work conducted for the model implemented for the Strait of Malacca reveals similar results between observations and predicted data (Hidromod, 2012). However, there are some particular locations where the discrepancies between sea surface elevations observations and the model predictions are higher. These discrepancies are mainly associated with the neap tide in the Singapore and Malacca Straits. It is important to understand the reasons for these inaccuracies, so that model predictions can be improved. Some of these places with higher differences in predicted and observed sea level data may be under important dynamic ocean processes.

1.1 Objectives and structure of the thesis

This work aims to deeply validate the MSYM model for the sea level, including the regions of South China Sea, Malacca and Singapore Straits, at different levels. The second stage of the validation process is the comparison between the highest discrepancies in predicted and observed sea level and the dynamic processes acting over the region (through wind speed and direction data).

The first part of this thesis is an introduction to the work, referring some important topics (Chapter 1). A brief characterisation of the important physical features and processes over the region is presented in Chapter 2, based on several scientific publications. The data and methods used for the MSYM validation are described in Chapter 3 and the results are summarized in Chapter 4. Finally, Chapter 5 exposes the conclusions of this work.

Chapter 2 | South China Sea and Malacca and Singapore Straits

The study area is composed by three main regions: Malacca Strait, Singapore Strait and South China Sea. In this chapter some important characteristics of these regions are described: the geographical location and bottom topography; the weather and regional circulation patterns; interannual and annual variations on the sea level for these regions; the astronomical tide and the geographical distribution of tidal types in Southeast Asia and finally the storm surges and how they are generated in the Singapore Strait due to winds in the South China Sea.

2.1 Geography and topography

The Singapore Strait is enclosed by the Malacca Strait and the South China Sea and these three regions comprise the study area, as show in Figure 1.

The Singapore Strait is a channel, extending for 105 km, connected to the South China Sea and Pacific Ocean to the east, and to the Indian Ocean via the Malacca Strait to the west. The water depth in the Singapore Strait ranges between 30 and 120 m. It includes the Johor Strait and several small islands, resulting in an extremely complex topography.

The Malacca Strait is a passage with a complex topography between the Malaysia Peninsula and Sumatra and connects the Indian Ocean and Andaman Sea (at the North), with the South China Sea (at the South). It is approximately 980 km long and varies in width from 52 km in the south to 445 km in the north (Rizal *et al.*, 1994). Islands are numerous, especially in the southeast near Singapore, and water depth changes slightly from approximately 30 m in the south to 200 m at the line Indonesia with Thailand (Phuket).

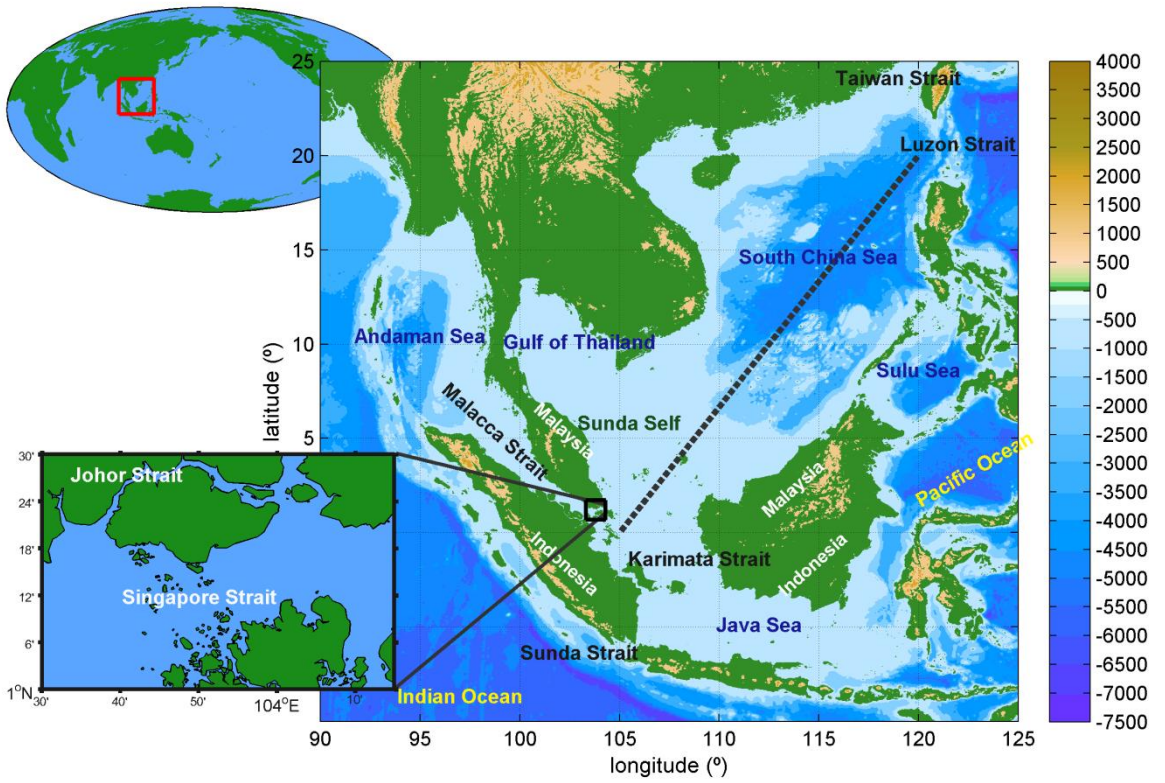

Figure 1 – Location and bathymetry of the area of study. Bathymetry values (central map) used in the plot is from NOAA (http://maps.ngdc.noaa.govn, and it is used the colorbar: Color Palette).

The South China Sea is the largest semi-enclosed marginal sea in the tropics, from 0^{o} - 23^{o} N and 99^{o} - 121^{o} E, with a width higher than 1100 km (Stewart, 2008) and a total area of about $3.5x10^{6}$ km^{2} (Tong *et al*., 2010). Between the Indian Ocean and the Pacific Ocean, the South China Sea is one of the most structurally complex regions on Earth. The bottom topography of the Malaysia Peninsula's eastern continental shelf has a moderate slope and progressively extends itself towards the South China Sea, and the coastal areas are not very deep, as shown in Figure 1. Extensive shallow water areas as well as deep oceanic basins can be found (Akdag, 1996). The South China Sea is composed for a deep central basin and two extensive continental shelves which occupy about 55% of South China Sea. Its mean water depth is approximately 1800 m and the main topographic characteristic of the oceanic regions in the northern and central parts of the South China Sea is the V-shaped basin (Akdag, 1996), with a maximum depth of more than 5400 m. The shelf in the south is composed by the Gulf of Thailand and the Sunda Shelf; while the shelf in the north encompasses the Gulf of Tonkin and the coasts of South China (Malanotte-Rizzoli, 2011).

2.2 Weather conditions

The climate in the study area is typically equatorial and tropical, humid with little variation in temperatures around the year. The South China Sea experiences two seasonal monsoon systems: northeast (NE) monsoon, from November to March (averaged wind velocity can be as high as 8 ms^{-1}) and southwest (SW) monsoon, from May to September (averaged wind velocity of about 4 ms^{-1}).

Specifically for Singapore, air temperature varies between 26^{o}C and 34^{o}C and humidity is above 90%. Regarding the precipitation, a seasonal variation was identified and for Peninsular Malaysia/ Singapore, this variation is different for the east and west coast, as seen in Figure 2. On the side of the Malacca Strait, there are two maximums (April/May and October/November) while to the west, the maximums are higher and correspond to the months of November/ December.

The interannual variability of temperatures in the equatorial Pacific modulates the oceanic forcing of the atmosphere and this interannual variability is associated with El Niño, causing the highest changes in equatorial dynamics (Stewart, 2008). Therefore, changes in sea level are directly linked to a number of atmospheric and oceanic processes.

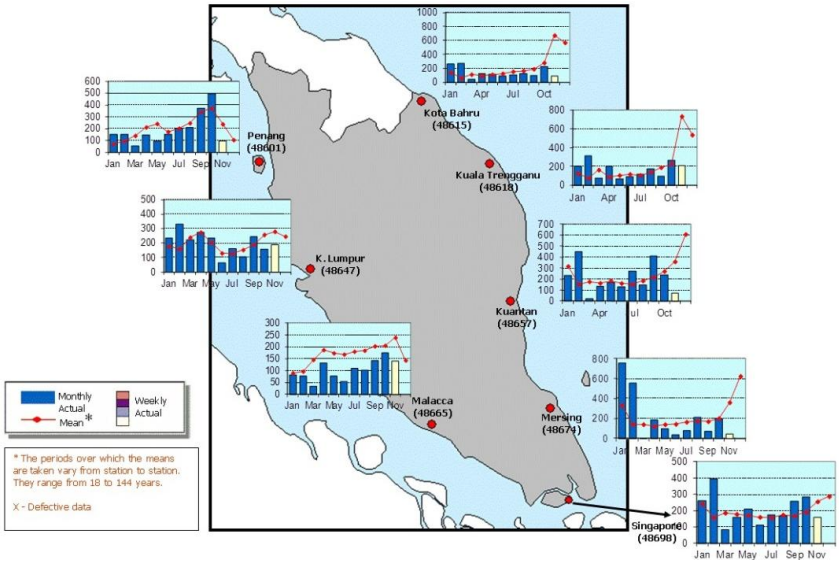

Figure 2 – Spatial and monthly rainfall distributions for Peninsular Malaysia/ Singapore.
Source: http://www.weather.gov.sg/wip/c/portal/layout?p_l_id=PUB.1003.647.

2.3 Sea level

Tide-stations or tide-gauges measure Local Sea Level, which is the height of the water as measured along the coast relative to a specific point on land (bench marks). However, the measurements at any given tide station include both global sea level rise and vertical land motion (such as subsidence or glacial rebound), so that the land-water interface can vary spatially and temporally. Therefore, it is necessary to evaluate the tide at several time-scales.

Figure 3 displays every type of wave, arranged by their period. Various factors can contribute to the variations in sea level, at different time scales: long and short-term. Long-term variations in sea level occur over various time scales, from months to several years, and may be periodic, gradual trends, or intermittent anomalies. Short-term variations generally occur on a daily basis and include waves, tides, or specific flood events, such as those associated with a winter snow melt, or hurricane or other coastal storms (http://tidesandcurrents.noaa.gov/sltrends/faq.shtml#q1).

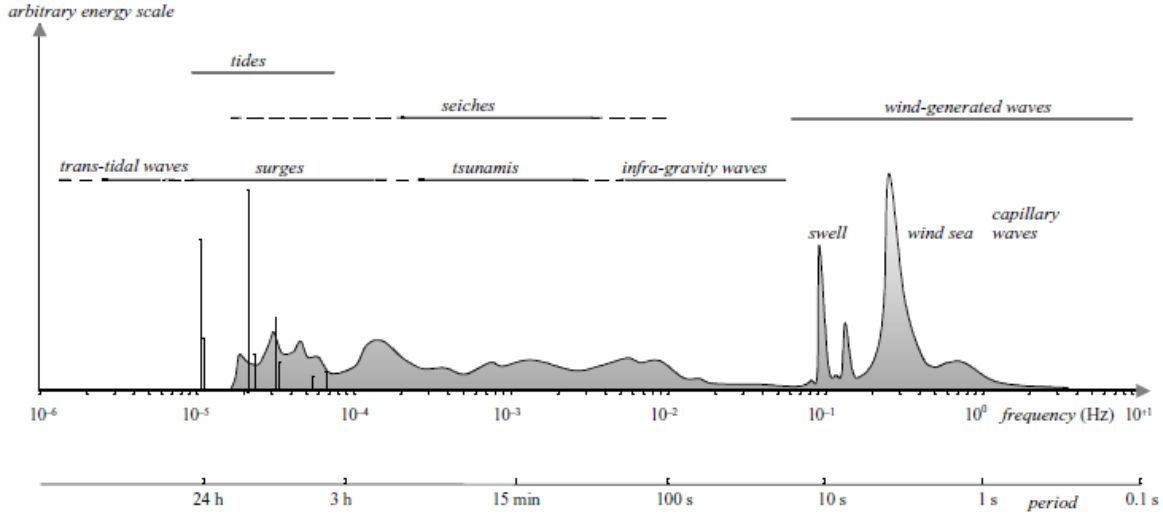

Figure 3 – Frequencies and periods of the vertical motions of the ocean surface. Source: Holthuijsen, 2007.

2.3.1 Annual and interannual variability of the sea level

There are a number of factors which change the sea level over time, such as seasonal weather patterns, changes in coastal and ocean circulation, dredging and the El Niño Southern Oscillation (ENSO). Thus, sea level trend analysis is especially important in the sea level variation studies. In recent decades, numerous studies have been carried out to estimate long-term sea level trends (e. g. Douglas, 1991; Church *et al.*, 2001; Bindoff *et al.*, 2007). Global sea-level has been rising at a rate of 1.5+0.5 $mmyr^{-1}$ over the last century (Church *et al.*, 2001) and between 1993 and 2003 the rise was estimated at 3.1±0.7 $mmyr^{-1}$ (Collins *et al.*, 2008). On the other hand, many studies have indicated that the spatial distribution of the SL presents regional differences, e. g., there are larger SL variations in the Western tropical Pacific, Eastern Indian and Southern Ocean during the past decade (e.g., Cheng and Qi, 2007). According to Chambers *et al.* (2002) and Cheng and Qi (2007) the tropical Pacific and Indian Ocean regions have considerable inter-annual and decadal SL variability associated with the ENSO, the Asian-Australian monsoon and phenomena like the North Pacific Decadal Oscillation. NOAA (http://tidesandcurrents.noaa.gov/sltrends/) also presents the analysis for some of the regions used in this study. Table 1 is a summary of SL trends calculated by NOAA and also by Cheng and Qi (2007); Fang *et al.* (2006a); Fang *et al.* (2006b); Tkalich *et al.* (2013) and Li *et al.* (2002). Moreover, Fang *et al.* (2006a) identified abnormal events in 1994-1995, in 1997-1988 and in 2002 with different spatial scales for the South China Sea.

Table 1 – Mean Sea Level Trend for important tidal stations of the study area using data with the average seasonal cycle removed. Source: (http://tidesandcurrents.noaa.gov/sltrends/)

Sources	***Location***	***Period***	***Mean sea level trend***
NOAA	Ko Taphao Noi	1940 - 2010	0.90 ± 0.96 $mmyr^{-1}$
	Ko Lak	1940 - 2010	0.08 ± 0.27 $mmyr^{-1}$
	Sembawang, Singapore	1954 – 2011 (data gaps of 10 yrs)	-0.82 ± 0.69 $mmyr^{-1}$
	Zhapo	1959 - 2011	2.11 ± 0.45 $mmyr^{-1}$
Cheng and Qi (2007)	South China Sea	1993 – 2000	11.3 $mmyr^{-1}$
		2001 - 2005	11.8 $mmyr^{-1}$
Fang *et al.* (2006a)	South China Sea	1993 - 2003	6.7 $mmyr^{-1}$
Tkalich *et al.* (2013)	Singapore Strait	1975 – 2009	1.2 – 1.7 $mmyr^{-1}$
		1984 – 2009	1.8 – 2.3 $mmyr^{-1}$
		1993 - 2009	1.9 – 4.6 $mmyr^{-1}$
Li *et al.* (2002)	South China Sea	1993 - 1999	10.0 $mmyr^{-1}$

During the course of a year, the sea level also varies (Marmer, 1952). On the basis of monthly tidal averages, an obvious seasonal effect on the tides is observable. The seasonal variation can be up to 20 cm. As an Asian marginal sea, the South China Sea reveals pronounced seasonal variability under the influence of the East Asian monsoon. Further, as a tropical Pacific marginal sea, the South China Sea exhibits remarkable interannual variability (e.g., Chu *et al.*, 1997; Liang *et al.*, 2000).

For the particular case of the Singapore Strait, at a regional scale, annual and interannual sea level variability are also caused by the Asian monsoon system (Tkalich *et al.*, 2013), modulated by coupled ocean–atmosphere oscillations (ENSO variations are in the range of ± 5cm). At a local (hourly) scale, the sea level elevation is driven by astronomic tides and distorted by bathymetry gradients.

2.3.2 Circulations and currents

Strong currents along the continental margin of the South China Sea form mean basin-wide cyclonic and anticyclonic circulations in the winter and summer, respectively, (Gan *et al.*, 2006). They reveal that the circulation in the South China Sea is generally dominated by the geostrophic currents; a positive nonlinearity in the zonal direction is locally intensified in the North of the Luzon Strait (which leads to the formation of centripetal acceleration for the mainstream of the Kuroshio to turn eastward) and that the weakening of the Kuroshio markedly enhances Kuroshio's intrusion (Figure 4, right), and forms an anticyclonic eddy west of the Luzon Strait.

The South China Sea and also the Straits of Malacca and Singapore are under the strong influences of the Asian monsoon which greatly affects their circulations. In the NE monsoon, the major circulation in South China Sea forms a large anti-clockwise gyre in the central area and a strong clockwise gyre is observed in the Gulf of Thailand, (Figure 4, left). In the SW monsoon, the major clockwise circulations can be noticed in the middle of South China Sea and two gyres can be observed in the Gulf of Thailand (a smaller anti-clockwise and a bigger clockwise), (Figure 4, centre).

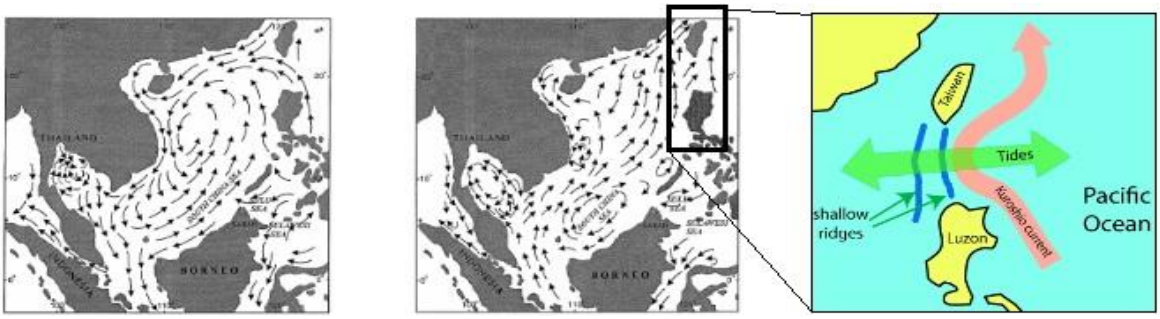

Figure 4 - Observed surface currents of South China Sea during Northeast Monsoon (left); Southwest Monsoon (centre). Source: (Choon *et al.*, 2006). Kuroshio Current between Taiwan and Luzon (right). Source: http://www.michw.com.

In the NE monsoon, the major currents that flow in the SW direction split into two at the east coast of Peninsular Malaysia: one to the north, heading toward the Gulf of Thailand and another to the south, flowing out to the Southern Indian Ocean through the Kalimantan Straits and the Java Sea (Figure 4, right). In the SW monsoon, the weaker south-westerly winds induce net north-eastern currents which flow through the Luzon and Taiwan Straits and eventually to the Pacific Ocean (Choon *et al.*, 2006).

Because of the position of the Malacca and Singapore Straits, they are also highly influenced by seasonal surges associated with monsoon winds. The monsoonal effects are not severe in the Malacca Strait because of the sheltering effect of the Malaysia Peninsula and of the island of Sumatra. Indirectly, however, the monsoon seasons greatly influence the circulation in the strait. There are two rainy seasons of unequal magnitude occurring without any really dry period (Keller and Richards, 1967). The currents flow through the strait generally in a northwest direction throughout the year, due to differences in sea level from the south-eastern to the north-western entrance of the strait, with the slope towards the Andaman Sea (Wyrtki, 1961). The low sea level in the NE monsoon months can be explained by the prevailing wind patterns. From January to March, the NE monsoon blows over the Bay of Bengal, drastically lowering the sea level in the Andaman Sea and in the northern entrance of the Malacca Strait. Thus, the NE monsoon causes a lowering of sea level in the adjoining Malacca Strait, producing a slope of sea level from the Singapore Strait to the Andaman Sea (which intensifies the transport based on baroclinic pressure gradients and this transport is also amplified by southerly winds, during the SW monsoon, Wyrtki 1961, 1991).

More rapidly changing sea levels are generated by short-term forces, including the astronomical tides and storm surges (with rates of water level rise in the order of meters per hour). These two sea level variations are described in the next two sections.

2.3.3 Astronomical tide

Tides are long waves and that result from the gravitational attraction of the moon and sun acting on the water particles on the surface of the earth. The mutual attraction between the earth and moon must be balanced by a centrifugal force, which results in a rotating system with an axis of rotation located within the earth (Dean *et al.*, 2002). The rotation of the earth causes the cyclical rise and fall of the ocean levels on a daily (diurnal) and half-daily (semidiurnal) basis. Variations in the relative positions of the earth, moon, and sun cause fluctuations in the strength of the astronomical forcing. The periods of the interactions between the oceans, moon and sun range from a few hours to somewhat more than a day and their wave lengths, accordingly, vary between a few hundred and a few thousand kilometres (Holthuijsen, 2007) (Table 2).

Table 2 – The important constituents of the astronomical tides. Source: Doodson (1921).

Tidal Type	**Symbol**	**Relative Amplitude**	**Description**
Semidiurnal	M_2	100.0	Principal lunar tide
	S_2	46.6	Principal solar tide
	N_2	19.1	Monthly variation in lunar distance
	K_2	12.7	Changes in declination of sun and moon
Diurnal	K_1	58.4	Solar-lunar constituent
	O_1	41.5	Principal lunar diurnal constituent
	P_1	19.3	Principal solar diurnal constituent
Longer	M_f	17.2	Moon's fortnightly constituent

Tides have precise frequencies and their spectrum is not continuous. It consists of discrete lines. Doodon's expansion included 399 constituents, of which 100 are long period, 160 are daily, 115 are twice per day and 14 are thrice per day. It is possible to exactly reproduce the sea level as the sum of a finite set of independent harmonic waves.

The region of the South China Sea and the Indonesian waters are characterized by a very complex tidal behaviour (Akdag, 1996), entangled with the co-oscillating nature of the tide from the Pacific and Indian Ocean, mainly in response to the geographical configuration of the area. The South China Sea together with the Indonesian Sea work functioned as a system of several connected basins each with own characteristics. Due to the various subdivisions of this region, each basin is different, with its own primary oscillation.

The tidal patterns in the deep basin are simple and weakly tidal currents, whereas the tidal regimes on the shelf, particularly the semidiurnal tides, are complex and with strong tidal currents (the pattern is manifold and in each basin a different oscillation is primarily stimulated (Wyrtki, 1961). Tides and currents in the South China Sea, Andaman Sea, Gulf of Thailand, Singapore and Malacca Straits have been studied by numerous oceanographers (Fang, 1986; Rizal and Sündermann, 1994; Fang *et al.*, 1999; Zu *et al.*, 2008; Aungsakul *et al.*, 2007; Breemen, 2008; Tong *et al.*, 2010). Tkalich *et al.* (2012a, 2012b) and Kurniawan *et al.* (2011) have focused on the tidal analysis in the Singapore Strait. In the study area, large differences are noted depending on the analysis location (Figure 5).

Diurnal tides predominate in the China and Java Seas, mixed tides in the Eastern Archipelago and in the Philippine Waters. According to Zu *et al.* (2008), the amplitude of the semidiurnal tide, M_2, decreases, while the amplitude of the diurnal tide, K_1, increases, after the tidal waves propagate from the western Pacific into the South China Sea through the Luzon Strait. The tides in the Malacca Strait are strongly influenced by the tidal propagation along the northern Indian Ocean. The tidal ranges of 1.6–3.7 m, depending on the location, and can partly reach 4–5 m (Thia-Eng *et al.*, 2000). However, in further detail, there are two types of tidal distribution: part of the Indian Ocean and in the middle of the Malacca Strait, the type is mixed tide prevailing semidiurnal, while in the Andaman Sea and the southern part of this Strait the type is semidiurnal tide (Rizal *et al.*, 2012).

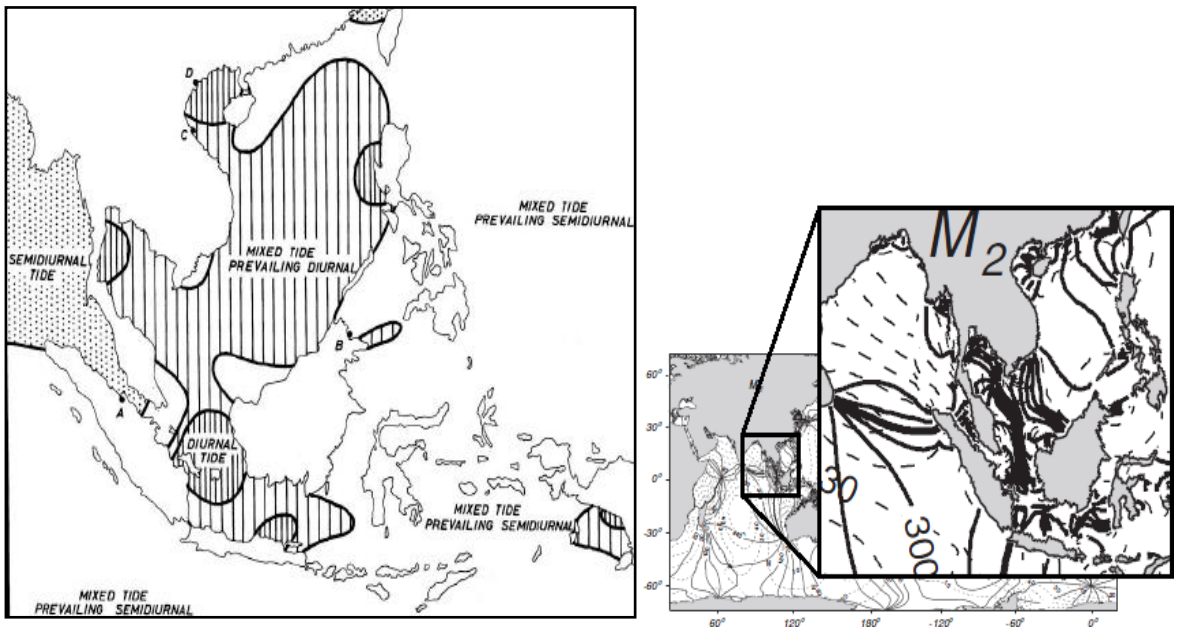

Figure 5 – Geographical distribution of tidal types in Southeast Asia (left). Source: Wyrtki (1961). Global map of M2 tide calculated from Topex/Poseidon observations of the height of the sea surface. Full lines are contours of constant tidal phase (contour interval: 30◦). Dashed lines are lines of constant amplitude (contour interval: 10 cm) (right). Source: Holthuijsen (2007).

The Singapore region also has a complex tidal pattern. This complexity of the tide in this region is primarily due to the fact that here, the main interaction takes place between predominantly different tidal signals from two oceans (Indian, mainly semidiurnal; and Pacific, mainly diurnal). It is further complicated by factors such as sharply varying bottom topography toward the predominant shallow Sunda Shelf, which acts as a separator of two deep basins (South China Sea/Pacific Ocean and Andaman Sea/Indian Ocean), and the complicated coastal geometries due to the narrow straits and numerous small islands.

Astronomic tide can be decomposed in numerous constituents; however there are only four main constituents (M_2, S_2, K_1, O_1) that are important in generating shallow water constituents (Aungsakul *et al.*, 2007). They give a relatively complete picture of the tidal pattern at a station, and their representation seems to be sufficient for general information (Wyrtki, 1961). Table 3 summarizes amplitude and phase of the main constituents of the astronomical tide presented by different authors, for specific periods of time and different tidal stations of the study area.

Table 3 – Amplitude and phase of the principal harmonic constituents for some important places for this work, from different authors. The phase of Fang *et al*. (1999) was transformed to Greenwich phase-lag, G_i, by $G_i = g_i - 8\ \omega_i$, where g_i is the Beijing time phase-lag (local phase lag, 8 hours before GMT at 120°E) with i standing for constituents and ω_i the angular velocity (28.984, 30.000, 15.041 and 13.943 for M_2, S_2, K_1 and O_1, respectively, in degrees per hour).

Tidal Station	Latitude	Longitude	Sources	Amplitude (cm)				Phase (°)			
				O_1	K_1	M_2	S_2	O_1	K_1	M_2	S_2
Lumut Pier	~4° 10′	~100° 30′	Breemen (2008)	03	22	75	35	161	247	241	276
B. DaToh	~4° 10′	~100° 30′	Rizal *et al*. (1994)			79				253	
Ko Raet	11° 48′	99° 49′	Fang (1999)	30	52	06	00	20.5	63.7	296.1	2.0
Terengganu	5° 21′	103° 08′	Fang (1999)	30	30	27	12	203.5	291.7	11.1	49.0
Hailingshan	21° 35′	111° 49′	Fang (1999)	36	42	68	28	153.5	193.7	62.1	93.0
Tanjong Pagar	1° 16′	103° 51′	Tkalich *et al.* (2012b)	30.14	31.26	79.26	32.12	56.6	109.37	322.6	16.8

The tide is divided into astronomical tide (described in this section) and residual tide, the sea level anomalies. The residual tide is, mostly, caused by atmospheric conditions, thus, it is also designated by meteorological tide or storm surge. The storm surge is an abnormal anomaly in sea water level generated by a storm, over and above the predicted astronomical tides, explained in the next section.

2.3.4 Storm surges

In space and time scales roughly equal to those of the generating storm (typically a few hundred kilometres and one or two days) there are storm surges, with a wave length and period generally slightly shorter than tides. As a result of meteorological conditions (e.g., wind stress, a reduction in atmospheric pressure due to a tropical cyclone), they can be either positive or negative. The South China Sea is under the main southwest-northeast patterns of the seasonal monsoons which dominate the larger-scale sea level dynamics. The geographical distribution of the sea level variations over the South China Sea is asymmetric, with a pronounced variation in the deep water (Cheng and Qi, 2007), as represented in Figure 6.

The entire region, bounded by Gulf of Thailand on the north, Karimata Strait on the south, east coast of Peninsular Malaysia on the west, and break of the Sunda Shelf on the east, could experience positive or negative SLAs, depending on the wind direction and speed (Tkalich *et al.*, 2012a). If strong sea level surges during NE monsoon coincide with spring tide, they usually lead to coastal floods in the region.

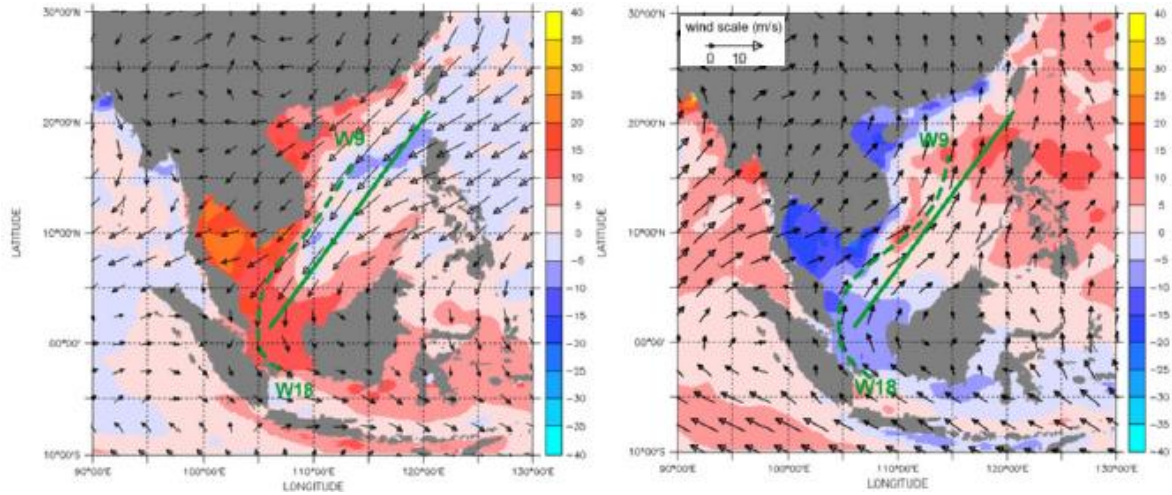

Figure 6 - Climatological seasonal 6-hourly wind and satellite altimetry averaged over 1993–2008 years: NE Monsoon (November–February), (left) and SW Monsoon (June–August), (right). Solid line is the longest axis of Taiwan– Singapore, and dash-lines are the wind speed streamlines. Source: Tkalich *et al.* (2012a).

Tkalich *et al.* (2012a, b) noted that if the sea level slope is in the direction from Taiwan to Singapore (i.e., NE monsoon), a positive anomaly occurs in the South China Sea (Figure 6), leading to surges near the Gulf of Thailand and the Singapore Strait. Storm surge, monsoons, circulations and other constituents of the circulation in Singapore Strait Region have been studied by several oceanographers (Camerlengo and Demmler, 1997; Choon *et al.*, 2006; Chen *et al.*, 2010a, 2010b; Kurniawan et al, 2011; Tkalich *et al.*, 2012a, 2012b). Some of them developed numerical models based on the shallow water equations to simulate, as well as possible, the complex systems in the South China Sea, Andaman Sea, Malacca and Singapore Straits.

Storm winds blowing over shallow, continental shelves pile water against the coast (Figure 7, left). Tkalich *et al.* (2012a) reveal that all major past sea level extremes in Singapore Strait have been generated by monsoon surges, manifested as an increase in monsoonal wind above the usual range for a few consecutive days. The climatological NE and SW wind is aligned roughly along the longest axis of South China Sea depicted by solid lines, or in more refined terms, along the streamlines depicted by dashed curves having a sharp turn almost 90^0 at the southernmost tip of the Malaysia Peninsula (Figure 7, right).

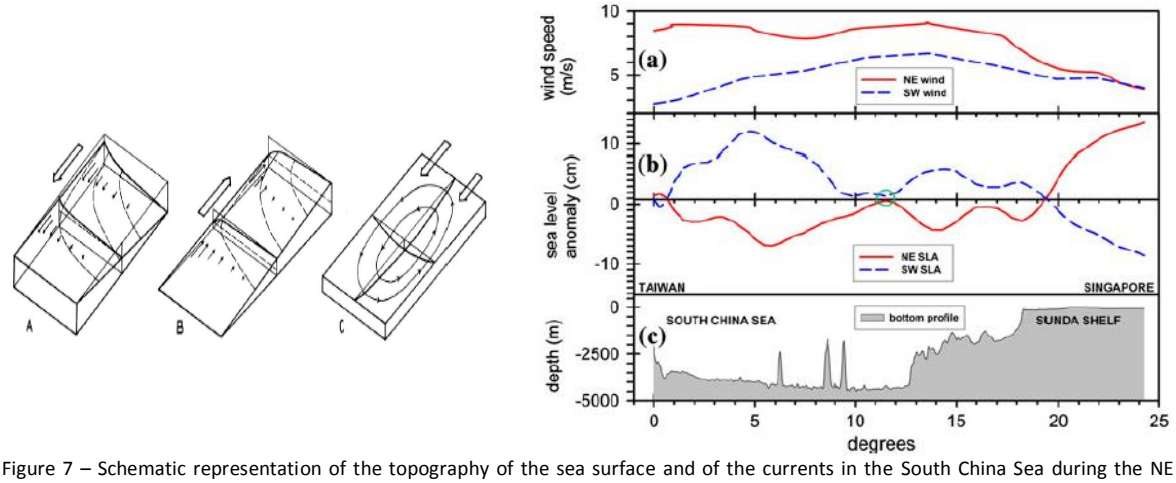

Figure 7 – Schematic representation of the topography of the sea surface and of the currents in the South China Sea during the NE monsoon (A), during the SW monsoon (B) and of the rotating circulation due to the variation of wind stress across the South China Sea (C) (left). Source: Wyrtki (1961). Cross-section of the South China Sea from Taiwan to Singapore (dashed line in Figure 1). Climatology wind and SLA for the period 1993–2008 (a), (b) and bottom profile (c). A nodal point at seasonal sea level is shown by a circle (right). Source: Tkalich *et al.* (2012a).

Chapter 3 | Data and Methods

The methodology followed in this study is focused on the analysis of sea level (SL) data. Predicted and observed astronomical tides for six tide-gauges are compared. Then, a more detailed analysis for the SL in the Singapore and Malacca Straits is studied. This analysis is mainly centred in the Sea Level Anomalies (SLAs) and their relationship with the dynamic processes occurring in the region (generally associated with the wind stress). This chapter presents the data sets and the methodologies used to achieve the proposed goals.

3.1 Observations

The SL data observations used in the model validation were provided by the Global Sea Level Observing System (GLOSS), the Marine Electronic Highway Project (MEH) and the Hydraulic-Environmental-Civil Engineering Company under an engineering project (HYDEC) presented in Table 4 and Figure 8. Meteorological values for three-hourly wind speed and direction, taken from the Global Forecast System of the National Oceanic and Atmospheric Administration (GFS NOOA) were also used.

Table 4 – Coordinates of the Global Sea Level Observing System, Marine Electronic Highway Project and the Hydraulic-Environmental-Civil Engineering Company Project tide-gauges used with the respective available data and sample interval.

Sources	Stations	Latitude	Longitude	Available data	Sample interval
GLOSS, ID - 42	Ko Tapthao Noi	7° 50’	98° 26’	1st of January 1985 to 31st of December 2010	1 hour
GLOSS, ID - 39	KoLak	11° 47’	99° 49’	1st of January 1985 to 31st of December 2010	1 hour
GLOSS, ID - 293	Kuala Terengganu	5° 16’	103° 11’	31st of October 1984 to 31st of December 2006	1 hour
GLOSS, ID – 43	Pengkalan	4° 14’	100° 37’	12th of December 1984 to 31st of December 2006	1 hour
GLOSS, ID – 44	Singapore	1° 28’	103° 50’	13th of August 1981 to 31st of January 1990	1 hour
GLOSS, ID – 78	Zhapo	21° 35’	111° 50’	1st of January 1975 to 31st of December 1997	1 hour
MEH	Tanjong Pagar	1° 16’	103° 51’	24th November 2012 and 6th April 2013	30 min
HYDEC	Pangkor, TG1	4° 26’	100° 36’	5th to 19th April 2010	10 min
HYDEC	Pangkor, TG2	4° 11’	100° 35’	5th to 19th April 2010	10 min

The first SL data sets were extracted from GLOSS, for six-hourly tide gauges located between the South China Sea, Malacca and Singapore Straits, enclosed by the Pacific and the Indian Oceans (Table 4). However, all stations (except Zhapo), contain data gaps, varying from a few hours to less than one month. The second SL data set was extracted by sensors implemented during the MEH Project for Tanjong Pagar with a sample interval of 6 minutes and 10 minutes (Table 4). To compare the results with the same sample interval, observations were filtered with a sample interval of 30 minutes, containing data gaps ranging from 2 hours to 20 days. Finally, the SL data set was provided by HYDEC for two tide-gauges in Pangkor, with a sample interval of 10 minutes, without any data gaps (Table 4).

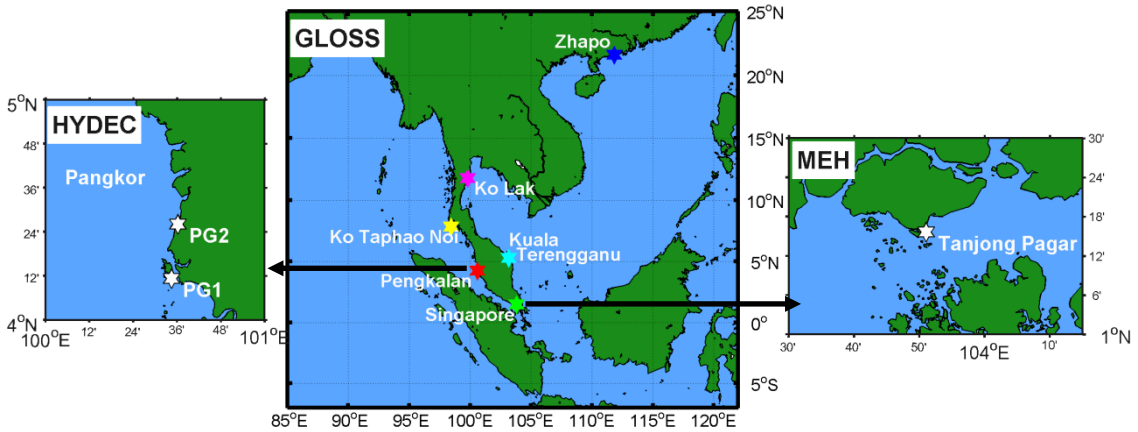

Figure 8 – Location of the GLOSS (Ko Taphao Noi, Ko Lak, Kuala Terengganu, Pengkalan, Singapore, Zhapo), MEH (Tanjong Pagar, in the Singapore Strait) and HYDEC (two tide-gauges in Pangkor (TG1, TG2)) analysed monitoring stations (tide-gauges).

3.2 Model implementation

The predicted sea level data was generated using the Strait of Malacca conceptual model called the Malacca Strait Hydrodynamic Model (MSYM) with the MOHID Water Modelling System model. The MOHID, developed by the Marine and Environmental Technology Research Center (MARETEC) at Instituto Superior Técnico (www.mohid.com/), is an integrated water modelling software that can be used to simulate the dynamics of water bodies, porous media flow and infiltration, and watersheds. Initially, MOHID was a two-dimensional tidal model which, with further developments, came to include a 3D setup, baroclinic effects, and a full discretization to finite volumes approach, allowing the use of generic vertical coordinates. Currently written in ANSI FORTRAN 95, it boasts new features such as the ability to produce object-oriented programming (www.maretec.org/#!mohid-model). This model has been applied to several coastal and estuarine areas worldwide and has shown its ability to simulate complex features of the flows. An example is the MSYM model, which consists of a downscaling method using four levels (Figure 9) of grid nesting (Level 1 to Level 4) with different dimensions and horizontal resolution. The nesting is done only in one way: the large-scale models influences the local models, but not the opposite. At this stage, all of the levels are 2D-H barotropic, using only 1 sigma layer in the vertical dimension (Hidromod, 2012).

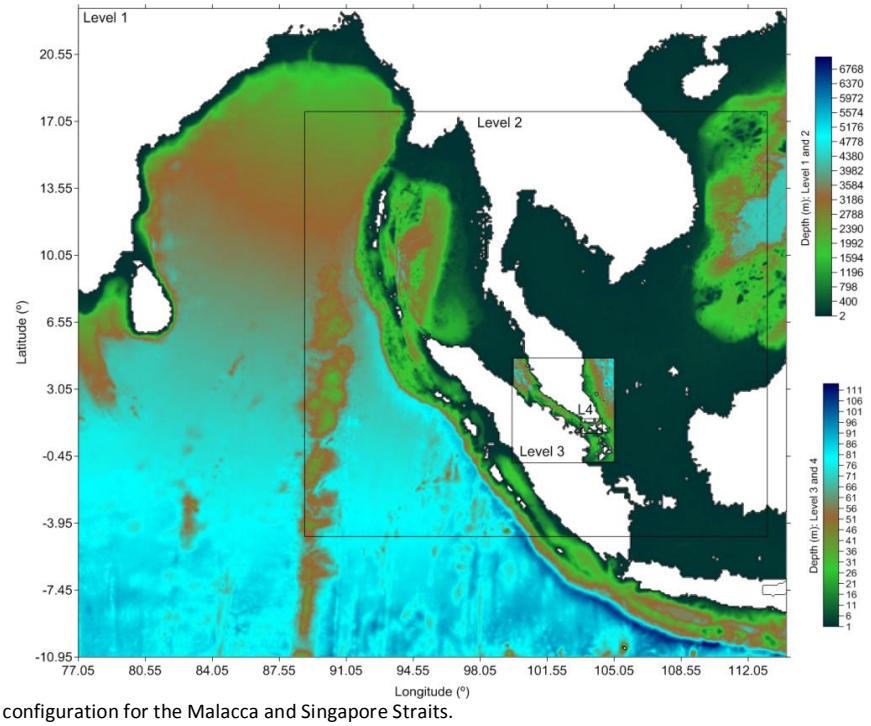

Figure 9 - Nested configuration for the Malacca and Singapore Straits.

The first domain (Level 1) has a horizontal resolution of about 10 km ~0.089° (Figure 9). This grid data domain is coarse, since the objective is to simulate large-scale processes (e.g., tide). In the open boundary of Level 1 a sea level interpolated from the FES2004 global tidal solution (Lyard *et al.*, 2006) was imposed. As initial conditions, zero free surface gradient and zero velocity at all grid points were used. The second domain (Level 2) is regional, and it has a horizontal resolution of about 5 km~0.044°. The Open Boundary Conditions (OBCs) for this level were defined by adding the inverted barometer effect (sea level variation due to pressure gradients) to the solution of Level 1 (high frequency). The surface boundary condition for wind stress and atmospheric pressure is applied by using the GFS weather prediction solution (spatial resolution of 0.5°). The third domain (Level 3) comprises the Malacca Strait with a horizontal resolution of about 1 km~0.0089°. The fourth domain (Level 4) is local

and includes the Singapore Strait with 200 m (0.0018°) horizontal resolution. The OBCs for these levels are prescribed from the upper levels, and meteorological forcing (wind and atmospheric pressure) are still being applied using the GFS solution. Table 5 presents the main characteristics of the implemented model configuration for the Malacca Strait.

Table 5 - Main characteristics of the nested models configuration for the Malacca Strait.

	Level 1	Level 2	Level 3	Level 4
Domain	West Indian Ocean and South China Sea	Andaman and South China Sea	Malacca Strait	Singapore Strait
Grid Corners	lon: 77.0° to 114.1° lat: 23.0° to -11°	lon: 88.90° to 113.1° lat: 17.6° to -4.7°	lon: 99.8° to 105.0° lat: 4.65° to -0.75°	lon: 103.3° to 104.4° lat: 1.52° to 1.04°
Dimension/Nº of Cells	371x340/126140	483x445/214935	524x539/282436	540x240/129600
Δx (°)	0.089	0.044	0.0089	0.0018
Δt (s)	240	120	120	30
Horizontal eddy viscosity	100 m^2s^{-1}	50 m^2s^{-1}	10 m^2s^{-1}	2 m^2s^{-1}
Vertical Discretization	1 sigma layer	1 sigma layer	1 sigma layer	1 sigma layer
Simulated Properties	Sea level and current velocities	Sea level and current velocities	Sea level and current velocities	Sea level and current velocities
Open Boundary Condition	Tidal global solution (FES2004)	Level 1+Inverted Barometer	Level 2	Level 3
Surface Boundary Condition	-	Wind and atmospheric pressure	Wind and atmospheric pressure	Wind and atmospheric pressure

3.2.1 Simulated periods

The model was run for three different time intervals: 17th of December 1988 to 23rd of December 1989; 24th of November 2012 to 6th of April 2013 and 5th to 19th of April 2010, displayed in Table 6. Three days of spin-up for the simulations (not included in the aforementioned periods) were considered. The first time interval is the lengthiest period of continuous data common to all six GLOSS tide-gauges. The model was run only for the astronomic tide forcing. The second time interval corresponds to the available observed SL for Tanjong Pagar and the predicted data was forced with the astronomic tide and wind data. For this station, the model was also run for the following specific values of wind speed and direction (scenarios): 5 ms^{-1} from SW and typical values during storm surges of 18 ms^{-1} from NE. These constant winds were used as model input with a specific pressure, according to each situation (Hasegawa *et al.*, 2012). The last interval is related with the available observed data for the tide-gauges of Pangkor (TG1 and TG2) and the model was forced only with astronomic tide and with the astronomic tide and wind (Table 6).

Table 6 – Simulated period according to the available data from GLOSS (six tide-gauges), MEH and HYDEC.

Period Compared	Validated Area	Forcing	Levels	Tide-gauges	Frequency
17th Dec. 1988 to 23rd Dec. 1989	South China Sea and Andaman Sea	Astronomic tide	L1, L2, L3 and L4	GLOSS	1 hour
24th Nov. 2012 to 6th Apr. 2013	Singapore Strait	Astronomic tide + wind	L4	MEH	30 min
5th to 19th Apr. 2010	Pangkor	Astronomic tide and Astronomic tide + wind	L3	HYDEC	10 min

3.3 Characteristics of the sea level

To understand some characteristics of the SL in each tide-gauge, Mean Sea Level, MSL, Seasonal SL (winter/ spring/ autumn/ summer), Yearly mean of the Sea Level Anomalies (yearly SLAs) and Monthly mean of the Sea Level Anomalies (monthly SLA) were calculated for the SL data set according to the available data interval. For the latter two variables, its corresponding MSL was removed. Due to the data breaks, the number of samples was different according to the station. Table 7 shows the number of samples used for the yearly SLAs and Table 8 present the number of samples for the monthly SLAs.

Table 7 – Total number of samples for the yearly mean sea level for GLOSS Stations.

Ko Taphao Noi		Ko Lak		Kuala Terengganu		Pengkalan		Singapore		Zhapo	
Year	*NºSample*	*Year*	*NºSample*	*Year*	*NºSample*	*Year*	*NºSample*	*Year*	*NºSample*	*Year*	*NºSample*
1985	8760	**1985**	8760	**1985**	8224	**1985**	7667	**1982**	8760	**1975**	8760
1986	8760	**1986**	7657	**1986**	8624	**1986**	8760	**1983**	8653	**1976**	8784
1987	8753	**1987**	8543	**1987**	8760	**1987**	8396	**1984**	8784	**1977**	8760
1988	6580	**1988**	8595	**1988**	8784	**1988**	8784	**1985**	8760	**1978**	8760
1989	8760	**1989**	8760	**1989**	8760	**1989**	8760	**1986**	8760	**1979**	8760
1990	8760	**1990**	8009	**1990**	8760	**1990**	8760	**1987**	8760	**1980**	8784
1991	8760	**1991**	8295	**1991**	8760	**1991**	8760	**1988**	8304	**1981**	8760
1992	8736	**1992**	8784	**1992**	8756	**1992**	8784	**1989**	8640	**1982**	8760
1993	8760	**1993**	8717	**1993**	8712	**1993**	7853			**1983**	8760
1994	8760	**1994**	7501	**1994**	8545	**1994**	8054			**1984**	8784
1995	8760	**1995**	8601	**1995**	8760	**1995**	8760			**1985**	8760
1996	8784	**1996**	8408	**1996**	7910	**1996**	8784			**1986**	8760
1997	8760	**1997**	8760	**1997**	8760	**1997**	7927			**1987**	8760
1998	8760	**1998**	8760	**1998**	8760	**1998**	8760			**1988**	8784
1999	8760	**1999**	8402	**1999**	8760	**1999**	8760			**1989**	8760
2000	8784	**2000**	8714	**2000**	8784	**2000**	8784			**1990**	8760
2001	8016	**2001**	8488	**2001**	8760	**2001**	8760			**1991**	8760
2002	7897	**2002**	7901	**2002**	8760	**2002**	8760			**1992**	8784
2003	7222	**2003**	8385	**2003**	8760	**2003**	7721			**1993**	8760
2004	8753	**2004**	8450	**2004**	8784	**2004**	8684			**1994**	8760
2005	8760	**2005**	7159	**2005**	8760	**2005**	8760			**1995**	8760
2006	8760	**2006**	7275	**2006**	8752	**2006**	8565			**1996**	8784
2007	8760	**2007**	8247							**1997**	8752
2008	8784	**2008**	8437								
2009	8728	**2009**	8259								
2010	8753	**2010**	8445								

Table 8 - Total number of samples for the monthly mean sea level for GLOSS Stations and Tanjong Pagar.

	Ko Taphao Noi	Ko Lak	Kuala Terengganu	Pengkalan	Singapore	Zhapo	Tanjong
January	18575	18624	16368	16192	6688	17112	1421
February	16917	17499	14904	14755	5424	15600	640
March	18575	18584	15912	16279	5896	17112	1108
April	18720	17219	15495	15814	5720	16560	241
May	19234	18392	16111	15536	5952	17112	
June	18630	16877	15840	14068	5760	16560	
July	17856	18069	16368	15685	5952	17112	
August	18611	18982	15961	16321	6406	17112	
September	18713	18249	15712	15418	6480	16560	
October	18607	18903	16385	16368	6432	17112	
November	18693	17433	16390	15172	6304	16560	289
December	19299	17481	17030	16466	6453	17104	1350

3.4 Harmonic analysis

Tides and tidal currents are predictable far into the future due to the predictability of the astronomical forcing. These forces are expressed as the tidal potential which consists of a limited number of discrete frequencies whose amplitudes and phases are well known at any time (Zervas, 1999). It is possible to reproduce a tidal record as the sum (Figure 10) of a larger number of harmonic wave constituents (a Fourier series), according to classical harmonic analysis. The tidal forcing is predicted as a set of spectral lines:

$$\eta\,(t) = \sum_{i=1}^{N} a_i \cos\,(2\pi f_i t + \alpha_i) \qquad (3.1)$$

where, a_i and α_i are the amplitude and phase, respectively, of each frequency f_i and t, the time. The harmonic method applied in this work is the t_tide function which separates the tidal and non-tidal energies (Pawlowicz *et al*., 2002). In order to select the main constituents, a previous analysis to the six tide-gauges of GLOSS (longest time-series available) was done, and the harmonics with higher amplitude were selected. These also took into account the harmonics produced by FES2004 (used by the model as boundary conditions - hydrodynamic wave including the tidal harmonics: M_2, S_2, K_1, K_2, N_2, $2N_2$, O_1, Q_1, P_1, M_4, M_f, M_m, M_{tm}, M_{Sqm}). Thus, the harmonics selected were: higher harmonics (M_4); Semidiurnal (N_2, M_2, S_2, K_2) and Diurnal (Q_1, O_1, P_1, K_1).

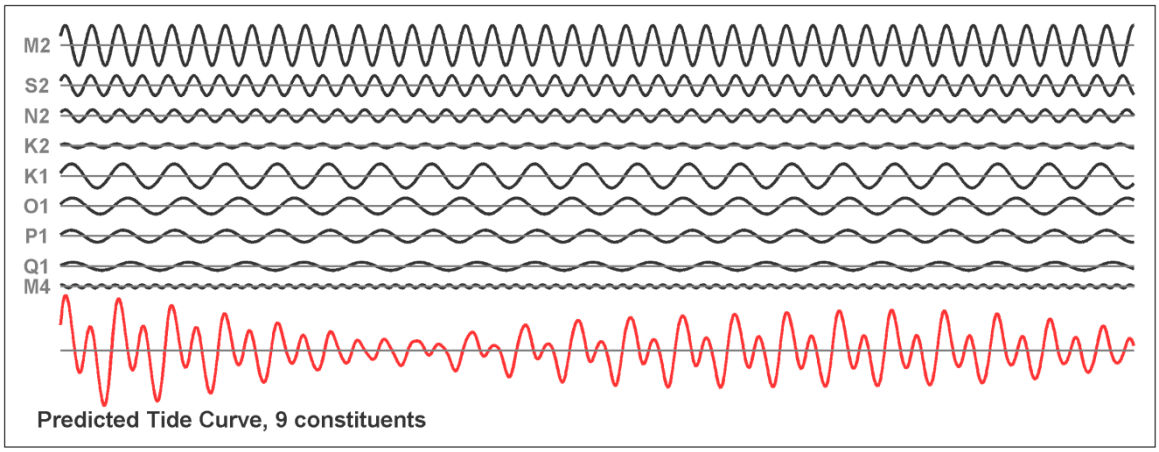

Figure 10 - Semidiurnal constituents (M_2, S_2, N_2, K_2) diurnal harmonics constituents (K_1, O_1, P_1, Q_1) and the shallow water constituent M_4. Red line is the reconstruction using the 9 constituents.

Table 9 presents the period, angular velocity, frequency and the difference between the closest constituents. Long harmonics (S_{sa} and S_a) are also computed, but only for the largest continuous periods of each GLOSS tide-gauges.

In general, the constituents with higher amplitude are M_2, S_2, O_1 and K_1. Using their amplitudes, the form factor (F) can be calculated (equation (3.2)). According to the result, the tide is classified, quantitatively, as: - semidiurnal (if the F ratio is less than 0.25, i.e. two main cycles per day); - mixed with mainly semidiurnal (if the F ratio was from 0.25 to 1.5); - mixed with dominantly diurnal (if the F ratio was from 1.5 to 3.0); - diurnal (if the F ratio was greater than 3.0, i.e. one cycle per day).

$$F = \frac{K_1 + O_1}{M_2 + S_2} \tag{3.2}$$

When the harmonic analysis is applied, there are some important aspects that have been taken into account, among them, the Rayleigh criterion (the minimum period to separate two constituents), the time of the analysis data (the start time) and the Nyquist frequency (the sample time).

The observation period needed to distinguish between the various constituents may be established according to the Rayleigh criterion, which takes into account only the separated constituents with at least one complete cycle. The minimum observation time for separating constituents of a pair of harmonics has the name of synodic period (Pugh, 2004), and depends on the frequency of the constituents to be determined, given by:

$$t = \frac{360}{\Delta\omega_c} = \frac{360}{360(f_2 - f_1)} = \frac{1}{(f_2 - f_1)} \tag{3.3}$$

The value $\Delta\omega_c$ is the difference between the angular velocities.

Table 9 – The characteristics of the main tidal constituents: period, angular velocity and frequency. The last column is the difference between the frequencies, used to select the minimum period of analysis.

Symbol Tidal used	**Period** (hr)	**Angular velocity** (°/hr)	**Frequency** (hr^{-1})	**Difference**
Q_1	26.87	13.40	0.0372185	
O_1	25.82	13.94	0.0387307	0.0015122
P_1	24.07	14.96	0.0415526	0.0028219
K_1	23.93	15.04	0.0417807	0.0002281
N_2	12.66	28.44	0.0789992	0.0372185
M_2	12.42	28.98	0.0805114	0.0015122
S_2	12.00	30.00	0.0833333	0.0028219
K_2	11.97	30.08	0.0835615	0.0002282
M_4	6.21	57.97	0.1610228	0.0774613

The goal was to apply the harmonic analysis to separate the nine constituents seen in Table 9. Thus, the harmonic analysis must be applied to a period which should be sufficient to separate the two constituents which present the smaller difference (last column of the Table 9, the underlined value is the smaller difference between two frequencies). For these constituents the minimum observation time to separate the nine constituents is 182.7 days. According to the time period, different constituents can be separated. For example, to separate the main constituents M_2, S_2 K_1, O_1 14.76 days were necessary, but to separated Q_1, O_1, P_1, K_1, N_2, M_2, S_2, K_2, M_4, the harmonic analysis must include 27.55 days.

Another important aspect to the harmonic analysis is the time reference (including in the start time of the t_tide (Pawlowicz et al., 2002) routine) which affects the results of the harmonics phase. In this work, the harmonic analysis was applied to sea level data at the Greenwich Mean Time (GMT).

Finally, to a sample wave of frequency ω the time step Δt may not exceed $\Delta t_{max} = \pi/\omega = T/2$, which implies that at least two samples of the signal must be taken per period. This minimum required sampling frequency is called the Nyquist frequency. Looking at the problem in a different way, with a given sampling interval Δt (rather than a given frequency), we recognize that the highest resolved frequency is $\pi/\Delta t$, called the cutoff frequency. If higher frequencies are present, aliasing inevitably occurs, as illustrated by a sinusoidal function sampled with increasingly fewer points per period, shown in Figure 11 (Cushman-Roisin and Beckers, 2006). The M_4 is the harmonic constituent with the highest frequency analysed (period of 6.21 hours, displayed as a blue line on the Figure 11). Therefore, the maximum time step is 3.105 hours. As previously mentioned, the time series used in this work have 1-hour; 30-minutes and 10-minutes data sets, which are lower than of the Nyquist frequency.

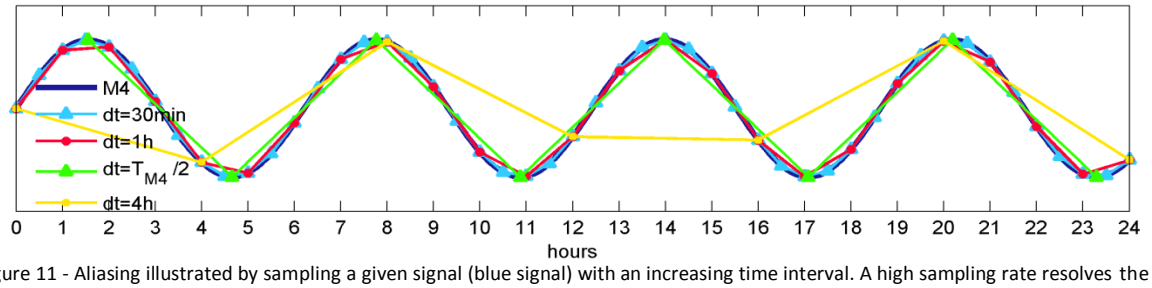

Figure 11 - Aliasing illustrated by sampling a given signal (blue signal) with an increasing time interval. A high sampling rate resolves the signal properly. The green signal corresponds to the cut-off frequency, and the sampled signal appears as a seesaw. The yellow signal corresponds to excessively long time intervals that alias the signal, making it appear as if it had a longer period than it actually has.

3.4.1 Astronomic and residual tides analysis

The tide is a combination of the astronomic and the residual tides. The astronomic tide analysis was performed with tide-gauges data from GLOSS, MEH and HYDEC while the residual tide (SLAs) was analysed using tide-gauges data from MEH and HYDEC only (Figure 12). Note that the harmonic analyses applied to the SL data from GLOSS with continuous data only (not including data gaps) as well as to the SL data from HYDEC. However, the SL data from MEH include data gaps (due to the limited data available and in order to separate a greater number of harmonic constituents). For the data gaps, the t_tide routine uses interpolations between data: FIXGAPS which linearly interpolates gaps in a time series, but ignores trailing and leading NaN (Pawlowicz *et al.*, 2002).

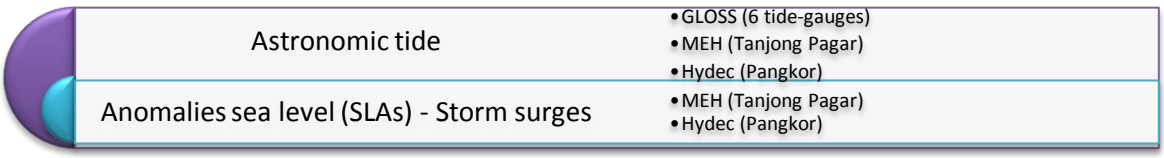

Figure 12 – Astronomic and residual tide analysed according to the available data per area.

3.5 Statistical calculations

To compare observed and predicted data, parameters and error measures were calcuted. The Root Mean Squared Error, *RMSE* (3.4) was computed where f is predictions, r is either observations and *N* is the total number of points in a temporal or spatial domain, or spatial-temporal combined space. The centred pattern of Root Mean Squared Error difference, *RMSE'*, is given by (3.5) and the Mean Squared Error, $RMSE^2$, (Yang, 2010) is obtained by the equation (3.6).

$$RMSE = \sqrt{\frac{1}{n}\sum_{i=1}^{n}(f_n - r_n)^2} \tag{3.4}$$

$$RMSE' = \sqrt{\frac{1}{n}\sum_{i=1}^{n}\left[(f_n - \bar{f}) - (r_n - \bar{r})\right]^2} \tag{3.5}$$

$$RMSE^2 = RMSE'^2 + \overline{Bias}^2 = \sigma_f^2 + \sigma_r^2 - 2\sigma_f\sigma_r R + \left(\bar{f} - \bar{r}\right)^2 \tag{3.6}$$

$$RMSE'^2 = \sigma_f^2 + \sigma_r^2 - 2\sigma_f\sigma_r R^2 \qquad \overline{Bias}^2 = \left(\bar{f} - \bar{r}\right)^2$$

Total $RMSE^2$ can be decomposed into two parts: the error due to differences in the mean ($RMSE'^2$) and the error due to differences in pattern variation ($\overline{Bias}^2$), which depends on standard deviation over the domain and on the anomalous pattern correlation between predictions and observations. Considering two dimensional variables, f and r, the Pattern Correlation (*R*) is expressed as:

$$R = \frac{1}{n}\sum_{i=1}^{n}\frac{(f_n - \bar{f}).(r_n - \bar{r})}{\sigma_f\sigma_r} \tag{3.7}$$

The variables σ_f and σ_r represent the variances of f (predictions) and r (observations), respectively:

$$\sigma_f^2 = \frac{1}{n}\sum_{i=1}^{n}\left(f_n - \bar{f}\right)^2 \qquad \sigma_r^2 = \frac{1}{n}\sum_{i=1}^{n}(r_n - \bar{r})^2 \tag{3.8 a,b}$$

If a forecast has a larger mean bias than another, its $RMSE^2$ can still be smaller if it has much smaller error in pattern variation, and vice versa. If two forecasts are verified against different observations, differences in analysis variance and mean complicate the interpretation of forecast $RMSE^2$. However, in this work, the mean sea level is removed for each analysis, according to their interval, and for both the observed and predicted data.

The main focus is on the anomalies in sea level and to present these statistical measures, the Taylor Diagram (Taylor, 2001) was computed. It offers a way to examine how closely a pattern matches observations, including the correlation coefficient, *RMSE'*, and the standard deviations. These values are used to define a single point in the Taylor diagram (Figure 13). In general, the Taylor diagram characterizes the statistical relationship between two fields, a "test" field and a "reference" field (usually representing "truth", based on observations) (Taylor, 2005).

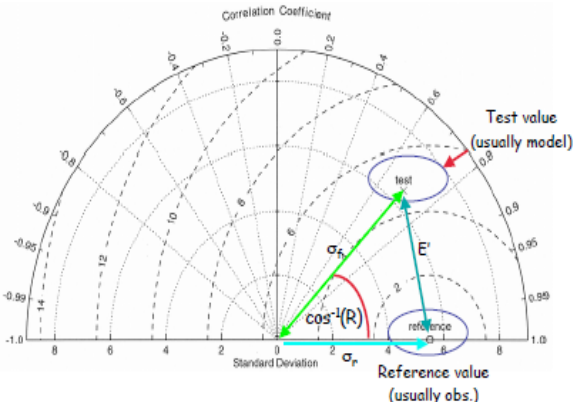

Figure 13 - Taylor diagram scheme. Forecast standard deviations, as a green line; Observation standard deviations as a cyan line and the resulting E' (= RMSE') value. Source: Fletcher, 2006.

To compare observations with predicted data, another parameter was defined: the *Relative Error*. Expressed in percentage, the *Relative Error* uses the *RMSE* values and the standard deviations of the observed and predicted data.

$$Relative\ Error(\%) = (RMSE/4\sigma r_n) \times 100 \quad (3.9)$$

Finally, to compare the results (amplitude and phase) of each harmonic constituent i, the Mean Complex Amplitude Error (*HC*) was computed (equation (3.10)), where h_{mod}, h_{obs}, φ_{mod} and φ_{obs} are amplitudes and phases as simulated in the model and in observations, respectively (Chanut *et al.*, 2008). To evaluated the relative value of this parameter the Relative Mean complex amplitude error (*Relative HC*), as expressed by the equation (3.11), was also computed.

$$HC_i = \left\{\left[h_{mod_i}\cos(\varphi_{mod_i}) - h_{obs_i}\cos(\varphi_{obs_i})\right]^2 + \left[h_{mod_i}\sin(\varphi_{mod_i}) - h_{obs_i}\sin(\varphi_{obs_i})\right]^2\right\}^{\frac{1}{2}} \quad (3.10)$$

$$Relative\ HC_i = \frac{HC_i}{h_{obs_i}} \times 100 \quad (3.11)$$

3.6 Tanjong Pagar analysis

Tkalich *et al.* (2012a) identified that the NE (SW) monsoon's climatological and extreme wind, when aligned along the longest axis of South China Sea Taiwan–Singapore, produces the strongest positive (negative) sea level surges in the Singapore Strait. Thus, they simplify the sea level surge generation problem in South China Sea using a rectangular domain, with the longest axis parallel to the direction of the NE/SW monsoon (Figure 14). It was based on a rather complex analytical treatment by Malanotte-Rizzoli (2011) which can be simplified by assuming uniformity of sea level and wind stress in cross-basin (y) direction, idealizing the sea level response under the monsoon system. The resulting analytical solution consists of opposite steady-state set-up at the two ends of the basin under the wind blowing along the main axis, with superimposed two oppositely traveling waves. The boundary conditions at the two-end side walls give rise to a standing wave, the seiche. The shallow water equations are expressed by the equations of the velocity *u* and of the SL η:

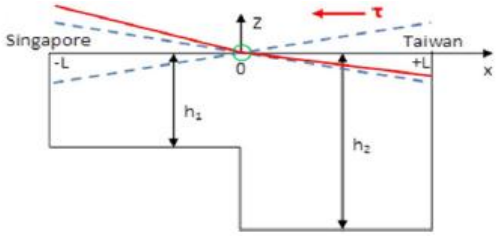

$$\frac{\partial u}{\partial t} = -g\frac{\partial \eta}{\partial x} + \frac{\tau}{\rho_0 h} \quad (3.11)$$

$$\frac{\partial \eta}{\partial t} + h\frac{\partial \mu}{\partial x} = 0 \quad (3.12)$$

$$\eta = \frac{1}{\rho_0 g h}\tau x \quad (3.13)$$

$$\tau = C_d \rho_a W^2 \quad (3.14)$$

Figure 14 - Conceptual model of storm surges in a channel 1-D model of the steady-state set-up (solid red line) and free oscillations (dashes gray lines) along the main axis of the South China Sea shown in Figure 1 during the northeast monsoon. Nodal point over shelf break is shown by a circle; existence of sea level node over the edge of the shelf break is supported by observations in Figure 7 (right). Source: Tkalich *et al.* (2012a).

If the wind stress is constant in x, the solution for the steady-state set-up can be written as 3.13 and varies only with the depth of each region. The sea level response by a NE wind ($-x$) is higher in Singapore ($x = -L$) and smaller in Taiwan ($x = +L$) due to a deeper basin. Therefore, the simplified model for storm surge in Singapore Strait presents the steady-state sea level setup that is linearly dependent on the wind shear stress. Typical values were used for the Sunda Shelf of depth, h =100 m and fetch, x =1 km. The other parameters used were the density of air, ρ_0 =1.025 kgm^{-3}, the gravitational acceleration, g =9.810 ms^{-2}, and the wind shear stress expressed by (3.14). The density of water is ρ_a =1.25 kgm^{-3}, the wind speed at 10 m, W and the drag coefficient, $C_d = 10^{-3}(0.8 + 0.065W)$, by Wu (1982). The goal was to evaluate how well the solution of this model fit the observed values. Tkalich *et al.* (2012a) shown that there is a good agreement between the observed and predicted values for the representing area offshore of Vietnam and Hainam Island.

Chapter 4 | Results and Discussion

The analysis presented in this chapter is divided into two main parts: in the first part, the available SL data from six tide-gauges from GLOSS was compared with MSYM predictions using tidal forcing, whereas in the second part the SL data available from MEH and HYDEC was compared with MSYM predictions using tidal and wind forcing.

Previously, only the SL data from the six selected GLOSS tide-gauges from (observed data) has been analysed allowing a brief characterization of the tidal behaviour in this region. Beside the co-oscillating nature of the tide from the Pacific and Indian Ocean, the topography, geography and the associated coastal waters system of each GLOSS station are also important parameters in the complex tidal behaviour. Therefore, a sequence of maps was displayed to detail the each location: a smaller map varying from 2^{o} of latitude to 3^{o} in longitude; a middle map varying in 0.3^{o} of latitude and longitude; a background image presents the scale on the bottom (3 km for all tide-gauges, except Kuala Terengganu of 5.2 km). The first two maps were created using data from CISL Research Data and the background image was taken from Google Earth. Then, the SL variability was analysed, evaluating the highest and lowest record of the tide, the MSL, the Seasonal SL and the Yearly and Monthly SLAs. Tidal harmonic analysis was also performed. This includes the: i) calculus of amplitude and phase of principal tidal constituents and ii) evaluation annual oscillation of the main constituents and the sensibility of the harmonic analysis by refining specific time periods: 1 year, 7, 4, 2 and 1 month(s) and 15 days. The amplitude and phase of the major harmonics for the 1 year analysis was shown and standard deviations (STD) for the remaining periods were summarized on tables. Afterward, a comparison with SL model predictions was performed. The SL data from GLOSS and MSYM predictions were compared, for the larger continuous records common to the six GLOSS tide-gauges. Comparisons include: amplitude and phase obtained with the tidal harmonic analysis and calculus of Mean Complex Amplitude Error (*HC*) and Relative Mean Complex Amplitude Error (*Relative HC*) for each harmonic constituent. Further, the Taylor Diagram was applied to astronomical tide generated by observations (GLOSS) and predicted data (MSYM). Only the astronomic tide was analysed in the first part.

The second part was centred in the astronomic and residual tides. To understand the phenomena of the positive or negative SLAs depending on the speed and wind direction, the SL data from the tide-gauge of Tanjong Pagar, located on the Singapore Strait was analysed. After the recognition of the tide-gauge, the MSL and the Monthly mean SL, for observed and predicted data, was also calculated. Daily *RMSE* to these two data sets were calculated, as well as the monthly *RMSE'*, *R* and *Relative Error* between the predicted and observed data. Next, harmonic analysis was applied for all period under analysis, including the missing data. After removing the astronomical tide, the SLA (predicted and observed) were displayed, combined with the real wind speed (forcing in the predicted data). The SL data of this tide-gauge was crossed with winds of the South China Sea region, because of their effluence in the entire region, bounded by Gulf of Thailand on the north, Karimata Strait on the south, east cost of Peninsular Malaysia on the west, and break of Sunda Shelf on the east. Previous studies (Tkalich *et al*., 2012a, 2012b; Cheng and Qi 2007; Chen *et al.* 2010a, 2010b) revealed that the seasonal and extreme winds and their persistence and direction play the primary role in generating SLAs of different magnitudes in the Singapore Strait: positive during NE monsoon and negative during SW monsoon. The last part consisted in the analysis for two tide-gauges in Pangkor. Both of the tide-gauges data revealed some important discrepancies, mainly in neap tidal cycle. Harmonic analysis was applied and SLA was also evaluated and crossed with wind data from GFS.

4.1 Tidal analysis

Ko Taphao Noi tide-gauge, an island about 7 km southeast of Phuket City, is located in the Indian Ocean along the shelf of Thailand (time zone GMT + 7 h), where the depth ranges between 0 and 1 m. Near the GLOSS station there are two small islands (less than 1 km), which due to their size do not represent significant influence, as conveys in Figure 15.

Highest record of the tide	Lowest record of the tide	Mean	Seasonal mean	
4.00 m	0.41 m	2.21 m	*Winter*	2.12 m
			Spring	2.19 m
			Summer	2.26 m
			Autumn	2.25 m

Figure 15 - Location and tidal characteristics at Ko Taphao Noi tide-gauge. Source: Google Earth and Matlab (m_map) with data of CISL.

The available SL data for the Ko Taphao Noi tide-gauge includes the period from the 1st of January 1985 to the 31st of December 2010. For this period, the mean SL trend computed from the Yearly SLA (Figure 16, top) is 1.65 mmyr^{-1}, with some rising and falling of the SL. Seven distinct falls (important fall for 1996-1997) and seven sharp rises (important rise for 1995-1996, which can be related to ENSO events) were observed. In respect to monthly averages, data from May to November have a positive monthly mean SLA and the more negative SLA occurs between January and March. Then, the harmonic analyses for 1 year period (Figure 17) allowed the identification of the higher amplitude harmonics: M_2 and S_2. The largest STD corresponds to the harmonic constituent with largest amplitude (M_2), while regarding the phase, M_4 has higher STD.

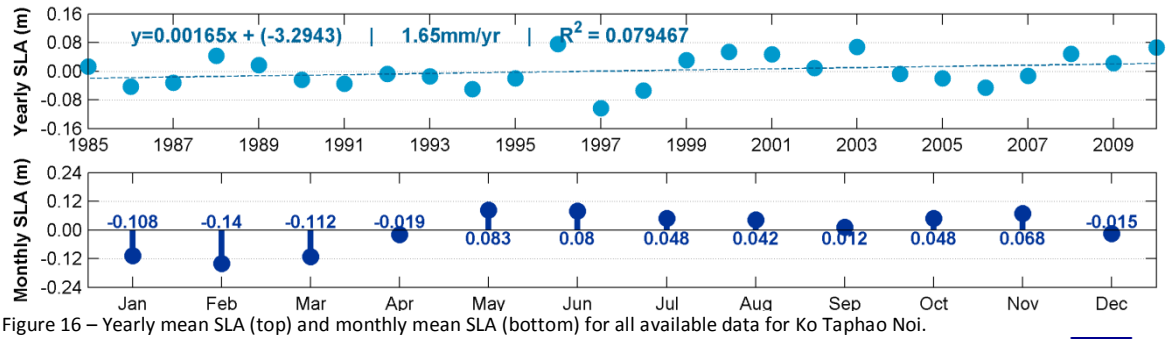

Figure 16 – Yearly mean SLA (top) and monthly mean SLA (bottom) for all available data for Ko Taphao Noi.

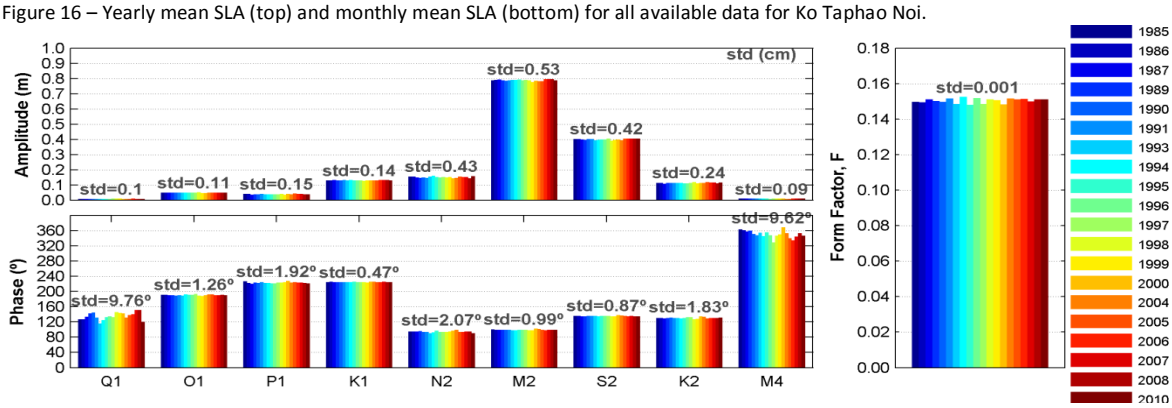

Figure 17 - Harmonic analysis of 1 year (color) for Ko Taphao Noi: amplitude (top), phase (bottom) and form factor (right).

Ko Lak tide-gauge is also located in Thailand (time zone GMT + 7 h) in the Pacific Ocean with a different associated hydrodynamic system: there are two bays and some small islands between the coordinates of the station. With a depth of around 0 m, the shallow water is exposed to winds from all directions and waves from adjacent energetic coastal zone (Figure 18).

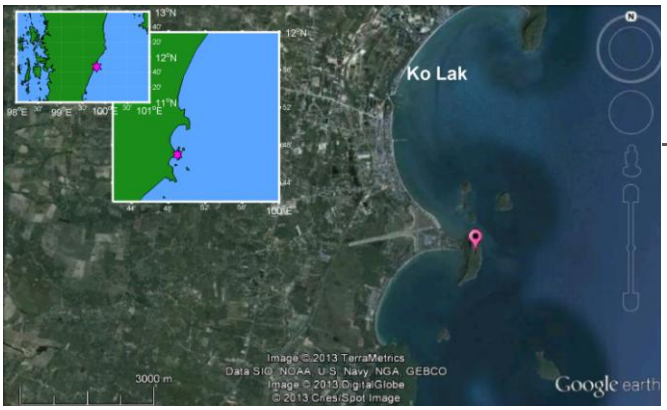

Highest record of the tide	Lowest record of the tide	Mean	Seasonal mean	
4.07 m	0.92 m	2.51 m	*Winter*	2.68 m
			Spring	2.50 m
			Summer	2.31 m
			Autumn	2.56 m

Figure 18 - Location and tidal characteristics at Ko Lak tide-gauge. Source: Google Earth and Matlab (m_map) with data of CISL.

The available data SL for the Ko Lak tide-gauge is from 1st of January 1985 to the 31st of December 2010. For this period, the mean SL trend computed from the yearly mean SLA (Figure 19, top) is 3.36 mmyr^{-1}, which is more significant in recent years (a rise of 41.39 mmyr^{-1} between 2007 and 2010). Rising and falling of the mean SL is noticed: four distinct falls (e. g., for 1991-1993 and 2006-2007) and five main rises (important rise for 2002-2004 and 2007-2010). The monthly variability (Figure 19, bottom) is intense with positive SLA for the months between October and March. This tide-gauge has many flaws and harmonic analysis for completed years was only possible before 1998. The major tidal harmonics are O_1 and K_1, as seen in Figure 20. The major STDs occur in the phase of the semidiurnal harmonics and a special variance was also found in the M_4; in the amplitude, they occur to the main constituents, K_1 and O_1.

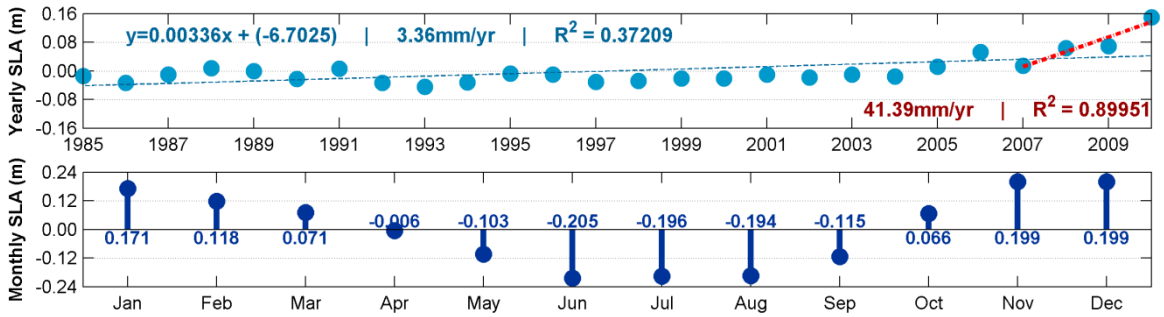

Figure 19 - Yearly mean SLA (top) and monthly mean SLA (bottom) for all available data for Ko Lak.

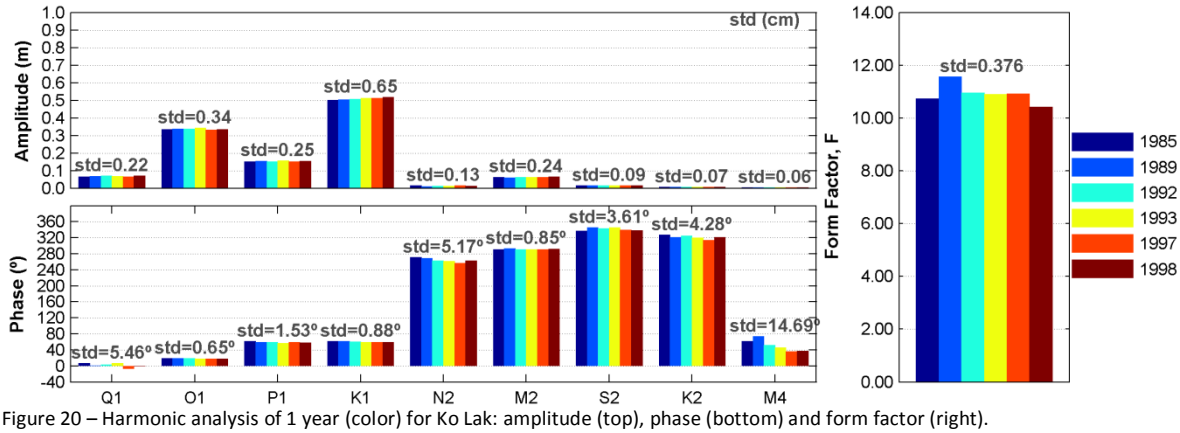

Figure 20 – Harmonic analysis of 1 year (color) for Ko Lak: amplitude (top), phase (bottom) and form factor (right).

Kuala Terengganu tide-gauge is located on the left corner of the T-junction on the jetty facing the Chendering Fisheries Complex (Figure 21). In the Pacific Ocean, along the shelf of Malaysia (time zone GMT + 8 h), it is located in a limited space (seawall on the left side and the depth is greatly reduced).

Highest record of the tide	Lowest record of the tide	Mean	Seasonal mean	
4.05 m	0.54 m	2.21 m	*Winter*	2.37 m
			Spring	2.18 m
			Summer	2.03 m
			Autumn	2.25 m

Figure 21 - Location and tidal characteristics at Kuala Terengganu tide-gauge. Source: Google Earth and Matlab with data of CISL.

The available data SL for the Kuala Terengganu station starts at the 31st of October 1984 and finished at the 31st of December of 2006. For this period, the mean SL trend computed from the yearly mean SLA (Figure 22, top) is 2.24 mmyr^{-1}, includes some rising and falling of the SL, e.g., higher rises occurs for the periods 1987-1988; 1994-1995 and falls for 1995-1996. As seen in the Ko Lak station (same side of coast), the monthly mean SLA is intense. Annually, difference between positive SLA in December and negative in June are probably caused by monsoons with negative SLA in spring and summer months (Figure 22, bottom). Through the harmonic analysis, shown in Figure 23, the main constituents for this station were identified: K_1, O_1 and M_2. The sum of amplitudes of the diurnal harmonics is higher than of the semidiurnal harmonics. The major annual variance in the amplitude occurred for O_1 and M_2, and in the phase for Q_1 and M_4.

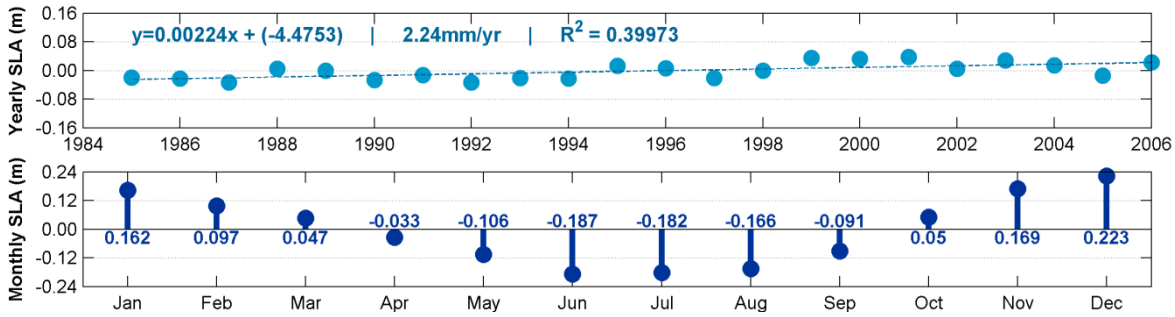

Figure 22 - Yearly mean SLA (top) and monthly mean SLA (bottom) for all available data for Kuala Terengganu.

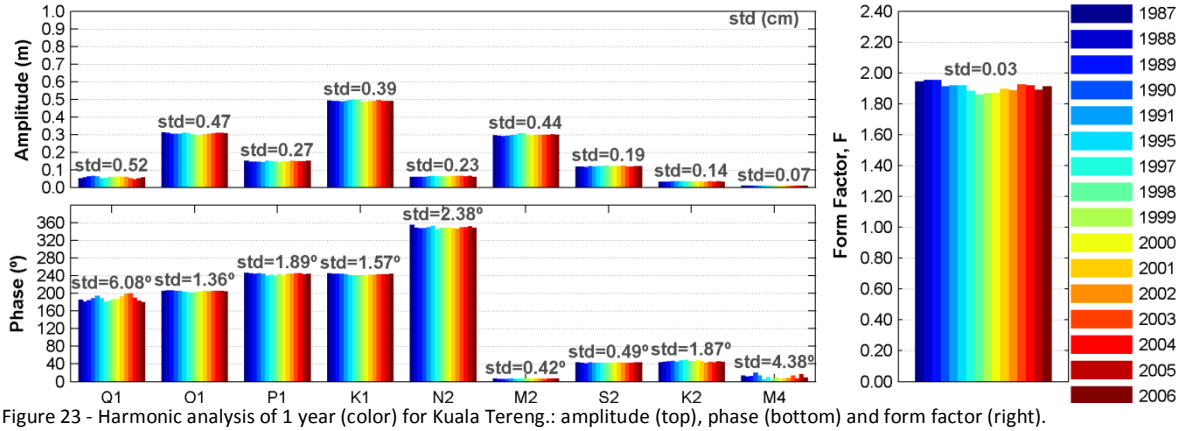

Figure 23 - Harmonic analysis of 1 year (color) for Kuala Tereng.: amplitude (top), phase (bottom) and form factor (right).

Pengkalan tide-gauge is located near the inner jetty of the Royal Malaysian Naval Base (time zone GMT + 8 h), on the side of Indian Ocean. The place is limited to an opening with just over 200 m, next to the mouth of a river, where there is a mixture of river water with ocean water. In front of the river discharge there is an island with about 10 km, which is an obstacle to the movement of water. Besides the importance of precipitation in river flow, the direction and intensity of the wind also has an impact on the water level, contributing to the entry or exit of water in this limited region (Figure 24).

Highest record of the tide	Lowest record of the tide	Mean	Seasonal mean	
3.97 m	0.25 m	2.19 m	*Winter*	2.12 m
			Spring	2.17 m
			Summer	2.24 m
			Autumn	2.24 m

Figure 24 - Location and tidal characteristics at Pengkalan tide-gauge. Source: Google Earth and Matlab (m_map) with data of CISL.

The available data SL includes the period from the 12th of December 1984 to the 31st of December 2006. For this period, the mean SL trend computed from the yearly mean SLA (Figure 25, top) is 1.38 mmyr^{-1}, with some rising and falling of the SL. Six distinct falls (important fall for 1993-1994; 1996-1997; 2001-2002) and five sharp rises (important rise for 1987-1988; 1994-1996; 1997-2000). In contrast to the monthly mean SLA for the other side of the coast, the SLA is negative from January to April (Figure 25, bottom) and two maximums for May and November. The major tidal harmonics identified by the harmonic analysis, shown in Figure 26, are M_2 and S_2. The annual amplitude variation is relatively low. Regarding to the phase, the largest STDs occur for Q_1, followed by O_1 and M_4.

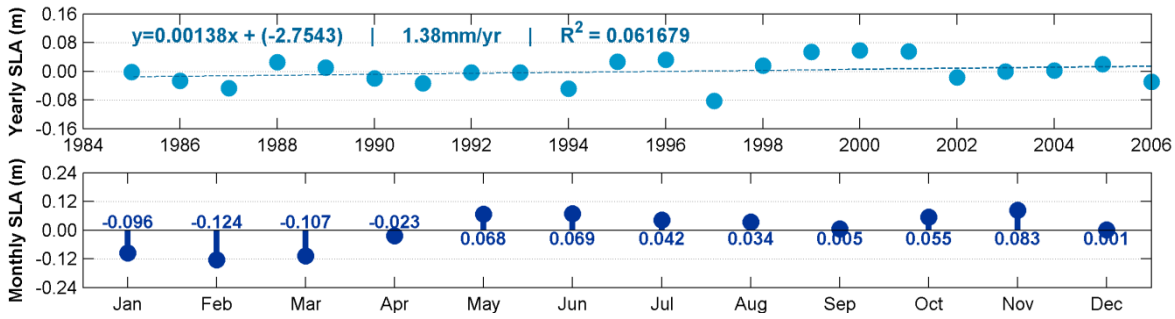

Figure 25 - Yearly mean SLA (top) and monthly mean SLA (bottom) for all available data for Pengkalan.

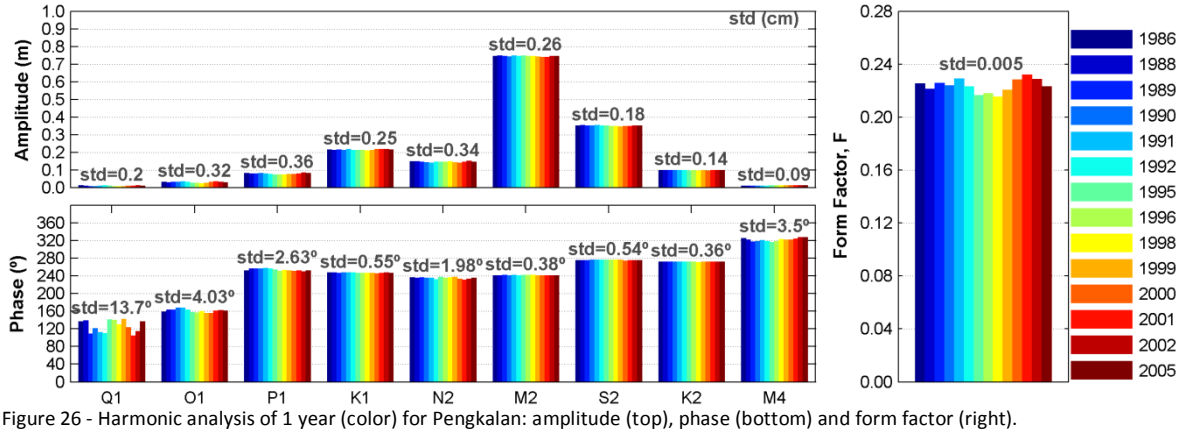

Figure 26 - Harmonic analysis of 1 year (color) for Pengkalan: amplitude (top), phase (bottom) and form factor (right).

Singapore tide-gauge (time zone GMT + 8 h), associated with the Indian Ocean, is located on a canal that begins on one side of the Singapore Strait and flows to the other side, Figure 27. The channel has a variable width (1 – 2 km) with various river discharging close to each other. Further, there are islands and Straits along the channel that interferes with the water movement. The SL is dominated by the tide and also by the local atmospheric conditions.

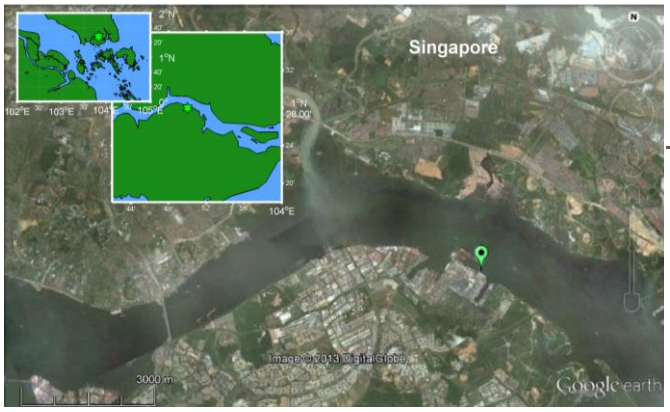

Highest record of the tide	Lowest record of the tide	Mean	Seasonal mean	
3.38 m	-0.28 m	1.58 m	*Winter*	1.67 m
			Spring	1.55 m
			Summer	1.51 m
			Autumn	1.61 m

Figure 27 - Location and tidal characteristics at Singapore tide-gauge. Source: Google Earth and Matlab (m_map) with data of CISL.

The available data SL for Singapore includes the period from the 13th of August 1981 to the 1st of January 1990. For this period, the mean trend computed from the yearly mean SLA (Figure 28, top) is 15.63 mmyr^{-1} (only seven years and between 1982 and 1989). Rising and falling of the SL is noticed: one fall (smooth fall for 1986-1987) and two rise (1982-1984 and 1987-1989, in agree with Tkalich *et al.* (2012b)). The monthly mean SLA are negative during the winter period, what can be explained by the prevailing wind patterns (Figure 28, bottom), confirmed by Tkalich *et al.* (2012a). The harmonic constituents with the highest amplitude are M_2, followed by S_2, K_1 and O_1, with similar amplitudes, as presented in Figure 29. The annual change in amplitude has a maximum STD for M_2 (the greater amplitude) and in the phase, the high STD is observed for the Q_1 and M_4 harmonics.

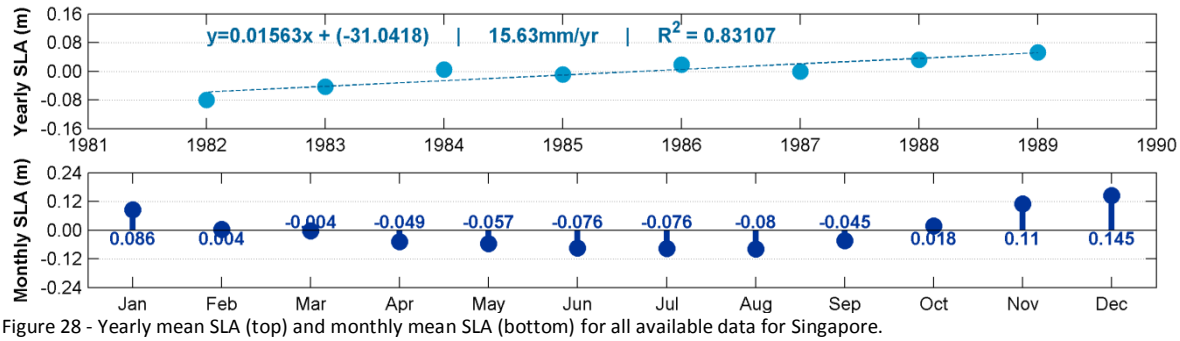

Figure 28 - Yearly mean SLA (top) and monthly mean SLA (bottom) for all available data for Singapore.

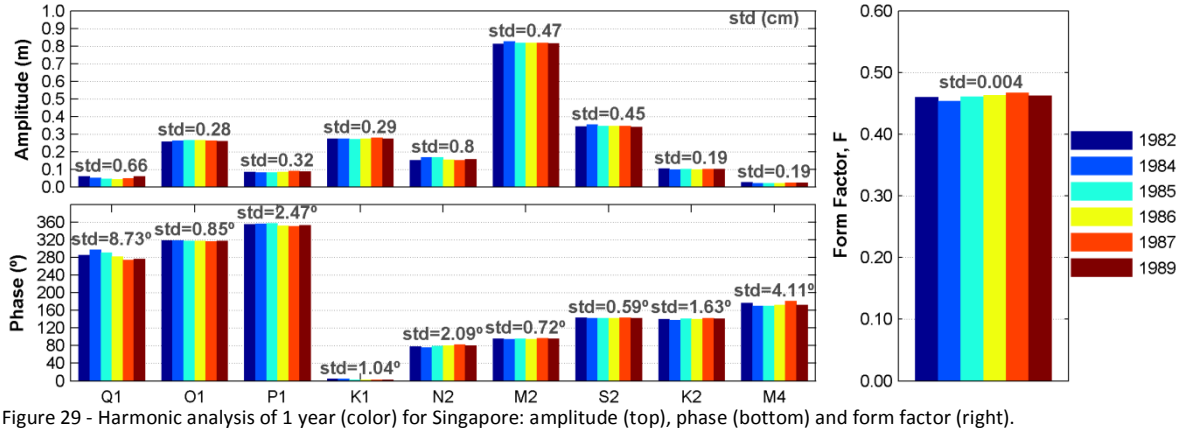

Figure 29 - Harmonic analysis of 1 year (color) for Singapore: amplitude (top), phase (bottom) and form factor (right).

Zhapo tide-gauge is located in a limited space of a Chinese island (time zone GMT + 8 h) with just over 10 km, in the Pacific Ocean. This place has an aperture of nearly 0.5 km, next to a wide mouth of a river. Beyond the influence of the ocean and the river, on the site of the station there is a current associated with the strait situated in the northeast, present in Figure 30.

Highest record of the tide	Lowest record of the tide	Mean	Seasonal mean	
4.58 m	0.11 m	2.11 m	*Winter*	2.09 m
			Spring	2.05 m
			Summer	2.04 m
			Autumn	2.26 m

Figure 30 - Location and tidal characteristics at Zhapo tide-gauge. Source: Google Earth and Matlab (m_map) with data of CISL.

The available GLOSS data SL for Zhapo includes the period from the 1st of January 1975 to the 12th of December 1997, without gaps. For this period, the SL trend determined from the yearly mean SLA in Figure 31 (top) indicates a rise of 2.17 mmyr^{-1}. Rising and falling of the SL is noticed: higher falls occur for 1976-1977; 1978-1979; 1981-1982; 1986-1987; 1989-1990 and rise for 1977-1978; 1987-1989; 1993-1994. The monthly SLA mean reveals a more intense positive anomaly between the months of September, October and November, and an anomaly that does not exceed 10 cm for the months from January to August (Figure 31, bottom). The harmonic analysis (Figure 32) reveals the main harmonics: M_2, K_1, O_1 and S_2. The annual variation has a maximum in the amplitude for M_2 and it is relatively low for the phase.

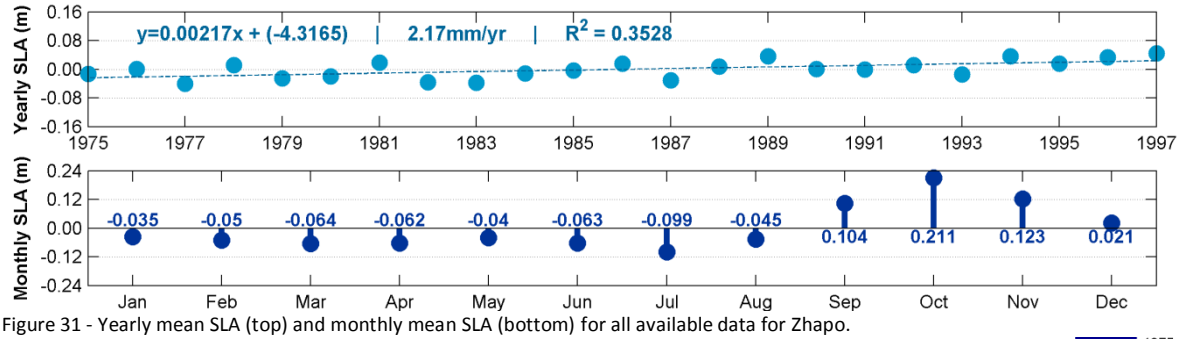

Figure 31 - Yearly mean SLA (top) and monthly mean SLA (bottom) for all available data for Zhapo.

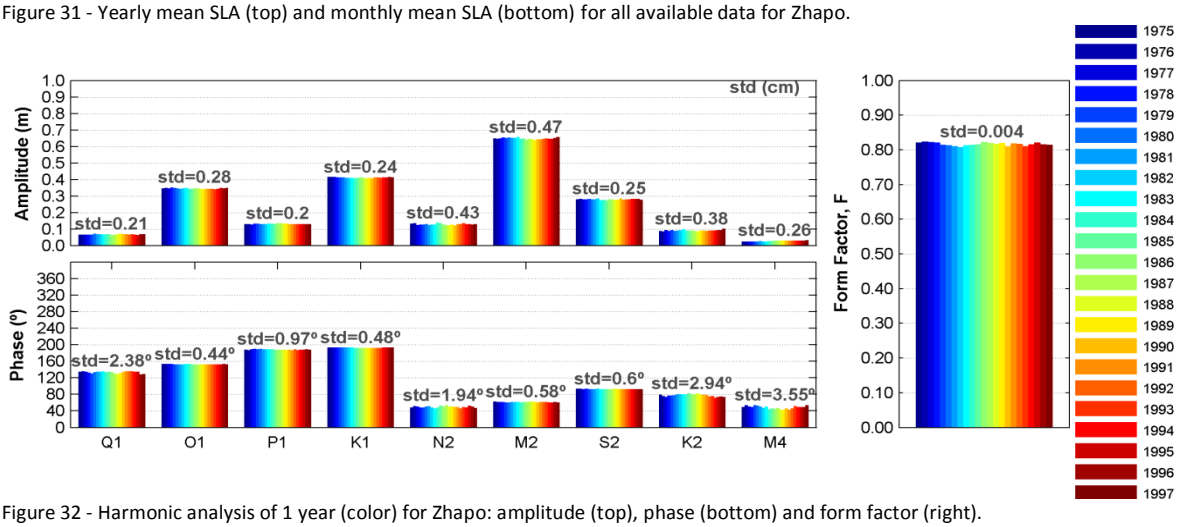

Figure 32 - Harmonic analysis of 1 year (color) for Zhapo: amplitude (top), phase (bottom) and form factor (right).

4.1.1 Harmonic analysis period sensitivity

Tidal harmonic analysis at each data station was applied for different periods. The goal is to study the sensitivity of the analysis range for different periods, excluding the missing data. The specific time periods are: 1 year; 7, 4, 2 and 1 month (s); and 15 days. For each period, some continuous data ranges weren't included due to failures in data (a few missing days). Therefore, conditions were imposed for each period taking into account the minimum data period needed to separate the harmonics. The minimum day's conditions are presented in Table 10. Note that for 15 days, data ranges must include 15 days; otherwise, it is not possible to separate the four major harmonics.

Table 10 – Minimum of days conditions available for each period range.

	Minimum days conditions
1 year	350
7 months	208
4 months	118
2 months	58
1 months	27
15 days	15

So, it is possible to include more data by reducing the time range of the harmonic analyses, however it is important to take into account the variations on the standard deviations (STD). For instance, for the Ko Lak station, from 2000 onwards there isn't continuous data for periods of over 350 days. However, by reducing the time period, harmonic analysis can be performed using smaller continuous data ranges (e.g., for 7 months, only 208 days is necessary). The STDs of the main harmonic, for all harmonic analysis, are summarized for amplitude in Table 11, and for phase in Table 12.

Table 11 - Standard deviation (STD) in relation to amplitude (in cm) of the harmonic constituents, for the six tide-gauges of GLOSS

	Period	**Q_1**	**O_1**	**P_1**	**K_1**	**N_2**	**M_2**	**S_2**	**K_2**	**M_4**
Ko Taphao Noi	*Year*	0.10	0.11	0.15	0.14	0.43	0.53	0.42	0.24	0.09
	7 Months	0.14	0.22	0.44	0.42	0.46	0.59	0.91	0.38	0.13
	4 Months		0.29		0.99		1.03	4.81		
	2 Months		0.41		2.36		1.24	7.33		
	1 Month		0.49		2.59		1.43	8.48		
	15 Days		0.75		2.76		5.20	9.16		
Ko Lak	*Year*	0.22	0.34	0.25	0.65	0.13	0.24	0.09	0.07	0.06
	7 Months	0.34	0.45	0.71	0.94	0.09	0.27	0.27	0.16	0.11
	4 Months		0.72		4.58		0.40	0.26		
	2 Months		1.09		7.93		0.52	0.64		
	1 Month		1.56		9.19		0.61	0.79		
	15 Days		2.77		9.78		0.85	0.82		
Kuala Terengganu	*Year*	0.52	0.47	0.27	0.39	0.23	0.44	0.19	0.14	0.07
	7 Months	0.53	0.47	0.38	0.56	0.28	0.61	0.41	0.31	0.10
	4 Months		0.66		3.64		1.05	0.64		
	2 Months		0.92		8.06		1.16	2.10		
	1 Month		1.17		9.09		1.30	2.47		
	15 Days		2.51		9.61		2.73	2.78		
Pengkalan	*Year*	0.20	0.32	0.36	0.25	0.34	0.26	0.18	0.14	0.09
	7 Months	0.27	0.36	1.24	0.94	0.31	0.39	0.72	0.26	0.10
	4 Months		0.78		1.00		0.84	4.19		
	2 Months		1.31		4.64		1.02	6.07		
	1 Month		1.53		5.24		1.18	7.19		
	15 Days		1.72		5.59		5.04	7.95		
Singapore	*Year*	0.66	0.28	0.32	0.29	0.80	0.47	0.45	0.19	0.19
	7 Months	0.65	0.52	0.96	0.57	0.56	0.99	0.74	0.51	0.46
	4 Months		0.50		2.10		1.91	4.83		
	2 Months		1.16		4.99		2.17	6.59		
	1 Month		1.34		5.67		2.31	7.95		
	15 Days		2.23		5.97		5.36	8.87		
Zhapo	*Year*	0.21	0.28	0.20	0.24	0.43	0.47	0.25	0.38	0.26
	7 Months	0.21	0.35	0.62	0.59	0.40	0.78	0.70	0.43	0.29
	4 Months		0.66		3.18		1.30	3.46		
	2 Months		0.87		7.81		1.63	5.35		
	1 Month		1.14		8.7		1.81	6.08		
	15 Days		2.74		9.19		4.94	6.79		

Table 12 - Standard deviation (STD) in relation to phase (°) of the harmonic constituents, for the six tide-gauges of GLOSS.

	Period	Q_1	O_1	P_1	K_1	N_2	M_2	S_2	K_2	M_4
Ko Taphao Noi	*Year*	9.76	1.26	1.92	0. 47	2.07	0.99	0.87	1.83	9.62
	7 Months	11.34	1.78	8.10	2.39	2.06	1.16	1.71	2.31	10.76
	4 Months		3.01		7.07		1.51	7.3		
	2 Months		4.98		10.14		1.76	10.96		
	1 Month		5.98		12.47		2.00	12.30		
	15 Days		9.27		13.07		5.92	13.43		
Ko Lak	*Year*	5.46	0.65	1.53	0.88	5.17	0.85	3.61	4.28	14.69
	7 Months	5.32	2.25	4.49	2.34	13.49	9.41	10.11	18	30.42
	4 Months		2.82		5.77		8.79	13.78		
	2 Months		3.10		11.73		10.89	34.05		
	1 Month		3.60		13.16		21.66	48.74		
	15 Days		7.25		13.8		24.83	62.71		
Kuala Terengganu	*Year*	6.08	1.36	1.89	1.57	2.38	0.42	0.49	1.87	4.38
	7 Months	6.08	1.40	2.77	1.53	2.66	1.54	1.63	2.84	8.82
	4 Months		1.78		5.80		2.38	4.31		
	2 Months		2.65		10.65		2.63	11.41		
	1 Month		3.16		12.77		2.84	12.37		
	15 Days		6.85		13.38		6.24	13.82		
Pengkalan	*Year*	13.70	4.03	2.63	0.55	1.98	0.38	0.54	0.36	3.50
	7 Months	19.10	8.18	7.63	3.62	1.71	0.44	1.60	0.79	4.06
	4 Months		14.96		10.88		0.84	7.29		
	2 Months		35.73		13.84		1.04	11.08		
	1 Month		44.24		15.89		1.15	12.14		
	15 Days		51.58		16.66		5.80	13.23		
Singapore	*Year*	8.73	0.85	2.47	1.04	2.09	0.72	0.59	1.63	4.11
	7 Months	8.86	1.13	5.30	2.17	2.23	0.73	1.80	2.03	15.44
	4 Months		1.26		6.77		0.98	7.48		
	2 Months		3.31		9.46		2.66	14.08		
	1 Month		3.66		11.63		2.94	14.81		
	15 Days		7.76		12.33		6.77	15.98		
Zhapo	*Year*	2.38	0.44	0.97	0.48	1.94	0.58	0.60	2.94	3.55
	7 Months	2.64	0.59	1.35	0.66	1.83	0.66	1.57	3.52	12.33
	4 Months		1.05		6.60		1.09	7.67		
	2 Months		1.36		10.74		1.29	11.32		
	1 Month		1.86		13.33		1.45	13.04		
	15 Days		6.33		13.97		5.56	14.00		

The major tidal harmonics of each tide-gauge are different, and consequently the associated STD can be related with the importance of each constituent in the tide-gauge. The reduction of the analysis periods increases the values of STD (amplitude and phase) and can include a data range that was not in the larger periods. As previously mentioned, Ko Lak is a clear example of this phenomenon. For this station, when the analysis was applied for 1 year of records, there were few full years and these were before 2000 (did not reveal a very marked variability). It is important to remember that this tide-gauge (Ko Lak) was located between two bays and near smaller islands, and that M_4 was the largest of the shallow water constituents. Therefore, for period ranges smaller than 7 months, because fewer observations can be used, more recent recorded data was included. This point to: increase in the phases of M_2 and S_2, and a slight decrease in amplitude for O_1 and slight increase for M_2 (not shown).

In general, taking every tide-gauge into account, the highest amplitude variations were observed for the largest amplitude. However for Zhapo, for instance, K_1 and S_2 have the highest variations. For the phase, maximum STD for the harmonic analysis for 15 days was around 7° for O_1 (except for Pengkalan, where STD is 51.58°); 14° for K_1; 6° for M_2 (except for Ko Lak where STD is 24.83°); and 14° for S_2 (except for Ko Lak where STD is 62°71). Finally, Table 13 presents the amplitude of S_A and S_{SA}.

Table 13 – Amplitude of the annual SA and semiannual SSA for the larger continuous period of each tide-gauge, in centimetres.

	Larger continuous	Nº of Days	S_A (cm)	S_{SA} (cm)
Ko Taphao Noi	May/1992 to Sep/2001	3433.58	7.59	5.36
Ko Lak	Jan/1991 to Dec/1993	1066.33	20.88	6.44
Kuala Terengganu	May/1996 to Dec/2006	3878.54	19.65	2.79
Pengkalan	Dec/1997 to May/2003	1972.92	6.70	6.29
Singapore	Dec/1983 to Mar/1988	1560.54	9.65	3.47
Zhapo	Jan/1975 to Dec/1997	8400.67	10.45	7.54

4.1.2 Concluding remarks

Yearly SLAs are useful to identify the trend of the mean SL as well as the variability over the years, and the monthly SLAs allow evaluating the variability of the SL throughout the year. NOAA mean SL trends are lower than the results found for tide-gauges data. This happens for two main reasons: NOAA's (Table 1) mean SL is based on monthly mean SL data while the mean SL trend for GLOSS data (red line on the Figures 16, 19, 22, 25, 28 and 31) were calculated with yearly mean SLA; the different time intervals used for the mean SL trend analysis is the second reason (for the period present in Table 14).

Table 14 – Available data to calculate the yearly mean SL and mean SL trend shown in Figure 33 (left).

	GLOSS data	Nº evaluated years
Ko Taphao Noi	1985 to 2010	26
Ko Lak	1985 to 2010	26
Kuala Terengganu	1985 to 2006	22
Pengkalan	1985 to 2006	22
Singapore	1982 to 1989	7
Zhapo	1975 to 1997	23

In addition, the recent years generally have higher trends compared to previous decades, and NOAA includes a larger and older data set of SL. This is easily visible in the Ko Lak, where the SL has increased, especially in the last five years. This can be an effect of climate changes or alterations to the bottom topography. To properly evaluate the SL trend, it is necessary to select a common time interval that is preferably continuous. But this did not occur in NOAA's mean SL trend calculation nor in the SL trend using the GLOSS. The data used by NOAA contains flaws ranging from a few hours to years, while the GLOSS data had failures ranging from a few hours to less than one month. Even though the NOAA trend for Singapore was negative between 1954 and 2011, for the period at study (1982-1989), the trend for GLOSS and NOAA were both positive (tidesandcurrents.noaa.gov/sltrends/).

The mean SL trend is positive for all analysed tide-gauges of GLOSS. However, the mean SL trends are higher on the side of M alacca Strait compared with Kuala Terengganu, Ko Lak and Zhapo. Singapore has the highest mean SL trends and Pengkalan the lower value from the available GLOSS data (Figure 33, left). Regarding the monthly variation, it is lower on the side of Malacca Strait. For Malacca Strait (Ko Taphao Noi and Pengkalan), the difference between maximum monthly SLA are of about 20 cm. The annual variance for Ko Lak and Kuala Terengganu are double those of Ko Taphao Noi and Pengkalan (about 40 cm) and occur between December and June (Figure 33, right and Table 15).

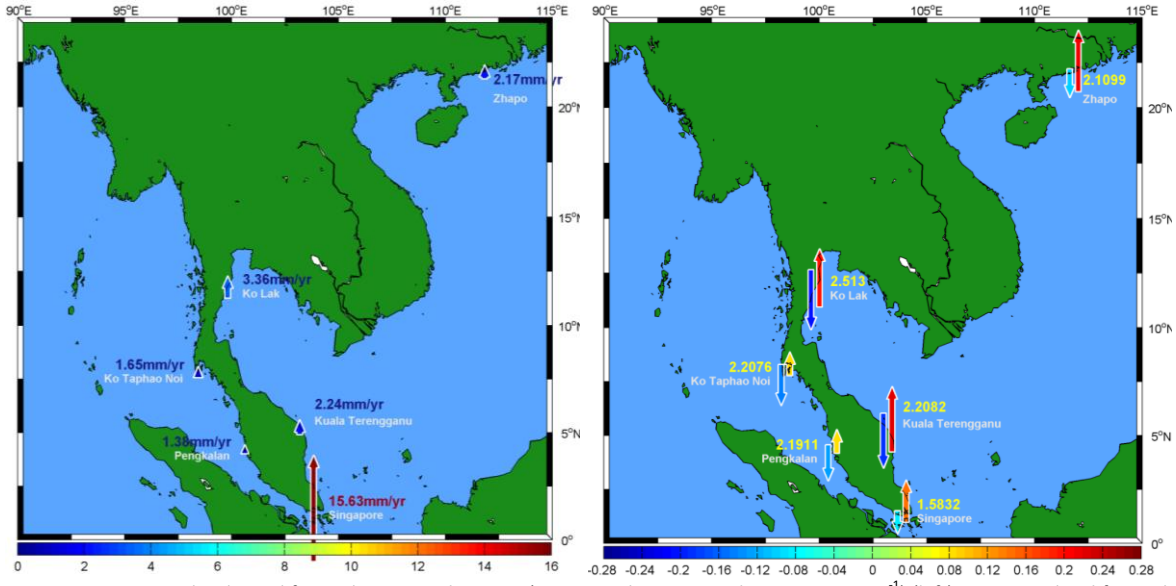

Figure 33 - Mean sea level trend for each GLOSS tide-gauge (arrows with corresponding text in $mmyr^{-1}$) (left). Mean sea level for each GLOSS tide-gauge (yellow text) and maximum (upward arrows) and minimum (downward arrows) Monthly SLAs, in meters (right).

Table 15 – Maximum and minimum monthly mean SL. Inter annual variances mean SL.

	Maximum monthly SLA	Minimum monthly SLA	Dif. (m)
Ko Taphao Noi	May	February	0.223
Ko Lak	December	June	0.404
Kuala Terengganu	December	June	0.410
Pengkalan	November	February	0.207
Singapore	December	August	0.224
Zhapo	October	July	0.310

The form factor uses the amplitude of the diurnal harmonic constituents K_1 and O_1 and semidiurnal M_2 and S_2 to classify the type of tide. The STD of amplitude increases with the decrease of the period of analysis, so minor deviations in the form factor occur in the harmonic analysis from one year, as expected. In some situations and especially for smaller periods of analysis, the classification of the tide can be different. It happens in Kuala Terengganu, Pengkalan and Singapore. The error bars in Figure 34 present the STD for the harmonic analysis applied. The last bar corresponds to the analysis for 15 days and the STD is proportional to the form factor value (Ko Lak). This factor gathers the STD of the four main harmonics: M_2, S_2, K_1 and O_1. Looking at Tables 11-12 (and Figure 35) it was possible to find the main harmonic constituents that contribute to STD in the form factor, at each tide-gauge.

The tide-gauge of GLOSS located on the side of Malacca Strait is semidiurnal: Ko Taphao Noi and Pengkalan. Singapore and Zhapo have mixed mainly semidiurnal tides, but for some analysed periods, Singapore can consider semidiurnal. In Ko Lak, the tide was classified as diurnal. It's also important to remember the large data gaps. For Kolak, the 7 month analyses include data sets not present in 1 year analysis, and, after 10 years, the amplitude or phase of the harmonics present some differences. The tide generates longer waves that move all around the ocean and the same amplitude and phase for harmonics is expected. However, the main variance found for these parameters, in general, can result from changes in the physical location of the tide-gauge (dredging operations, breakwaters, seawall, and artificial reef, among others).

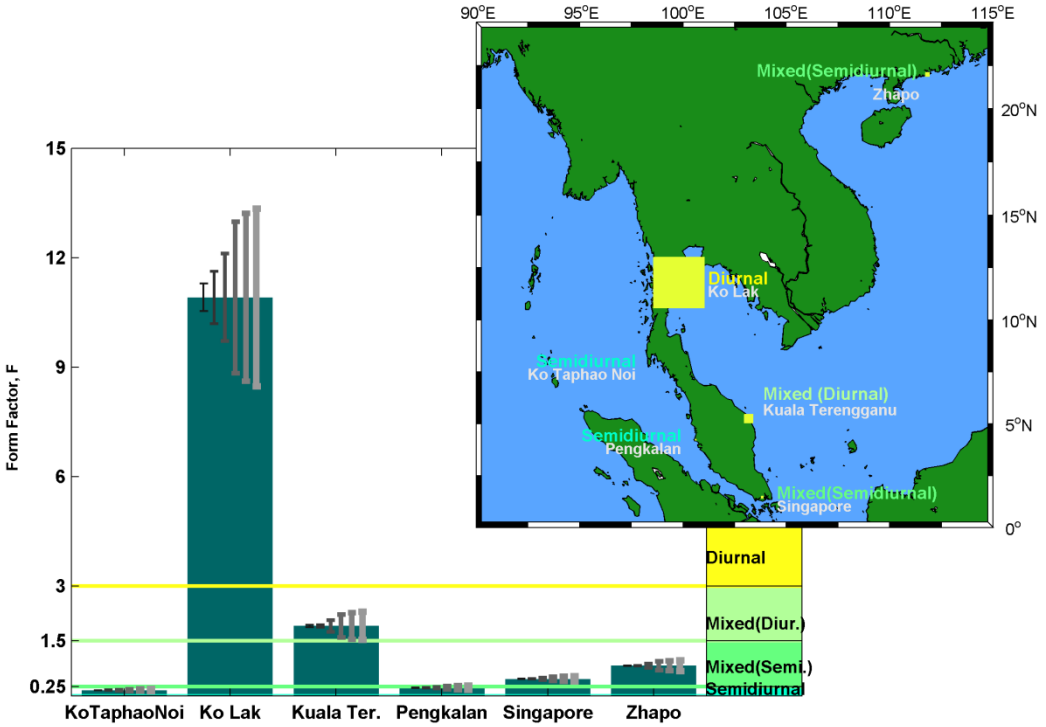

Figure 34 - Form factor for the GLOSS tide-gauges. The error bars represent the standard deviation of the form factor for the harmonic analysis of 1 year, 7 months, 4 months, 2 months, 1 month and 15 days (from left to the right, gray error bars). The horizontal lines identify the limits for diurnal tide, mixed mainly semidiurnal, mixed mainly diurnal and semidiurnal.

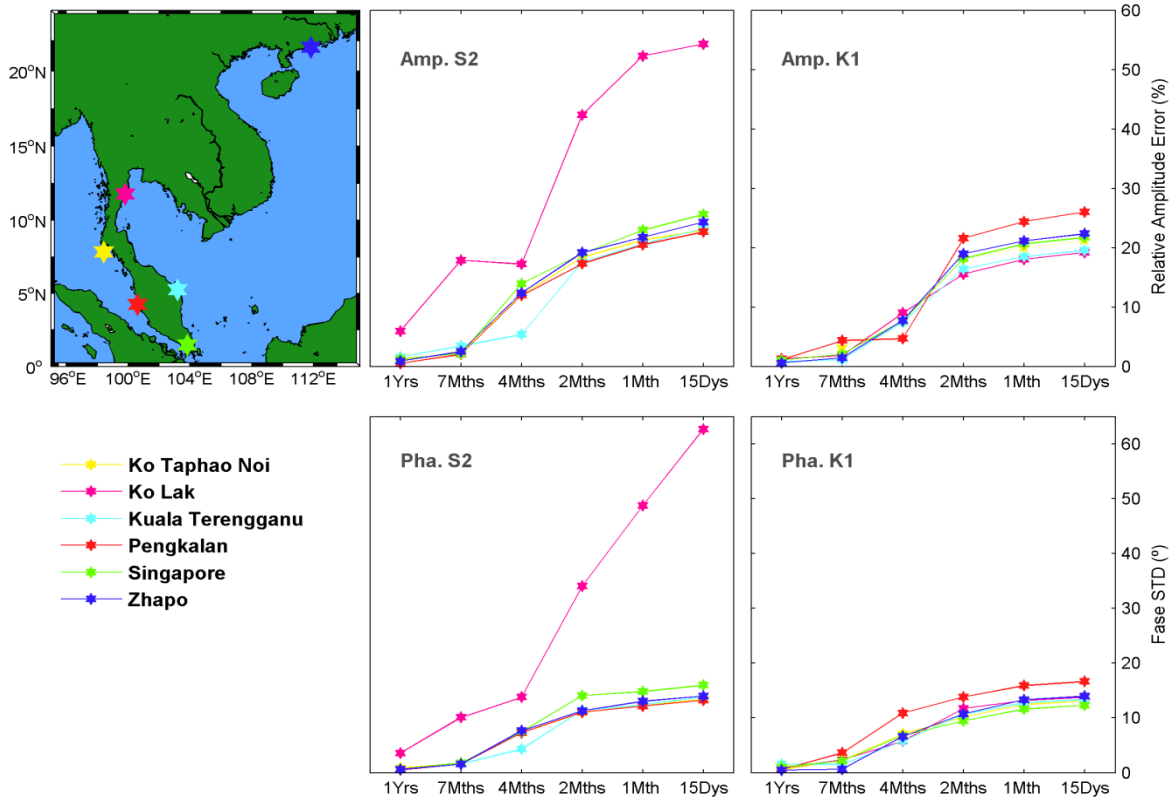

Figure 35 – Standard deviation for the constituents S_2 an K_1 for the harmonic analysis for 1 year, 7 months, 4 months, 2 months, 1 month and 15 days. Top left: map with the location of the GLOSS Stations. Top centre: Relative amplitude Error in percentage of S_2. Top right: Relative amplitude Error in percentage of K_1. Bottom centre: Phase STD of S_2. Bottom right: Phase STD of K_1, in degree.

Some conclusions about the STD of the harmonics are: when the STD increases in amplitude, it generally increases also in the phase of the harmonic constituent as well; the higher STD in the annual analysis occurs in constituents with higher amplitude; K_1 and S_2 have high STDs in amplitude and phase; STD in M_2 increases considerably for the analysis of 1 month and 15 days.

According to equation (3.3) – *Rayleigh criterion* - 15 days would be sufficient to separate the four major harmonic constituents: M_2, S_2, K_1 and O_1. However, as it turns out, the error would be too high in the site characterization to perform a harmonic analysis with this time interval. One year or 7 months are better when applying the harmonic analysis. Every harmonic analysis using less than 7 months can include a significant error in the results; in general, can be higher than 20% of the constituent amplitude. Note that a similar pattern for the error of the analysed tide-gauges (amplitude and phase). Comparing the results of the harmonics' amplitude and phase for similar locations, from previous studies (shown in Table 3) with the observed data from GLOSS, the highest discrepancies in amplitude occur for K_1, for the station of Kuala Terengganu, in particular. Regarding the phase, the most marked discrepancies also occur for K_1 with a maximum of 210 minutes of phase lag for Kuala Terengganu (Table 16). Moreover, M_2 shows a significant difference for Ko Lak and Kuala Terengganu.

Table 16 – Mean of the amplitude and phase given by the harmonic analysis to 1 year for O_1, K_1, M_2 and S_2, and respective form factor.

GLOSS Station	**Amplitude (cm)**				**Phase (°)**				**F**
	O_1	K_1	M_2	S_2	O_1	K_1	M_2	S_2	
Ko Taphao Noi	4.83	12.99	78.75	39.87	190.42	224.66	99.17	135.51	**0.15**
Ko Lak	33.64	50.91	6.24	1.51	18.46	60.33	291.57	341.69	**10.91**
Kuala Terengganu	30.49	49.14	29.78	11.96	204.70	242.76	6.85	42.86	**1.91**
Pengkalan	3.03	21.48	74.53	35.07	161.03	246.94	241.42	275.79	**0.22**
Singapore	26.20	27.47	81.76	34.63	317.58	3.55	95.58	142.94	**0.46**
Zhapo	34.54	41.13	64.76	27.92	152.76	192.71	61.37	92.84	**0.82**

4.2 Astronomic tide validation

To evaluate the MSYM SL predictions for the six GLOSS tide-gauges at study, harmonic analysis was applied, using the largest continuous period common to all stations: 17th of December 1988 to 23rd of December 1989. The harmonic analysis separated the astronomic tide from the residual tide, and only the first one is studied in this subsection. The amplitude and phase of the harmonic constituents – diurnal Q_1, O_1, P_1, K_1; semidiurnal: N_2, M_2, S_2, K_2; higher harmonic: M_4 – are presented in Figures 36-37 (right and left top). MSYM model was run for the four levels of grid nesting (L1-L4). GLOSS (blue bars – observations) values were compared with values for L1 (cyan bars - model) and with the smaller level that each station can include (red bars – model). To evaluate the results, the Mean Complex Amplitude Error (*HC*) (values text on bottom of Figures 36-37) was calculated as well as the Relative Mean Complex Amplitude Error (*Relative HC*) (graphic on the bottom of Figure 36-37). The *HC* and *Relative HC* comparing observations with L1 predicted data is displayed in cyan; the *HC* and *Relative HC* comparing observations with the smaller level, L2 or L3, is shown in red. The horizontal resolution of each level has a high impact on the M_4, as the bottom topography for the levels is different (Figure 1).

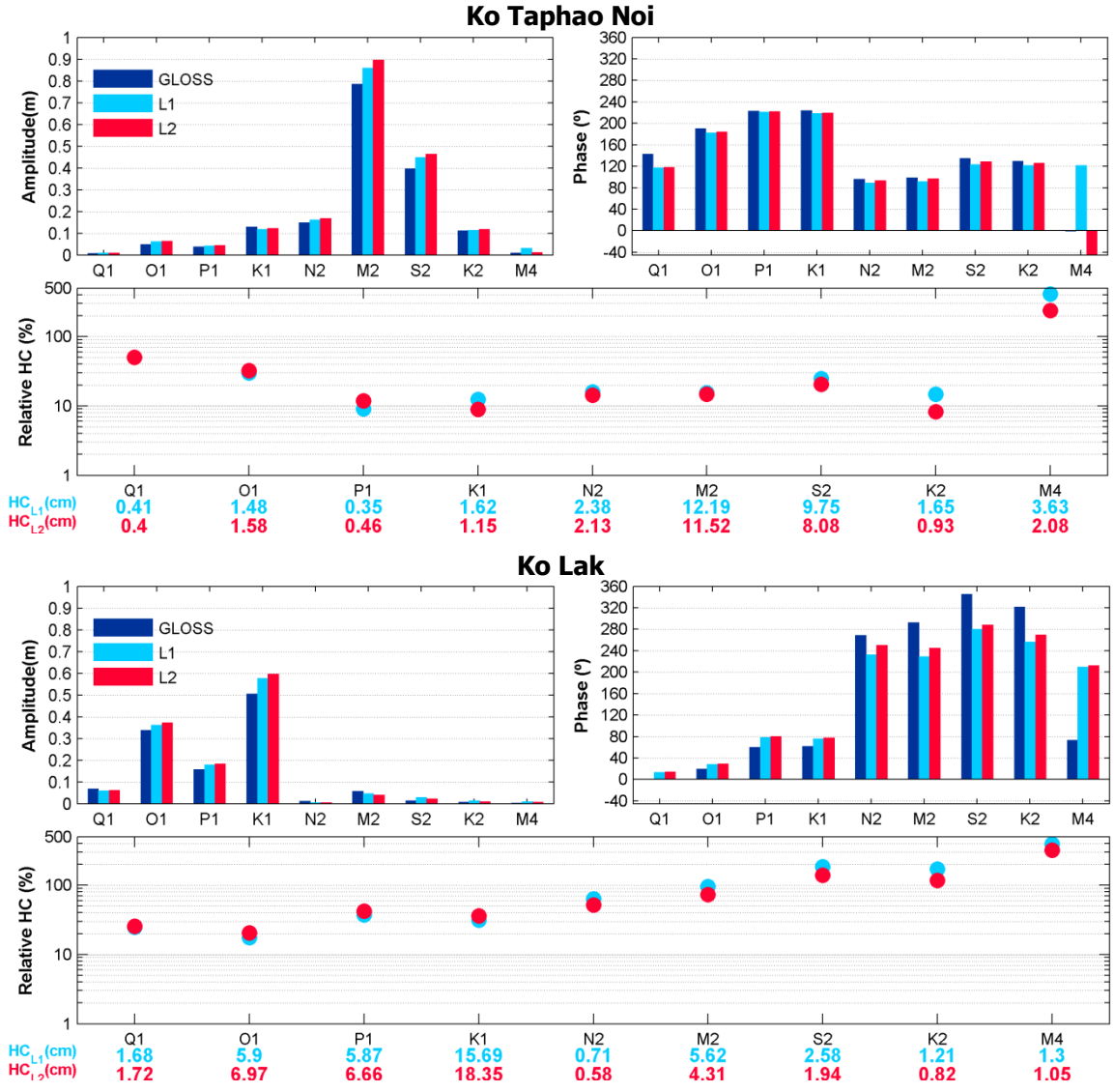

Figure 36 – Amplitude in meters (top left) , phase in degrees (top right) , *Relative HC* in percentage (graph on bottom) and *HC* (text) for the harmonic constituents - Q_1, O_1, P_1, K_1, N_2, M_2, S_2, K_2, M_4 - for Ko Taphao Noi and Ko Lak.

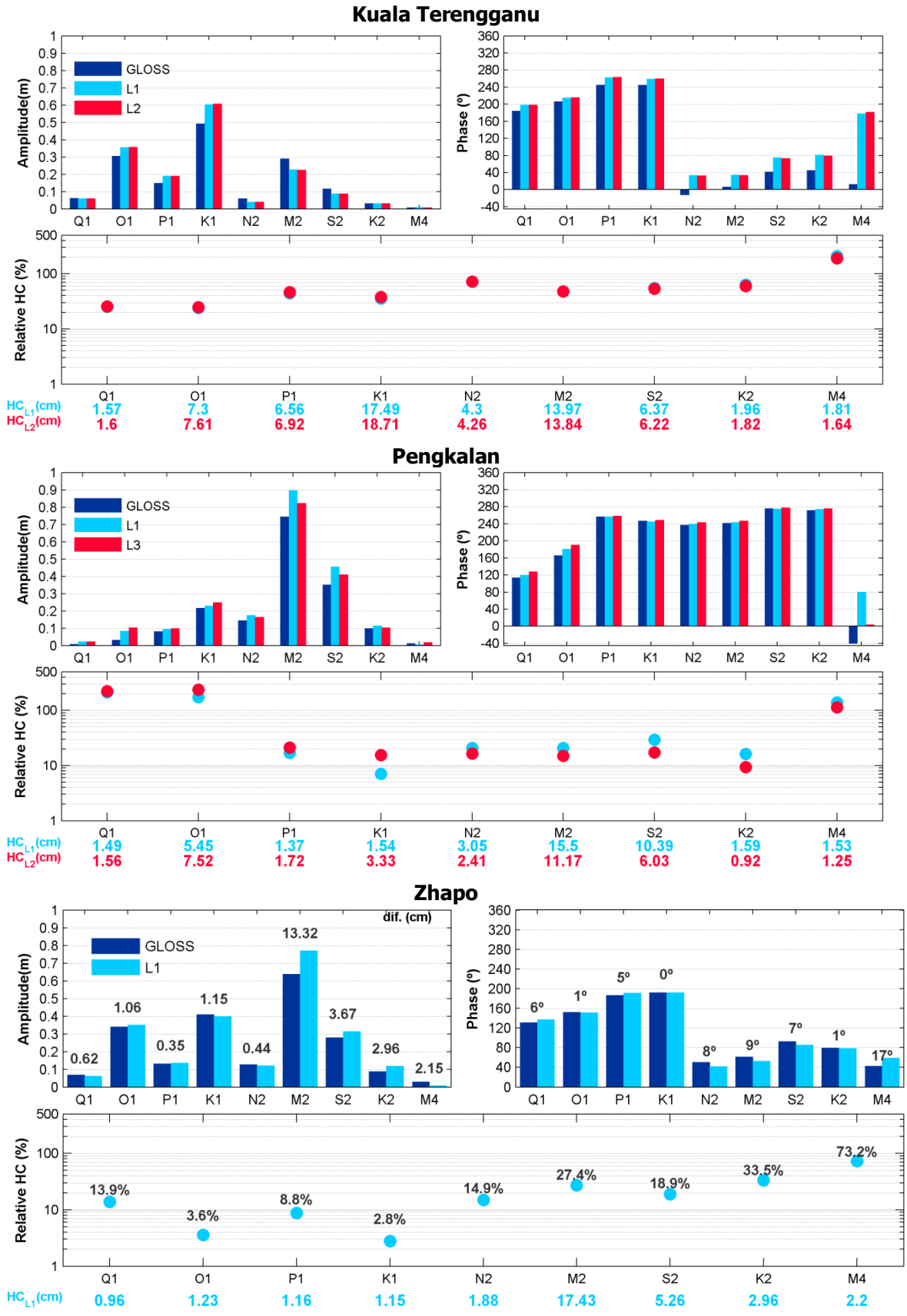

Figure 37 – Amplitude in meters (top left) , phase in degrees (top right) , *Relative HC* in percentage (graph on bottom) and *HC* (text) for the harmonic constituents - Q_1, O_1, P_1, K_1, N_2, M_2, S_2, K_2, M_4 - for Kuala Terengganu, Pengkalan and Zhapo. Zhapo only in level L1.

The horizontal resolution of each level has a significant impact on the M_4 (physical space). For a horizontal resolution of 5 km (L2) or 1 km (L3) the value of *HC* and *Relative HC* of M_4 is smaller in comparison with L1. Moreover, the *HC* and *Relative HC* of the semidiurnal harmonics decrease whereas the diurnal harmonics increase for L2 or L3 compared with the L1. The Singapore station, which is in the Johor Strait, as shown in Figure 39, isn't included in the model domain.

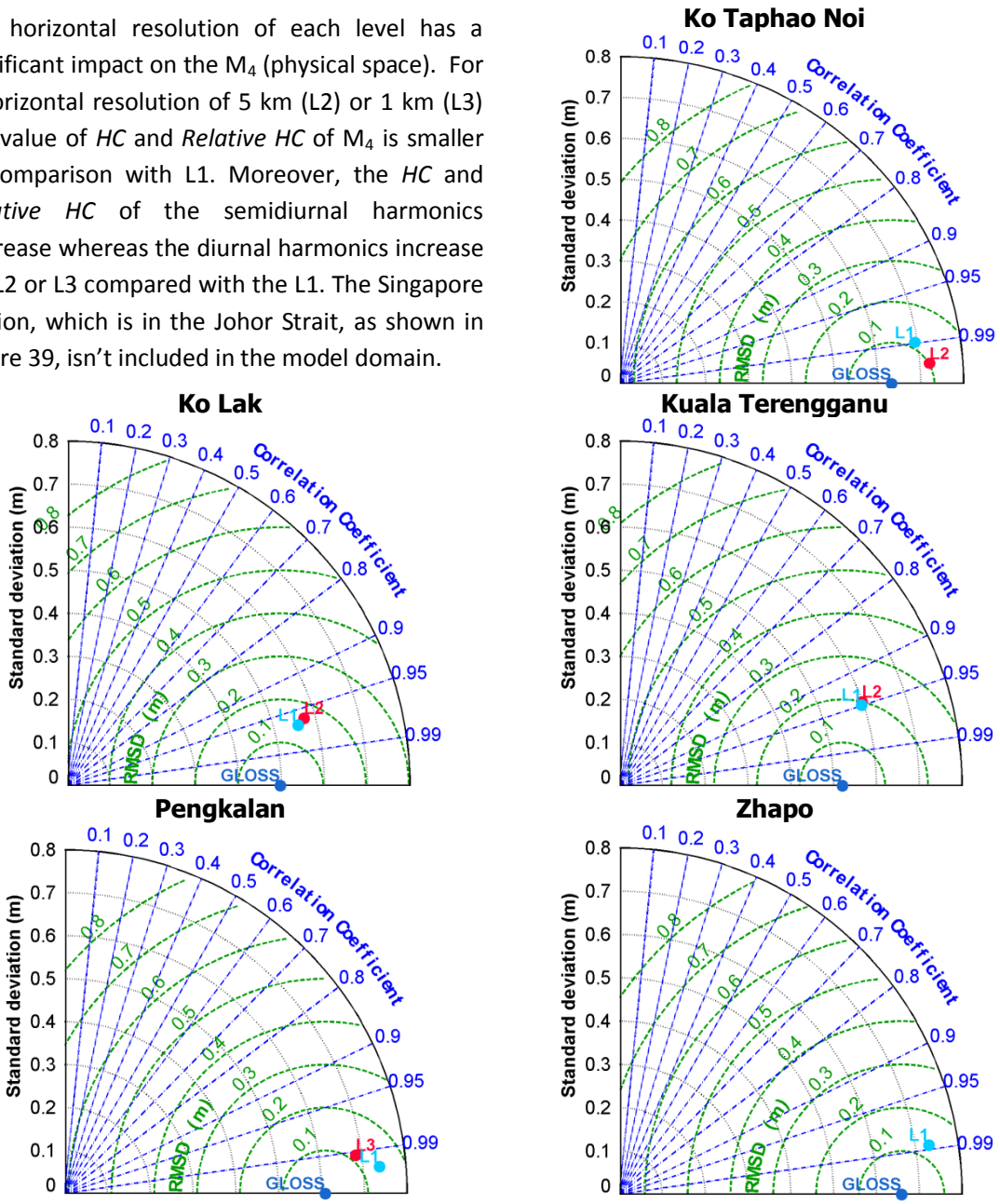

Figure 38 - Taylor diagram for astronomic tide (reconstructed with the 9 harmonic constituents) for GLOSS and MSYM (L1, L2, L3) between 17/12/1988 and 23/12/1989 for Ko Taphao Noi, Ko Lak, Kua Terengganu, Pengkalan and Zhapo. In the Taylor diagram the STD, Correlation Coefficient and *RMSE* of each series analysis are included.

Analysing Figure 38, it is evident that, in general, a smaller level (with higher resolution) reduces the errors measured differently, according to the station. The comparison in the Taylor Diagram of SL was done for the astronomical tide (reconstructed with the selected 9 harmonics) for both observations (GLOSS tide-gauges) and predictions (MSYM) data. When compared with L1, the correlation coefficient for the astronomic tide at Ko Taphao Noi presents better results for L2; at Pengkalan it is worse for L3; at Ko Lak and Kuala Terengganu the results for the two domains levels are similar. For Zhapo the results are close to 0.99, however, there are no other domain levels where this station is included. The domain level with higher resolution has a lower *RMSE* for Ko Taphao Noi and PengkalaN and a higher *RMSE* for Ko Lak and Kuala Terengganu. Moreover, the GLOSS STD of Ko Taphao Noi and Pengkalan is about 0.6 m, whereas for Ko Lak and Kuala Terengganu the STD is near 0.5 m and Zhapo shows the highest STD, of about 0.65 m.

4.2.1 Astronomic and residual observed tides

Figure 39 displays the observed SL (blue), the astronomic tide reconstructed with the nine analysed constituents (black) and the residual tide (red) for the six GLOSS tide-gauges. The high amplitude of the residual tide is clear (in order of 0.4 m), and its seasonal trend is similar to the monthly mean SLAs (in section 4.1), for each station, respectively. The variations are different according to the station. Ko Taphao Noi and Pengkalan (not shown), which presents identical characteristics, due to the location, have similar oscillations in time and amplitude, as happen for Kuala Terengganu (not shown) and Ko Lak (but Ko Lak presents more oscillations, in a short time). The residual tide in Singapore is more constant, because of its location (in a channel). On the other hand, Zhapo has a maximum residual tide of 1.2 m, on the 16th of July of 1989, and the residual has higher amplitude.

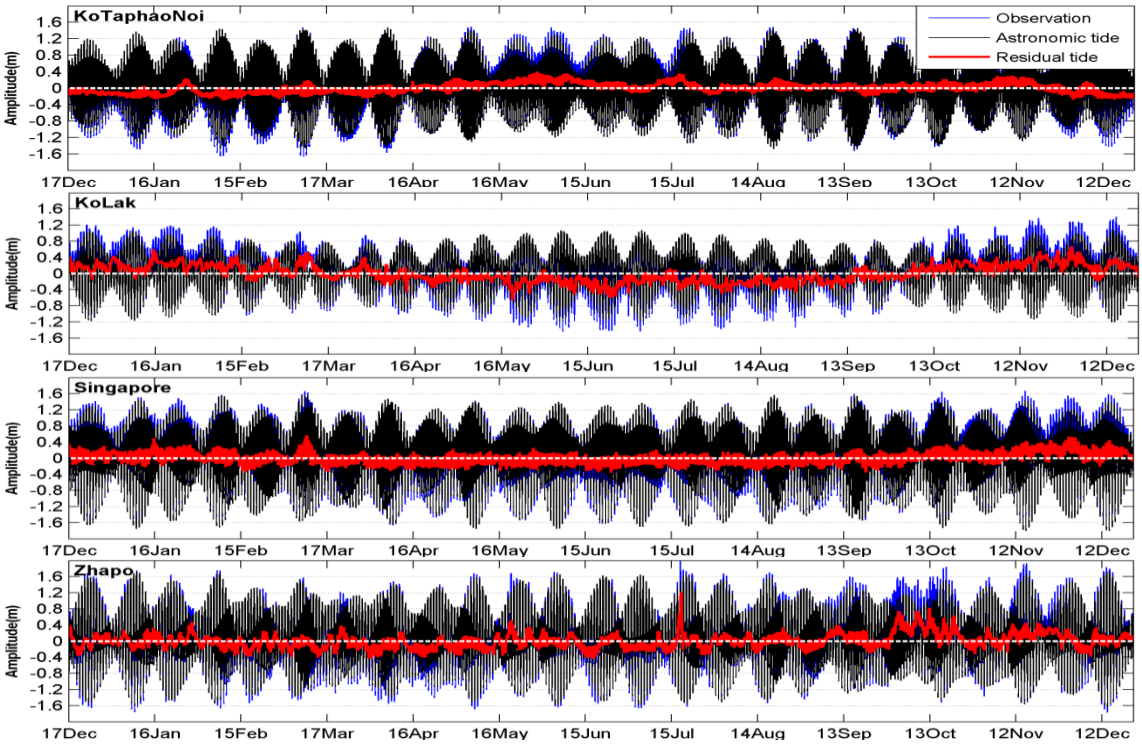

Figure 39 - Observed SL (blue line), astronomic tide reconstructed with the nine harmonic constituents (black line) and residual tide (included other oceanographic constituents, with small amplitude and the meteorological tide). Results for Ko Lak, Pengkalan, Singapore and Zhapo.

4.2.2 Concluding remarks

Analysing the Taylor diagram, which compares observed data with predictions (for both domains), it was concluded that the astronomical tide is better reproduced for the tide-gauges in the Malacca Strait, when compared with the tide-gauges in the east coast of Peninsular Malaysia. Even though the Correlation Coefficient is close to 1 (equal to and above 0.95, when considering all tide-gauges), indicating a good correlation between the data, it is important to take the *RMSE'* into account. While the *RMSE'* for the stations in Ko Taphao Noi, Pengkalan and Zhapo is between 10 and 15 cm (and even smaller for predictions using a higher horizontal resolution), for Ko Lak and Kuala Terengganu, the *RMSE'* has values between 15 and 20 cm (and higher for higher horizontal resolutions).

In further detail, Table 17 shows the *Relative HC* for each of the analyzed domains for the main constituents, including M_4. It also shows the tide classification for each station (through the analysis performed in section 4.1), the *RMSE'* and the *Relative Error*. The *Relative HC* decreases as the model

resolution increases, with the exception of O_1, in Ko Taphao Noi and of the diurnal constituents in Ko Lak, Kuala Terengganu and Pengkalan. However, an improvement is observed for all tide-gauges, for M_4 as the resolution increases, as expected, since M_4 is linked with the bathymetry. For each station in particular, a few key aspects should be noted: in Ko Taphao Noi (in a coastal system), the amplitude of O_1, N_2, M_2 and S_2 are overestimated in the model predictions, especially for L2 and the main differences in phase are essentially in the semidiurnal constituents and in M_4, as expected; in Ko Lak (a two bays system) the differences in amplitude are higher for the higher amplitude constituents and the phase lag is largest for the semidiurnal constituents, but the results improve for L2; in Kuala Terengganu (in a coastal system) the amplitude of the diurnal constituents are over estimated in opposite to the semidiurnal, and, again the differences are higher in the higher constituents and the higher difference in phase is for M_4; in Pengkalan (in an estuarine system on the same coast as Ko Taphao Noi) the M_2 and S_2 continue to be the constituents where the difference between amplitude predictions and observations is higher, and the phase of predictions are much closer to the phase of the observed results, except for Q_1, O_1 and M_4; in Zhapo the main difference in the amplitude occurred for M_2 and S_2 semidiurnal constituents, and in the phase M_4 presents the highest lag.

Table 17 – Classification of the tide, the *Relative HC* for each constituent, *RMSE*' and *Relative Error* for each tide-gauge and domain.

Tide-gauges	***Domain level***	***Classification of the tide***	***Relative HC(%)***					***RMSE'(cm)***	***Relative Error(%)***
			M_2	**S_2**	**K_1**	**O_1**	**M_4**		
Ko Taphao Noi	L1	Semidiurnal	15.5	24.6	12.5	30.1	412.9	11.44	4.1
	L2		14.7	20.4	8.9	32.2	236.0	10.10	3.5
Ko Lak	L1	Diurnal	96.0	184.0	31.1	17.5	394.0	14.57	6.5
	L2		73.6	138.5	36.4	20.6	319.0	16.52	7.2
Kuala Terengganu	L1	Mixed (Diurnal)	48.1	54.9	35.6	23.9	210.1	19.22	8.1
	L2		47.6	53.5	38.1	25.0	191.0	19.96	8.3
Pengkalan	L1	Semidiurnal	20.8	29.6	7.1	173.1	138.8	14.11	4.8
	L3		15.0	17.2	15.4	238.6	113.4	11.41	4.2
Zhapo	L1	Mixed (Semidiurnal)	27.4	18.9	2.8	3.6	73.2	13.07	4.5

The analysis for the Singapore tide-gauge wasn't done. This tide-gauge is located in the Johor Strait (blue marker in Figure 40, right) and this channel isn't included in the model, MSYM. The Level 4 includes only the Singapore Strait and therefore, a SL time-series was extracted, indicated with the red marker (Figure 40). The higher difference between the constituents of the predictions and observations (in Figure 40, the constituents' amplitude are on the left, and constituents' phase are in the centre) was expected, due to, the different location. Therefore, the observations for Singapore (GLOSS station) can't be compared with the model results.

The tide's amplitude for each tide-gauge should be taken into account when the *RMSE* is evaluated (Figure 39). The amplitude both in neap and spring tides is lower for Ko Lak (*RMSE* of 14-16 cm for a spring tide lower than 2.5 m) and is higher for Zhapo (*RMSE* of 13 cm for a spring tide higher than 3 m). These results suggest a good reproduction of the astronomical tide, with an error of about 5%.

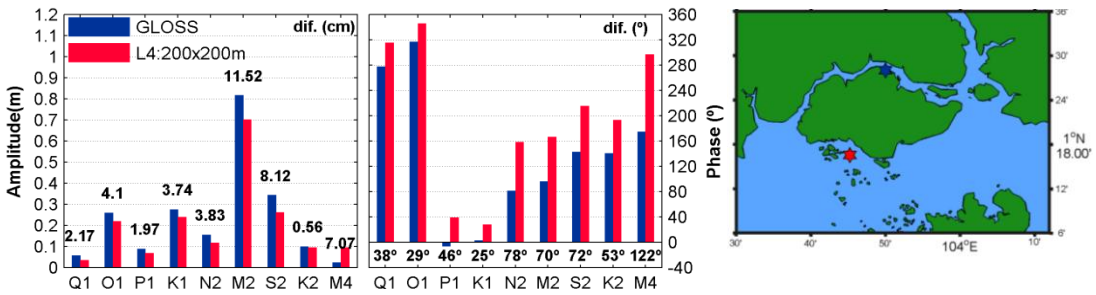

Figure 40 – Amplitude (left) and phase (right) of the harmonic constituents for prediction (red) and observations (blue). Location of the model results for Singapore (red marker) and GLOSS Singapore Station (blue).

4.3 Malacca and Singapore Straits sea level validation

Even though the astronomical tide has a larger amplitude, the effect of the residual tide on the SL can't be neglected, as revealed in the last section. With this in mind, this section is centered around not only the astronomical tide, but also on the residual tide for Tanjong Pagar (one tide-gauge) and Pangkor (two tide-gauges).

4.3.1 Tanjong Pagar analysis

In order to understand the effect of the wind (speed and direction) on the tide observed in the region at study, sea level and wind data were compared. The observed SL data sets are extracted from the Tanjong Pagar tide-gauge (Figure 41) and the predicted MSYM data sets are computed for the same coordinates as the tide-gauge, using tidal and wind forcing. The wind data was provided by GFS-NOAA with a grid of 50 by 50 km.

The Tanjong Pagar tide-gauge is located on the Singapore Strait, near the equator and is included in the L4 domain of the MSYM model. Since the implementation of the MSYM model for this station (on the 21st of November 2012), differences have been identified between observations and predicted data (which have been, in general, associated with neap tide). As such, the validation in this work was performed for the period between the 24th of November 2012 and the 6th of April 2013, with a 30-minute time-step.

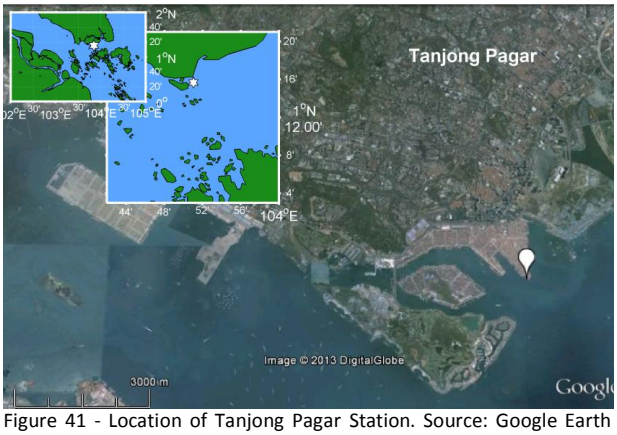

Figure 41 - Location of Tanjong Pagar Station. Source: Google Earth (background); Matlab with data of CISL Data Archive (m_map).

For the selected period, the mean sea level is 1.85 m, revealing an increase in monthly mean SL for December and January, as seen in Table 18. Apart from the monthly mean sea level, Table 18 also shows the *RMSE'* (centered *RMSE*, as the mean sea level has been removed from each data series) in meters, the Correlation Coefficient (*R*, adimensional) and the *Relative Error*, in percentage. November and April days show the lowest values for *RMSE'* (11.8 and 9.73 cm respectively), while the highest *RMSE'* values are seen for January (12.2 cm). Thus, for an amplitude in spring tide around 3 m, an *RMSE'* between 9.7 and 12.2 cm indicate an error of 4%. Looking at the correlation coefficient, the values are in the order of 0.98 for every month, revealing a good correlation, and the *Relative Error* is lower than 5%, which shows that the tide is well reproduced by the MSYM.

Table 18 – Monthly mean SL and *RMSE'* in meters, *R* and *Relative Error* (in percentage) for the available data observations/model.

	Monthly mean SL (m)	***RMSE'* (cm)**	***R***	***Relative Error* (%)**
November	Not complete	11.79	0.984	4.41
December	1.91	12.03	0.984	4.34
January	1.91	12.21	0.985	4.43
February	1.87	12.02	0.987	4.46
March	1.75	11.56	0.986	4.20
April	Not complete	9.73	0.989	3.65

Figure 42 displays the SL with the reference in zero, for each month (monthly mean SL computed for the observed and model data available was removed). Looking at the entire time series, the November and April days are not in neap tide (and the fit presents the fewer differences between predictions and observations). Thus, the daily *RMSE*' shown in the Figure 43, only includes the complete months.

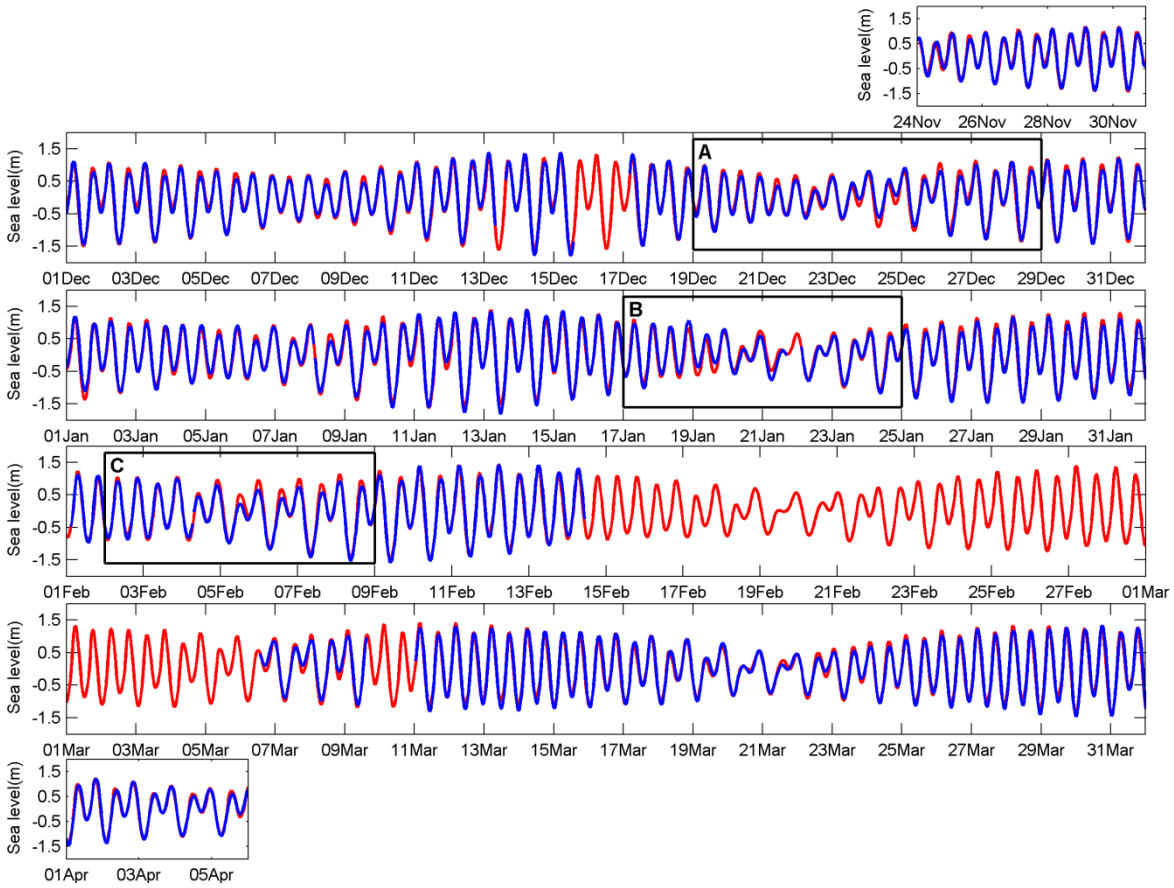

Figure 42 – Sea level observation from Tanjong Pagar tide-gauge (blue line) and prediction MSYM sea level (red line), in meters, for the period between the 24th of November 2012 to 6th of April 2013.

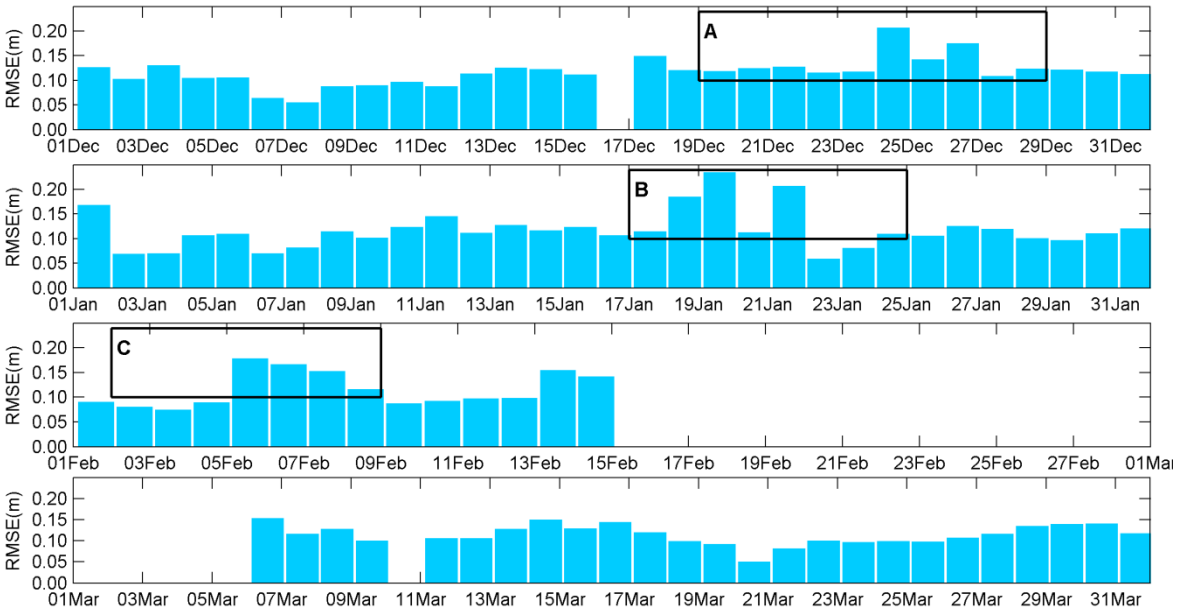

Figure 43 – *RMSE* (in meters) for each day of the months of December, January, February and March.

The daily *RMSE* shown in Figure 43 allows the evaluation of the fit between the observed and predicted sea level for comparable days. The daily *RMSE* varies between 5 and 23 cm: the lowest values were mainly found in March and the highest in December and January. The highlighted areas of the plots evidence the set of days where the error is higher, which generally corresponded to the neap tide of December and January (considering the analysis values).

The wind exerts a particularly important force on the sea surface, in this region: NE and SW monsoons are responsible for variations on the SL while the Sunda Shelf at the southern part of South China Sea tends to amplify SLAs. These can result from changes in wind direction and/or speed. Predicted SL was forced using the wind from GFS-NOAA of Tanjong Pagar, (as shown ahead, in page 40, in Figure 46). In order to test the contribution of the wind on the SL, two scenarios were created – one using a constant wind speed of 18 ms^{-1} with NE direction (the predominant direction in this region for the selected time period) and the other using a constant wind speed of 5 ms^{-1} with SW direction – shown in Figure 44. These scenarios are only presented for the highlighted areas, where the *RMSE* is higher (A, B and C of Figures 42-43) and, as expected, the different effects on the SL according to the characteristics of the wind are clear. The predictions using tidal and NE wind forcing caused a decrease in the amplitude during the low and high tide. On the 24th and 25th of December and 19th of January, the difference between observations and SL predictions (using the real wind) has a better fit during the low tide when compared with the predictions using the predictions using the NE wind forcing.

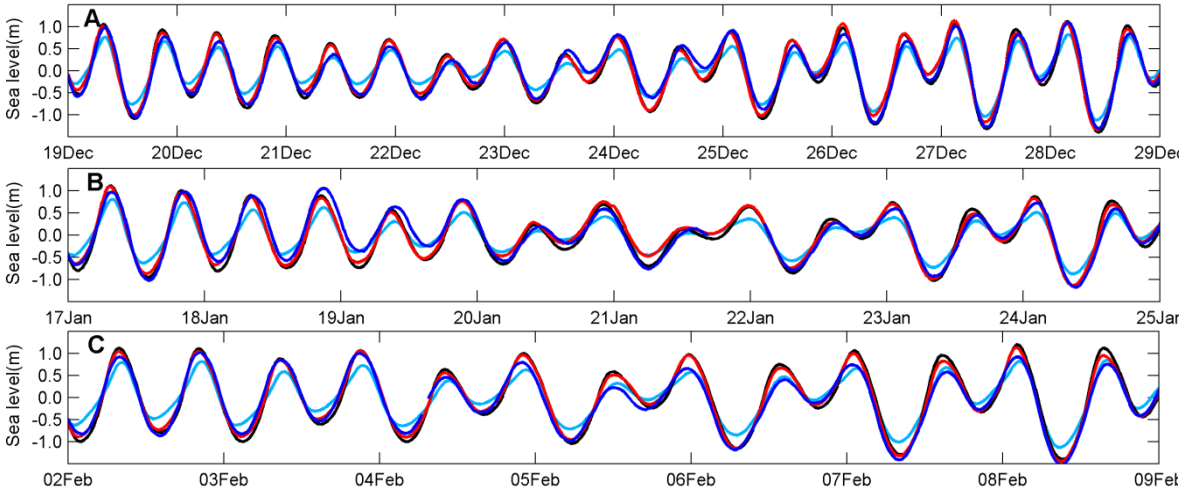

Figure 44 – Zoom of A (top), B (centre) and C (bottom) SL time series illustrated in Figure 43 using the 3 scenarios: constant wind speed of 18 ms^{-1} with a NE direction (cyan line); constant wind speed of 5 ms^{-1} with a SW direction (black line) and using the real wind (GFS-NOAA at red line) and observations from the tide-gauge (blue line).

In the highlighted area C, the fit with the predictions using the tidal and NE wind forcing improves during the high tide between the 5th and 9th of February. The data processing for these scenarios was the same as that applied to the data observations and predictions (there are compared with the same interval sample and the mean SL was removed). Regarding the SW scenario, the values are similar to the predictions using the real wind forcing. A higher wind speed at some specific times can reduce the difference between the amplitude of observed and predicted SL. However, the error between the observations and predictions can result from the astronomical or residual tides. To retrieve the non-tidal signal causing the SLAs for the period between the 24th of November 2012 and 6th of April 2013, the Tanjong Pagar tide-gauge data with a 30-minute sample interval, was underwent a harmonic analysis and every harmonic constituent separated with the t_tide function (Pawlowicz *et al.*, 2002) was obtained (Figure 45). The astronomic principal and major tidal harmonics in the observations data reveal amplitudes of: about 77.24 cm for M_2; about 33.83 cm for K_1; about 32.37 cm for S_2; about 30.71 cm for O_1; about 14.93 cm for N_2; about 5.32 cm for Q_1 and about 2.18 cm M_4. For the predictions, the amplitudes for the same constituents are: about 77.80 cm for M_2; about 31.88 cm for K_1; about 31.78 cm for S_2; about 30.18 cm for O_1; and about 13.20 cm for N_2; about 4.89 cm for Q_1 and about 5.03 cm for M_4. Comparing the results with those of Tkalich *et al.* (2013), the main difference to these harmonics occur for M_2 and K_1 (Table 3).

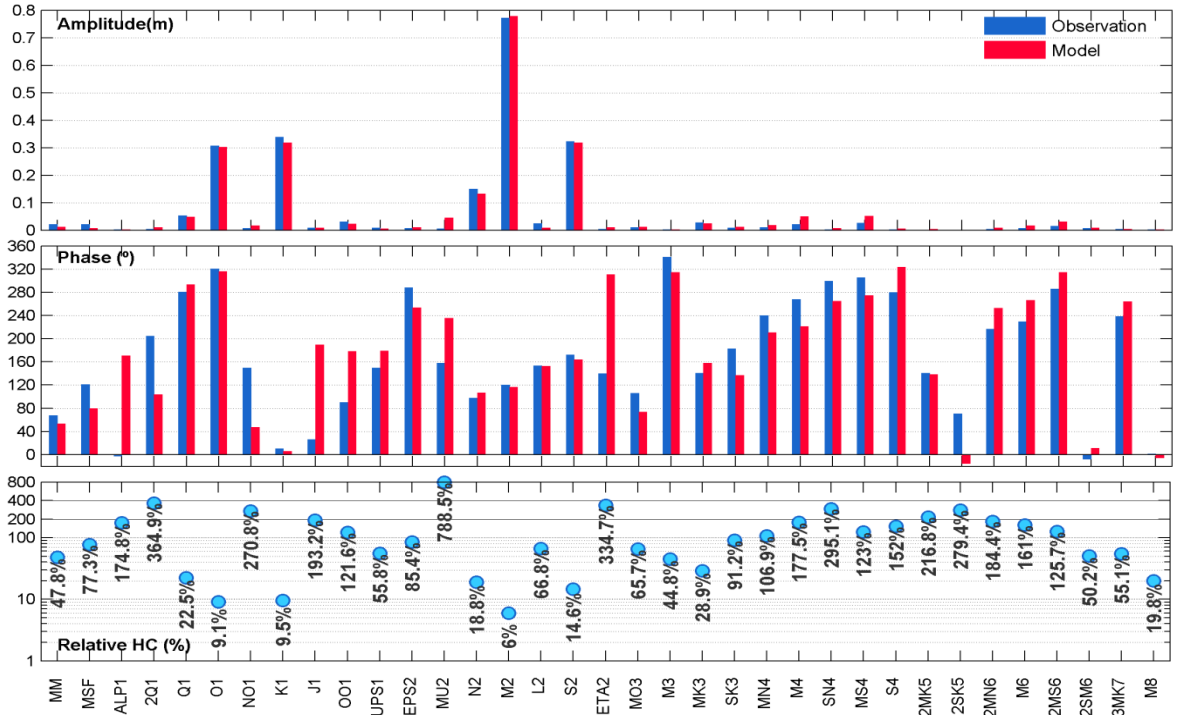

Figure 45 – Harmonic analysis for the Tanjong Pagar, amplitude (top), phase (centre) and *Relative HC* (bottom) for the 35 harmonic constituents separated with the t_tide function (Pawlowicz *et al*., 2002) for 133.02 days.

Looking at the bottom of Figure 45, the *Relative HCs* are smaller for the four main harmonics, less than 14.6% (for S_2). In general, for the constituents with higher amplitude, the differences in amplitude and phase between observations and predictions are lower. For the main constituents, the highest amplitude differences between predictions and observations were found for K_1. Moreover, differences in phase are observed for the shallow water constituents, but due their low amplitude, there aren't marked effects on the SL. Using the exact amplitude of the main harmonics (M_2, S_2, K_1, O_1), the value of the form factor is 0.5888 for the observations, and 0.5663 for the predictions (an error of 3.81%). On the left side of Tanjong Pagar, semidiurnal tides are predominant, while on the right side the tides are mixed or diurnal. These results show that the type of tide is mixed mainly semidiurnal in the Tanjong Pagar tide-gauge.

Next, the SLAs of the predictions (red line) and observations (blue line) are plotted in Figure 46 (after removing the astronomic tide which was reconstructed with the constituents separated by the t_tide function. The wind speed and direction in Tanjong Pagar is also shown on the same figure (as green dashed lines and vectors, respectively). Regarding the analysed time period, there are some important features, namely: the observed SLAs and the wind time series have a phase difference of approximately 1 day; the difference between observed and predicted SLAs is higher when the wind speeds increase, e.g., on the 23rd through 26th of December, on the 8th through 13th of January and 17th through 22nd of January. In March, November and April, the differences between the SLAs are smaller.

As previously described this is a very dynamic region, with consequences in the sea level patterns in the tide-gauge of Tanjong Pagar. Furthermore, the South China Sea is affected by NE and SW monsoons which dominate the larger-scale sea level dynamic of the South China Sea. The monsoons typical of the analysed period are NE monsoons, which occur from November to March. The spectral analysis of the observed and predicted SLAs data can be useful to identify the frequencies with higher amplitude (fsa), as well as the associated vertical motions of the ocean surface, as (as seen in Figure 3). These frequencies correspond to storms (10^{-5} to 10^{-4} Hz, i.e., from 3 hours to near 1 day), (Figure 47).

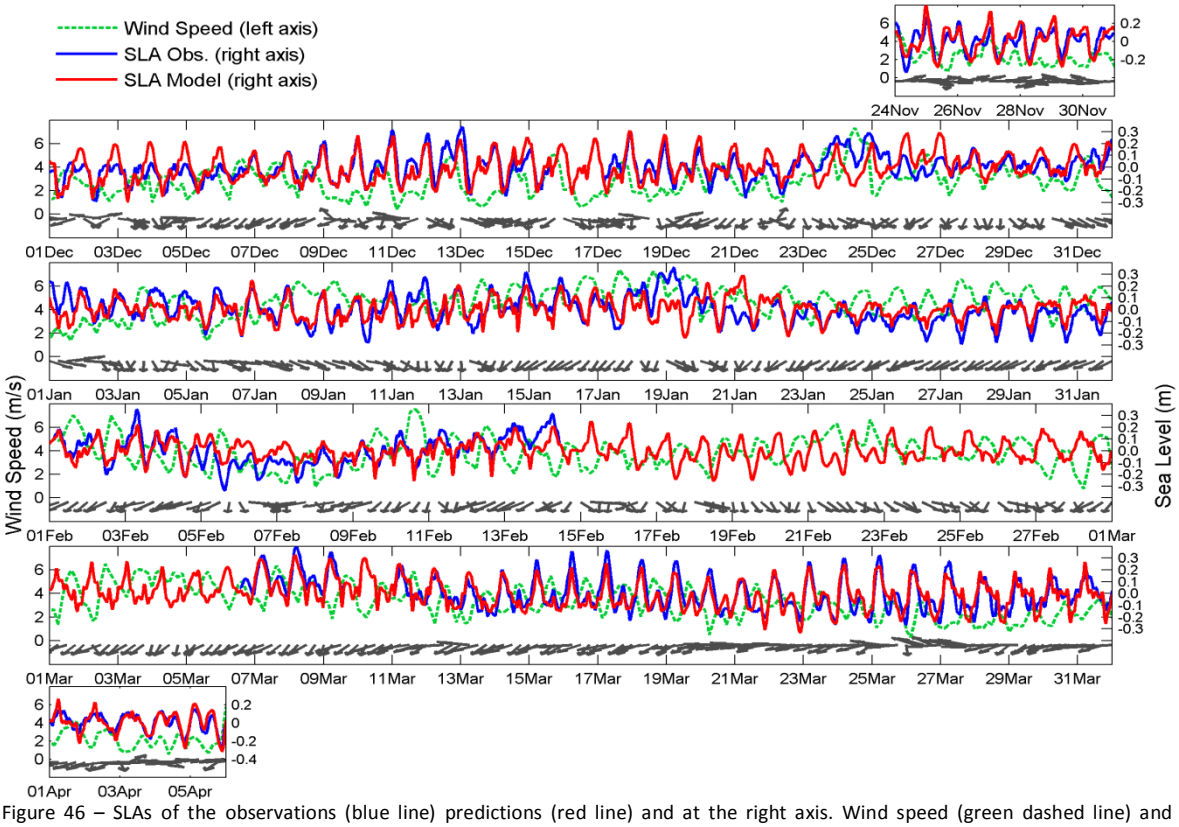

Figure 46 – SLAs of the observations (blue line) predictions (red line) and at the right axis. Wind speed (green dashed line) and direction (black vectors) in Tanjong Pagar for the period under analysis (GFS for 10 meters).

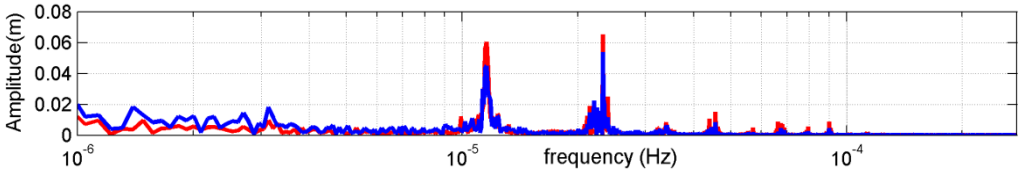

Figure 47 – Frequencies of the vertical SLA observations (blue line) and predictions (red line), in Hz (log-scale) and amplitude in meters.

Using the three-hourly wind fields (*u* and *v* components and wind speed, from GFS, at 10 m), the daily climatology was computed. Using the daily climatology, the monthly climatology was calculated and plotted in Figure 48 for: December (top left), January (top centre), February (bottom left) and March (bottom centre). The monthly climatology has shown a predominance of the highest wind speeds along the axis Taiwan-Singapore, in agreement with previous studies (Choon *et al.,* 2006; Tkalich *et al.*, 2012a; Chen *et al.*, 2010b). The January climatology presents the highest wind speed mean (near to 14 ms^{-1}, offshore of Vietnam). According to Tkalich *et al.* (2012a), the NE (SW) monsoon climatology and extreme wind, when aligned along the longest Taiwan–Singapore axis, produces the strongest positive (negative) SLA in Singapore Strait. In order to analyse the time series of the wind along this axis (so as to identify higher wind speeds), eight points are selected: the red points shown in the Figure 48, numbered from SW (Singapore) to NE (Taiwan): P1, P2, P3, P4, P5, P6, P7 and P8. On the right hand side of Figure 48, the wind rose for P2, P4 and P7 was plotted, revealing a similar wind direction. Even though the wind rose for P7 presents higher wind speed (yellow bar), the extreme wind speed occurs in P4 (maximum of 24 ms^{-1}). The wind rose for P2 shows a low wind speed (with maximums of 7-8 ms^{-1}) and the direction has a predominant easterly component, when compared with P7 and P4. The SLA in Tanjong Pagar was compared with these eight points (not shown). However, and with the goal of evaluating all wind grid data (50 by 50 km from GFS), the correlation coefficient (*R*) was computed, comparing every wind time series with the SLA in Tanjong Pagar.

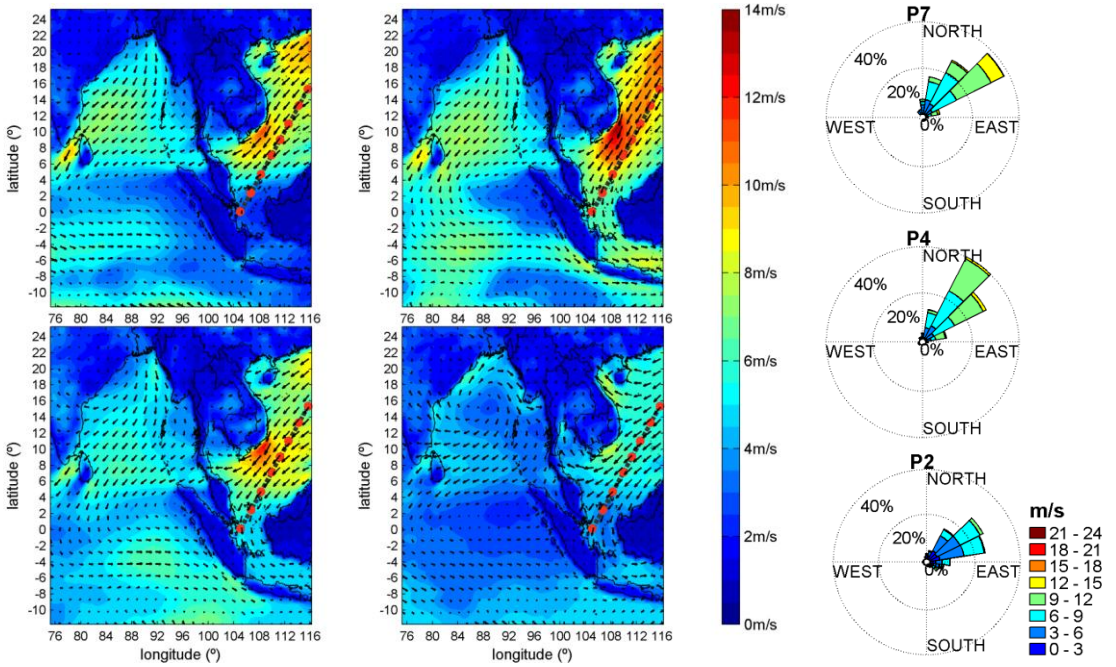

Figure 48 – Wind monthly climatologies at 10 m, for December (top left); January (top centre); February (bottom left); March (bottom centre). The red points are numbered from SW (Singapore) to NE (Taiwan): P1, P2, P3, P4, P5, P6, P7 and P8 and wind rose are represented for the P2 (top right), P4 (centre right) and P7 (bottom right).

In order to compare the SL with the wind, concurrent time series were selected and compared. Figure 49 presents the observed SLA with a sample time of 30 minutes (blue solid line), the three-hourly observed SLA (line solid black) and the daily observed SLA (smooth Matlab rotine of 24 hours at SLA – dashed red line). As seen in Figure 49, the major positive SLAs are developed between: 11th through 13th of December; 23rd through 26th of December; 11th through 19th of January; 3rd through 4th of February of 2012 and 13th through 17th of February. On other hand, the 5th of February presents the main negative SLAs, close to -35 cm. Looking at March, positive and negative SLAs are identified, but considering the daily mean SLAs, they present a straight line, close to zero. Moreover, the wind in March is less intense, according to Figure 48, and the SL is more stable (nodal point between Singapore-Taiwan is marked in NE and SW SLAs, Figure 7b). Next, the wind along the Singapore-Taiwan axis was correlated with the SLA in the Tanjong Pagar tide-gauge, in the entire MSYM (L1) domain level. Figure 50 plots the spatial distribution of *R*, with two higher correlations found for following coordinates: (108.25°E, 9.75°N); (108. 75°E, 10.25°N) with *R* values of 0.561 and 0.5426, respectively.

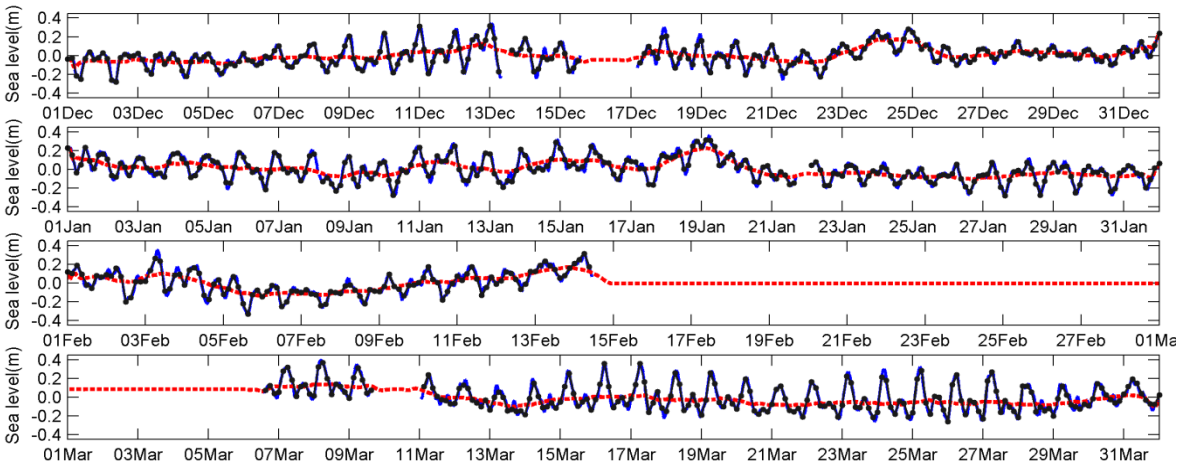

Figure 49 – Observed SLA in Tanjong Pagar: SLAs with 30-minutes sample time (blue solid line); Observed SLA filtered with a three-hourly (black solid line) and the daily observed mean SLA (dashed red line), between December and March.

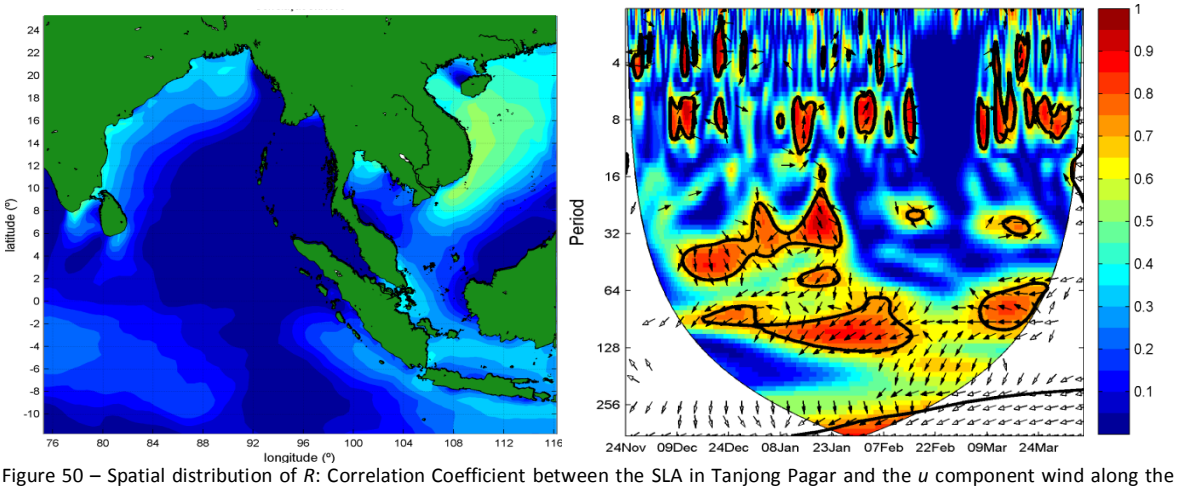

Figure 50 – Spatial distribution of *R*: Correlation Coefficient between the SLA in Tanjong Pagar and the *u* component wind along the Singapore-Taiwan axis (Figure 14), for the L1 domain (left). Wavelet Coherence, WTC (Grinsted *et al*., 2004) between the *u* component of the wind along the Singapore-Taiwan axis (U*) for the (9.75°N, 108.25°E) coordinates and the observed SLA in Tanjong Pagar (right). The vertical scale on the right side is respective both of the figures; they are plotted using the same Correlation Coefficient scale.

The best correlation between the SLA in Tanjong Pagar (3-hourly sample time, black solid line on Figure 49) and the *u* component wind along the Singapore-Taiwan axis (called by U*) is higher near area offshore of Vietnam and Hainam Island, as seen in Figure 50 (left). This area is located between the 108°-115°E and 8°-22°N coordinates. In Figure 50 (right), a wavelet coherence (WTC) was done between the SLA in Tanjong Pagar and the U* for the higher *R* coordinates (9.75°N, 108.25°E). The WTC, expands a time series into a time frequency space where oscillations can be seen visually with colour scale for *R* values and vector for the phase between series (right – in phase; left – anti-phase: noc.ac.uk/using-science/crosswavelet-wavelet-coherence). As the result has a 3-hourly sample time, the period on the *yy* axis of Figure 50 (right) present the period per 3 hours. Thus, coherence mainly in the daily and semidiurnal frequencies has been identified, i.e., the 4x3=12 h and 8x3=24 h, and the time series are in phase opposite (positive SLA generated by negative U*, i.e., from NE). From December to February, a frequency with 8 days (cyclone scale) was also identified. It was identifies a general connection between SL and wind speed. In order to evaluate the spatial distribution of the wind and identify where the wind changes its characteristics the distribution of the wind for each instant was plotted. The results are presented only for some of the cases that contributed to the positive/negative SLAs in Tanjong Pagar.

Significant events can be found over the time at study, namely: the development of a low pressure on the 7th of December (12°N and116°E) losing most of its energy on the 10th of December; a strong NE wind during 24th through 26th of December acting along the Taiwan-Singapore axis (maximum of over 20 ms^{-1} for the 25th of December); higher wind speeds on the 31st of December are identified near China's coast, moving southward, at near 20 ms^{-1}, decreasing on the 3rd of December; a low pressure system on the 6th of January, at 8°N and 116°E, moving westward until the 7th January (8°N and 110°E) completely dissipating its energy as it reaches the coast at 3°N and 111°E, on the 13rd of January; on the 18th of January near Vietnam a strong wind speed is found and is amplified in the following days, until the 21st of January; between the 5th February and the 9th of February lower wind speed covers the South China Sea (and for some places near Vietnam with SW direction); on the 10th of February, intense wind speeds are found in the domain at study, along the Singapore-Taiwan axis. Due to the data gap of the SLAs, between the 14th of February and the 7th of March 2013, the events occurring during this period weren't mentioned. Then, for March no significant changes in wind speed or direction were found; the mean wind speed is weak (below 6-7 ms^{-1}) and predominantly northeasterly for this month (in agreement with their climatology, Figure 48).

Two important wind events which generated SLAs in Tanjong Pagar are discussed below; one in December (positive SLAs) and another in February (negative SLAs). For December the analysis is focused on the positive SLAs on the 6th of December and on 28th of December. Figure 51 shows the SLAs in Tanjong Pagar (top right) and the U* component of the wind (bottom right). The wind that induces the positive SLA of 11th through 13th of December is lower than the wind speed that generated the SLA on the 24ththrough 25th of December (maximums near 20 ms^{-1}, as seen in Figure 51, left). However, both SLAs have similar values. This feature may be related when the NE monsoon coinciding with the spring or neap tide (strong SLAs during the NE monsoon, when coincident with spring tide can usually lead to coastal floods in the region of the Singapore Strait). Looking at Figure 42, the 11th through 13th are days associated with spring tide, while the 24th and 25th are days associated with neap tide (when the discrepancies between observed and predicted SL are higher). Conversely, in February, the wind acting over the South China Sea is weak (Figure 52, left), and for some places in the South of the Chinese coastal and East of Vietnam southwesterly winds were identified. According to Chen *et al.* (2010a) and Tkalich *et al.* (2012a), in the SW monsoon, the wind is blowing along the Singapore-Taiwan axis, resulting in SL elevation off Luzon and depression over the Sunda Shelf. Even though the analysis period doesn't typically encompass SW monsoons, in February the lower wind and the changes in direction caused a negative SLA in Tanjong Pagar of 35 cm for 5th of February (Figure 52).

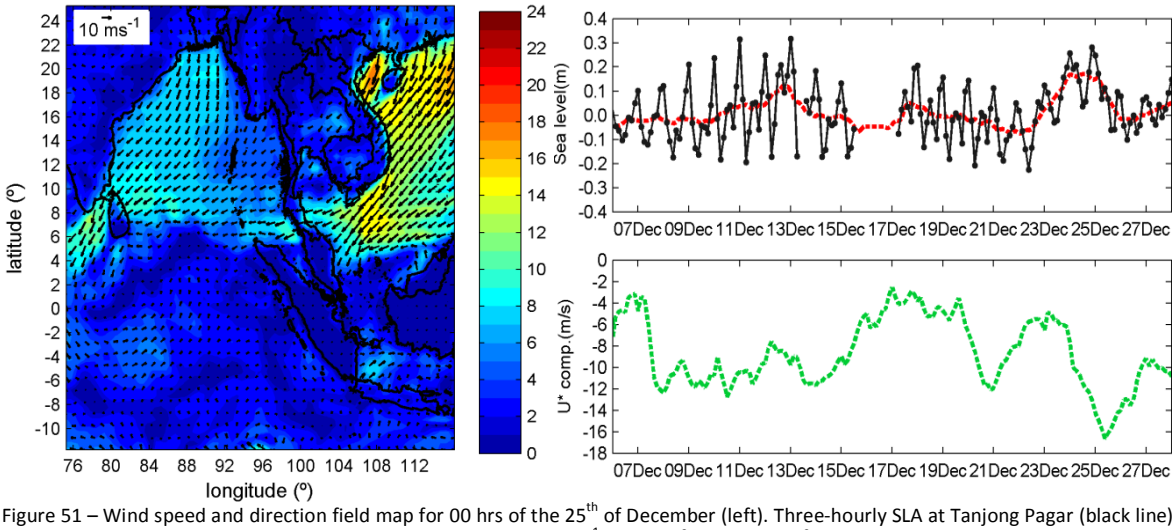

Figure 51 – Wind speed and direction field map for 00 hrs of the 25th of December (left). Three-hourly SLA at Tanjong Pagar (black line) and daily mean SLA (red line) (top right). Wind U*component, in ms^{-1}, at 16.25°N and 113.25°E (green line) (bottom right).

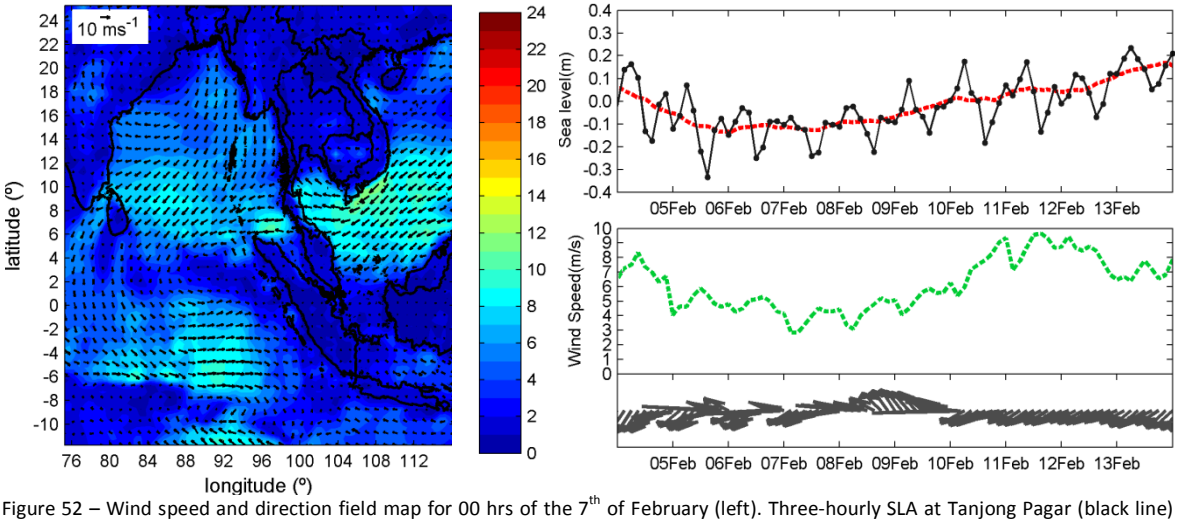

Figure 52 – Wind speed and direction field map for 00 hrs of the 7th of February (left). Three-hourly SLA at Tanjong Pagar (black line) and daily mean SLA (red line) (top right). Wind speed at 16.75°N and 109.75°E (green line) and direction (gray vectors) (bottom right).

4.3.2 Pangkor analysis

The last analysis done in this work used the sea level in Pangkor, using the data collected in two tide-gauges (designated by TG1 and TG2, Figure 53) to evaluated the astronomic and residual tides. Wind data set from GFS-NOAA were also used in the analysis, with a grid of 5 by 5 km.

Pangkor (time zone GMT + 8 h) is an island off the coast of Perak (longer than 9 km and with a width of over 3 km), in the north-west Peninsular Malaysia and in the Malacca Strait. Furthermore, this island is located near the mouth of the river of Manjung (Sungai Manjung), where there is a mixture of fresh water with ocean water, and it is also under the influence of the wind along the Malacca Strait. Figure 2 presents, the monthly precipitation for Penang and Kuala Lumpur, among others. As Pangkor is located between these two stations, the pattern of the monthly precipitation for Pangkor (between Penang and Kuala Lumpur) is expected to be similar.

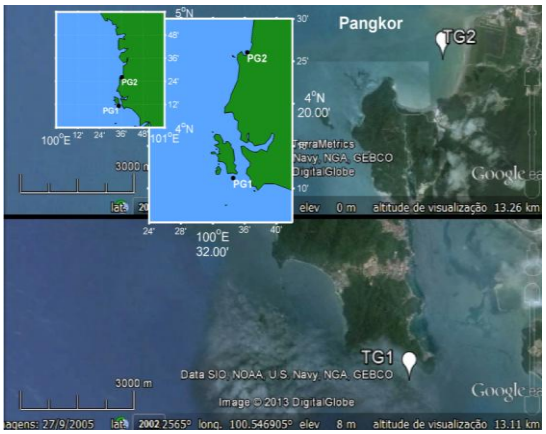

Figure 53 - Location of Pangkor area (m_map). The TG are situated with a white marker and labeled as TG1 and TG2.

In detail, PG1 is located on the south of the Pangkor Island while TG2 is located on a bay. At TG1, the tide was measured for the period between 12h30 of 5th and 16h00 of 9th of April 2010; while for TG2 was measured between 6h of 5th and 15h of 19th of April 2010. Both data sets have a sample interval of 10 minutes and are in GMT time. For the same time interval and at both sites, predicted SL was compared with the observed SL (blue line), for TG1 (top) and TG2 (bottom) (Figure 54). The predict SL resulted from simulations forced only with the tide (dashed black line) and the simulations forced with the tide and wind (red line). As seen in Figure 54, comparing the two predicted SL, the wind influence causes a reduction on the amplitude, especially in the neap tide. In further detail, for TG1, both predictions extrapolate the observed SL which has a better fitting only in the last 2 days, in opposite to TG2. Comparing the two solutions, the predicted SL with tide and wind has better results.

Then, the astronomic and residual tides were separated through harmonic analysis, applied to the observed and predicted SL, for TG1 and TG2. Figure 55 presents the amplitude and phase of the harmonics for the observed and predicted data, for TG1 (left) and TG2 (right). The results given identify some discrepancies in both amplitude and phase. These noteworthy discrepancies are more significant for the major harmonics. Looking at Figure 55 (bottom left), the *Relative HC*'s for TG1 are 19.5%, 81.4%, 28.3% and 46% for the main harmonics M_2, S_2, K_1, O_1, respectively. In Figure 55 (bottom right) is presented the *Relative HC* for TG2 are 13.2%, 51.9%, 44.5% and 218% for M_2, S_2, K_1, O_1.

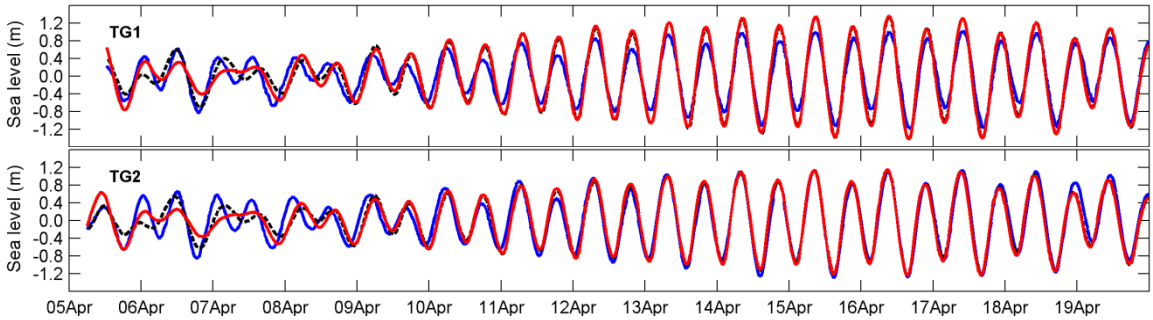

Figure 54 – Sea level (in meters) for TG1 (top) and TG2 (bottom) for the respective available time: blue line represents observations; dashed black line, the predictions with tide only; and red line represents the predictions with tide and wind.

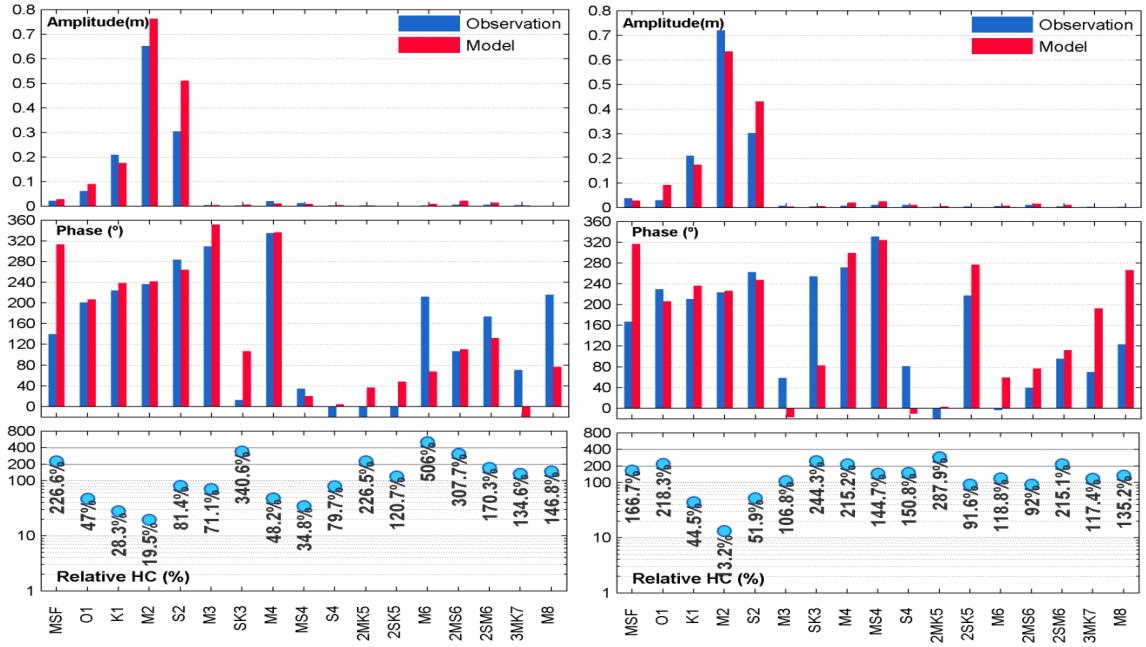

Figure 55 - Harmonic analysis for the Pangkor for TG1 (left) and TG2 (right). Amplitude (top), phase (centre) and *Relative HC* (bottom) for the 17 harmonic constituents separated with the t_tide function for analysis period (15 days).

The form factor was also calculated and the results were: 0.2822 (observations) and 0.2075 (predictions), for the TG1; 0.2355 (observations) and 0.2482 (predictions), for the TG2.Thus, relative errors in the form factor are 26.46% and 5.38%, for TG1 and TG2, respectively. Note that M_4 is higher in the TG2, which is on a bay. Moreover the harmonic analysis was applied to 15 days, and as seen on section 4.2, the amplitudes and phases for 15 days were not enough to give a good reconstruction of each harmonic. The highest errors should be observed for S_2, M_2 and K_1, when compared with the Pengkalan (GLOSS) results. Regarding to the SLA at Figure 56, the highest differences are in the neap tide, both in TG1 and in TG2, and the period between 5th and 8th of April is a clear example of that. Furthermore, the frequencies of the observations are similar for TG1 and TG2, which are not well reproduced by the model. The frequencies of the SLAs represented in Figure 57 can be related with frequencies of the astronomic tide that the harmonic analysis cannot separate due to the limited time interval. To identify these frequencies, a frequency spectrum was done. For the observed data of TG1 the highest two frequencies are: 0.0673 Hz (14.85 h) and 0.0054 Hz (185.67 h), both with an amplitude of 1.93 cm and frequency of 0.0592 Hz (16.88 h) with an amplitude of 1.83 cm. For TG2, the amplitudes are higher; the highest two are: 0.037 Hz (27.00 h) with an amplitude of 3.5 cm and 0.0053 Hz (189.00 h) with an amplitude of 3.11 cm. All these frequencies cannot be separated with a harmonic analysis of 15 days. Regarding the spectrum for the predictions, the frequency with higher amplitude is the same for both cases (12.80 h), with higher amplitude in TG1.

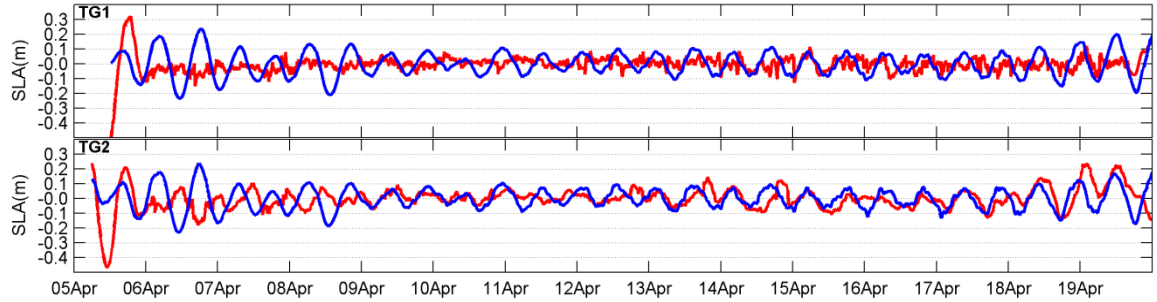

Figure 56 - SLA predictions (red line) and observations (blue line) for the TG1 (top) and for TG2 (bottom).

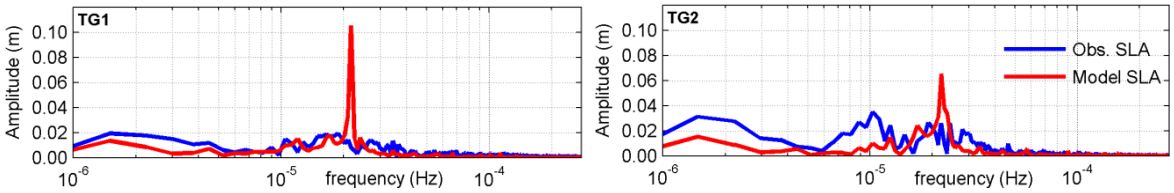

Figure 57 - Frequency spectrum, in log-scale, of the SLA observations (blue line) and predictions (red line), for TG1 (left) and TG2 (right).

Comparing the observed SL or SLA for TG1 and TG2, the time series are very similar, having a lag of around 20-40 minutes, depending if it is neap or spring tide. The main differences can be related with to the physical or meteorological factors for each place. The observed SLAs were also compared with the wind speed (in ms^{-1}) and wind direction (in vector) at each station, as seen in Figure 58 (right). During the analysed period, the maximum wind speeds are 5.5 ms^{-1} for 17th of April and around 4 ms^{-1} on the 9th, 13th and 14th of April. In general, no significant wind events happened during this time. Although the wind is weak in TG1 and TG2, it appears to change constantly, both in intensity and direction. These variations of the wind speeds don't appear to be a local event, but rather seem to occur for the entire surrounding region. In the days leading up the beginning of the analysis period, the wind was northeasterly. From day 7th of April onwards, the wind has a daily cycle (there exist a changes in the direction and wind speed along the day, e.g., at 9 h the wind field in Figure 58, left).
Furthermore, winds measured in TG1 have a special effect on the estuarine plume. The wind exerts a force on the ocean surface and according to its speed and direction; the SL near to TG1 can show different patterns: an eaterly/southeasterly wind facilitates the exit of water from the river, whereas a westerly/ southwesterly wind creates a pilling up of water at the Manjung river mouth.

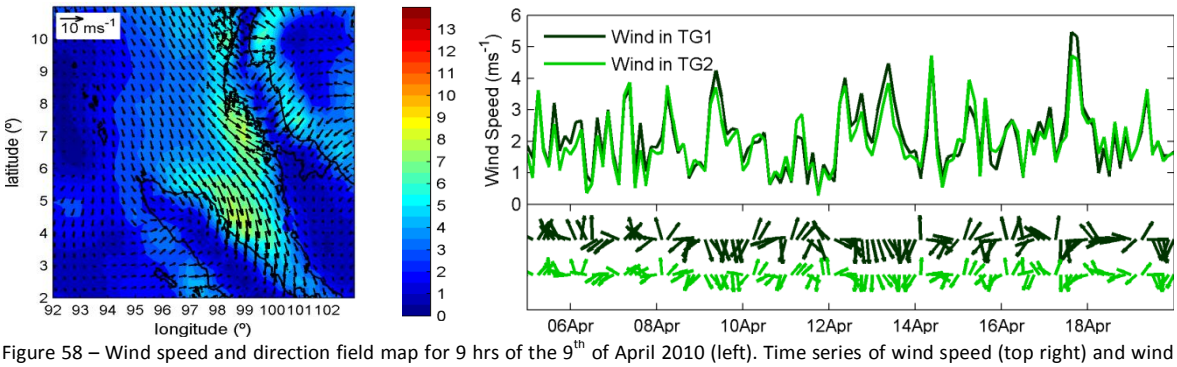

Figure 58 – Wind speed and direction field map for 9 hrs of the 9th of April 2010 (left). Time series of wind speed (top right) and wind direction (bottom right) for TG1 (dark green) and TG2 (light green).

4.3.3 Concluding remarks

In general and for the analysed period, during NE monsoons the wind changes direction or intensity causing mainly positive SLA in the Singapore Strait. A better agreement between the winds in the area offshore of Vietnam and Hainam Island and the SLA of Tanjong Pagar was shown. Figure 59 presents the storm surge height for Tanjong Pagar versus the mean wind speed (component along the Singapore-Taiwan) applying the analytical solution proposed by Tkalich *et al*. (2012a) (equation 3.13) for the Storm surges in the Singapore Strait due to winds in the South China Sea. On other hand, for the Pangkor analysis, the discrepancies between the observations and prediction can be associated with difference in the amplitude and phase, mainly of the major harmonics, which are strengthened during the neap tide. For TG1 the *RMSE'* is 22.45 cm whereas for TG2 is 18.74 cm.

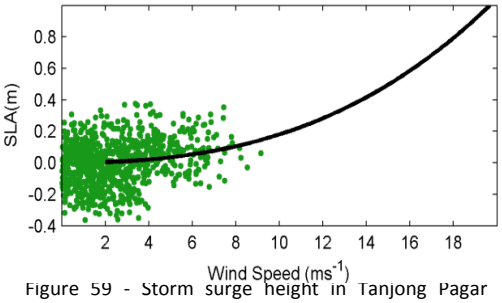

Figure 59 - Storm surge height in Tanjong Pagar versus wind speed (along the Singapore-Taiwan) between 24th of November and 6th April 2013.

Chapter 5 | Conclusion

The region of the South China Sea, entangled between the Pacific Ocean and the Indian Ocean, is characterized by a very complex tidal behaviour driven by these two oceans. This region can be thought of as a system of several connected basins with each basin having its own characteristics, like the coastal patterns and bottom topography. There is a strong variation of the bottom topography from the deep sea basins to the shallow areas, where the NE monsoon and SW monsoon dominate the large-scale sea level dynamics. Combining all these elements with the existence of many islands and small passages, the complexity of the tides in the study area can be explained. Consideration of hydrodynamic issues (water movement, predominantly caused by tides and wind) is important when major developments are proposed in estuarine or coastal settings. In addition to its dynamic complexities, this region is also known for its economic importance (e.g., it is important to guarantee its navigability). In this context, a numerical model was developed by Hidromod, for this region, with several levels, and special attention to the Malacca and Singapore Strait region (MSYM). Although this model can be used to study other parameters (such as currents) this study is focused on the validation of the MSYM sea level. And, centring this work on this parameter, the analysis performed was divided into two parts: the first part was focused on six tide-gauges from GLOSS; the second part was focused on the station of Tanjong Pagar (MEH) and the stations of Pangkor (HYDEC). Each of these sites has a set of observed data available that is compared with the data computed by the MSYM model.

In order to get acquainted with the area at study, in the first part of this work the most important characteristics of the region at study were identified. For that, data from the Ko Taphao Noi, Pengkalan, Singapore, Kuala Terengganu, Ko Lak and Zhapo GLOSS tide-gauges was used, and annual and interannual variations were studied, as well as the harmonic analysis for each station. The available data sets have revealed a trend of mean sea level rise across all stations at study, considering that the trend line, for some stations, has smoothed the ENSO events occurred during the available time. On the other hand, in the monthly analysis, a larger seasonal variation was observed for the stations in the east coast of Malaysia (with an interannual variation in the order of 40 cm) when compared with the stations in the Malacca Strait (in the order of 20 cm). The harmonic analysis allowed the characterization of the type of tide in each station: semidiurnal tide for Ko Taphao Noi and Pengkalan; mixed mainly semidiurnal tide for Singapore and Zhapo; diurnal tide for Ko Lak. The study of the harmonic analysis period sensitivity concludes that: 15 days is insufficient to separate the four major harmonic constituents, which can introduce errors in the amplitude (around 20%) and phase (around 15^{o}); the harmonic analysis should be applied for a minimum time-span of seven months. The first part of the work was concluded with the comparison between the observed astronomic tides and the astronomic tides predicted by the model (for the two levels with the best possible resolution for each station and the model predictions for both levels analysed are similar). The best fit between observed and predicted data for the higher resolution level was observed for Ko Taphao Noi, presenting a *RMSE'* around 10 cm for an amplitude in spring tide higher than 3 m and a *Relative Error* of 3.5%. The worst fit was found for Kuala Terengganu, which had a *RMSE'* near 20 cm and a *Relative Error* of 8.3%, for the higher resolution level. For the tide-gauges located in the Malacca Strait, the results are better in comparison with the Eastern Malaysia Peninsula coast, and are better for the higher resolution level. Conversely, for the tide-gauges located in the Eastern Malaysia Peninsula coast results were slightly better for the lower resolution level.

The second part of this study was centred on the Tanjong Pagar (Singapore Strait) sea level analysis, for a period of time under the influence of mainly NE monsoons. Due to the configuration of the bottom topography of the Sunda Shelf, the SLAs are amplified by the wind over the sea and,

depending on the wind speed and direction over the South China Sea, the Singapore Strait could experience positive or negative SLAs. In order to filter the SLAs from the sea level of observations and predictions data sets, harmonic analyses were applied. From this analysis was concluded that the main harmonics are reproduced well (*Relative HCs* less than 10%). Comparing the observed and predicted data, the highest discrepancies were identified during the neap tide. In an analysis of the spatial distribution of the wind, the positive SLAs are mainly coincident with periods of strong winds over the South China Sea, along the Singapore-Taiwan axis. The highest positive SLA are mainly identified in December and January, with an amplitude near 30 cm that seen generated by wind over the South China Sea from NE and with a speed of near 18 ms^{-1}. In spite of the predominant NE winds, a negative SLA was also identified, in February, resulting from weak winds with a change of direction into SW. Regarding the wind fields, the climatology of the wind at 10 m showed more intense winds offshore of Vietnam and in a region north of Vietnam, which is also the area where the correlation between SLAs in Tanjong Pagar and the wind speed is higher. The last part of this work consisted in the analysis of two tide-gauges in Pangkor, in the Malacca Strait, one located near the mouth of the river of Manjung (TG1) and the other on a bay (TG2). The comparison between observed and predicted data for both tide-gauges reveals higher discrepancies during neap tide. In order to explain these discrepancies, an analysis of the astronomic and residual tides (in SLAs) was performed through harmonic analysis. Concerning the astronomic tide, it was concluded that the main harmonics show a phase and amplitude difference that contributes to a *Relative HC* error for TG1 of 19.5% and 81.4% for M_2 and S_2, respectively. The combination of these discrepancies in relation to the observed data has a more visible influence during the neap tide and the *RMSE* are around 20 cm. For TG2, the differences in high and low tide in spring tide are smaller than for TG1, resulting in a *Relative HC*' of 13.2% and 51.9% for M_2 and S_2, respectively. Removing the astronomic tide, the SLAs are in the order of 10 – 20 cm, for both tide-gauges. Part of the residual tide is still due to the astronomic tide, which could not be separated due to the limited time interval of 15 days (this short period of time can introduce errors in the amplitude and phase calculations of the main harmonics).

In short, the MSYM model behaves in a different way when simulating the sea level, according to the site analysed. This is due to the region's complexity and to the local influence of several (physical and meteorological) factors. The analysis of astronomic tide (validated using GLOSS data) suggests a good model reproduction, with lowest errors for the Malacca Strait and Zhapo and higher errors for the East Coast of Malaysia Peninsula. For the Singapore Strait a good representation of the tide was also found (less than 4%), where the highest discrepancies between observations and predictions are usually associated with the meteorological tide due to the surface wind stress. On the other hand, for the Pangkor tide-gauge, the highest differences between predictions and observations are mainly related with the model's reproduction of the astronomical tide (amplitude and phase of the main constituents).

In future works, this study could be delved into deeper, in order to consolidate some of the achieved conclusions. For instance, the GLOSS data anomalies could be analysed (by running the MSYM model with meteorological and tidal forcing and also by changing some of the model parameters, such as the bottom friction). For the Singapore Strait, an analysis for a higher time period of observations should be done, for a better confirmation of the analytical solution proposed by Tkalich *et al*. (2012a), as well as the probability of the occurrence of storm surges (return period). Furthermore, in addition to the study of the relationship between wind and SLAs, a study between sea level pressure and SLAs could also be attempted. Finally, any of the analyses performed in this study could be programmed and applied in different study areas and time periods.

References

Akdag, C., 1996. Tidal analysis of the South China Sea. Delft University of Technology, Delft Hydraulics, pp. 85.

Aungsakul, K., Jaroensutasinee, M. and Jaroensutasinee, K., 2007. Numerical study of principal tidal constituents in the Gulf of Thailand and the Andaman Sea. Walailak *Journal of Science & Technology* 4, pp. 95-109.

Bindoff, N. L., Willebrand, J., Artale, V, Cazenave, A., Gregory, J., Gulev, S., Hanawa, K., Le Quéré, C., Levitus, S., Nojiri, Y., Shum, C. K., Talley L. D. and Unnikrishnan, A., 2007. Observations: Oceanic climate change and sea level, in: Climate Change 2007: The Physical Science Basis. Contribution of Working Group I to the Fourth Assessment Report of the Intergovernmental Panel on Climate Change, edited by: Solomon, S., Qin, D., Manning, M., Chen, Z., Marquis, M., Averyt, K. B., Tignor, M., and Miller, H. L., Cambridge Univ. Press, Cambridge, UK and New York, USA.

Breemen van, M.T.J., 2008. Salt intrusion in the Selangor: model study with Delft3D estuary in Malaysia.

Camerlengo, A. and Demmler, M. I., 1997. Wind-driven circulation of Peninsular Malaysia's eastern continental shelf, *Sci. Mar.,* pp. 61, 203–211.

Chambers, D. P., Melhaff, C. A., Urban, T. J., Fuji, D., and Nerem, R. S., 2002. Low frequency variations in global mean sea level: 1950–2000, *J. Geophys. Res*., pp. 107, 3026, doi:10.1029/2001JC001089.

Chanut, J., Galloudec, O. L. and Léger, F., 2008. Towards North East Atlantic Regional modelling at 1/12° and 1/36° at Mercator Ocean. Mercator Ocean Quarterly Newsletter.

Chen, H., Tkalich, P. and Malanotte-Rizzoli, P., 2010a. The Various Constituents of the Circulation in the Singapore Strait Region: Tidal, Wind and Eddy driven Circulations and Their Relative Importance. In Papers of the 20th International Offshore and Polar Engineering Conference, ISOPE-2010, Beijing, China, June 20-26.

Chen, H., Wei, J., Tkalich, P. and Malanotte-Rizzoli, P., 2010b. Data Analysis and Numerical Modeling of Sea Level Anomalies in the South China Sea. Proceedings of the 34th World Congress of the International Association for Hydro-Environment Research and Engineering: 33rd Hydrology and Water Resources Symposium and 10th Conference on Hydraulics in Water Engineering. Barton, A.C.T.: Engineers Australia, 2011, pp. 519-526.

Cheng, X. and Qi, Y., 2007. Trends of sea level variations in the South China Sea from merged altimetry data, *Glob. Planet. Change*, pp. 57, 371–382.

Choon, L.K, Lye, K.H., Juneng, L. and Tanggang, F., 2006. Simulation of circulation and storm surge in South China Sea. International Conference on Environment 2006 (ICENV 2006), 13-15 November 2006, Penang, Malaysia.

Chu, P.C., Lu, S. and Chen, Y., 1997. Temporal and spatial variabilities of the South China Sea surface temperature anomaly, *J. Geophys. Res*., 102(C9), pp. 20,937 – 20,955.

Church, J.A., Gregory, J.M., Huybrechts, P., Kuhn, M., Lambeck, K., Nhuan, M.T., Qin, D. and Woodworth, P.L., 2001. Changes in Sea Level, in Intergovernmental Panel on Climate Change, Third Assessment Report. Cambridge Univ. Press, New York, pp. 639–694.

Collins, W., Colman, R., Haywood, J., Manning, M.R. and Mote, P., 2008. The Physical Science Behind Climate Change. *Scientific American*. www.scientificamerican.com/article.cfm?id=science-behind-climate-change.

Color Palette. Kearney. http://www.mathworks.com/matlabcentral/fileexchange/28943-color-palette-tables-cpt-for-matlab, accessed in September 2013.

Cushman-Roisin, B. and Beckers J.-M., 2006. Introduction to Geophysical Fluid Dynamics. Physical and Numerical Aspects, Academic Press, pp. 721.

Dean, R.G., and Dalrymple, R.A., 2002. Coastal Processes with Engineering Application. Cambridge University Press, pp. 475.

Doodson, A. T., 1921. The Harmonic Development of the Tide-generating Potential, Proc. Roy. Soc. London, A, 100.

Douglas, B.C., 1991. Global sea level rise. *J. Geophys. Res*. 96 (C4), pp. 6981–6992.

Fang, G., Kwok, Y.-K. Yu, K. and Zhu, Y., 1999. Numerical simulation of principal tidal constituents in the South China Sea, Gulf of Tonkin and Gulf of Thailand. *Continental Shelf Research* (19), pp. 845-869.

Fang, W., Guo, J., Shi, P., and Mao, Q., 2006a, Low frequency variability of South China Sea surface circulation from 11 years of satellite altimeter data, *Geophys. Res*. Lett., 33, L22612, doi:10.1029/2006GL027431.

Fang, G., Chen, H., Wei, Z., Wang, Y., Wang, X. and Li, C., 2006b. Trends and interannual variability of the South China Sea surface winds, surface height, and surface temperature in the recent decade. *J. Geophys. Res.,* 111, C11S16, http://dx.doi.org/10.1029/2005JC003276

Fang, G., 1986. Tide and tidal current charts for the marginal seas adjacent to China. *Chinese Journal of Oceanology and Limnology* 4, 1-16.

fsa, martinho@fis.ua.pt. www.mathworks.com/matlabcentral/fileexchange/12886-teqcspec/content/Teqcspec/fsa.m, accessed in September 2013.

Gan, J., H. Li, Curchitser, E. N. and Haidvogel, D. B., 2006. Modeling South China Sea circulation. Response to seasonal forcing regimes. *J. Geophys. Res*., 111, C06034, doi:10.1029/2005JC003298.

Grinsted, A., Moore, J. C. and Jevrejeva, S., 2004. Application of the cross wavelet transform and wavelet coherence to geophysical time series. *Nonlinear Processes in Geophysics* 11, pp. 561–566

Hasegawa, H., Kohno N. and Hayashibara H., 2012. JMA's Storm Surge Prediction for the WMO Storm Surge Watch Scheme (SSWS).

Hidromod, 2012. Malhadas, M., Chambel, P., Malacca Strait Hydrodynamic Model (MSYM) Validation Report. Confidencial Document produced by Hidromod, Modelação em Engenharia, Lda.

Holthuijsen, Leo H., 2007. Waves in Oceanic and Coastal Waters, Cambridge University Press, ISBN 0-521-86028-8, pp. 387.

Keller, G.H. and A.F. Richards., 1967. Sediments of the Malacca Strait, Southeast Asia. *Journal of Sedimentary Petrology*, March, pp. 102-127.

Kurniawan, A., Ooi, S.K., Hummel, S. and Gerritsen, H., 2011. Sensitivity analysis of the tidal representation in Singapore regional waters in a data assimilation environment. *Ocean Dynamics*, DOI:10.1007/s10236-011-0415-6.

Li, L., Xu J., Cai, R., 2002. Trends of sea level rise in the South China Sea during the 1990s: An altimetry result, *Chin. Sci. Bull.*, pp. 47, 582–585.

Liang, W.D., Jan, J.C. and Tang, T.Y., 2000. Climatological wind and upper ocean heat content in the South China Sea, Acta Oceanogr. Taiwan., pp. 38, 91– 114.

Lyard, F., Lefèvre, F., Letellier, T. and Francis, O., 2006. Modelling the global ocean tides: a modern insight from FES2004,*Ocean Dynamics*, pp. 56, 394-415.

m_map. Pawlowicz, R., http://www.eos.ubc.ca/~rich/private/, accessed in May-September 2013.

Malanotte-Rizzoli P., 2011. An analytical model for sea level set-up and seiche response in semi-enclosed basins. MIT internal report, pp. 9.

Marmer, H. A., 1952. Changes in Sea Level Determined from Tide Observations. Proc. 2nd Intl. Conf. Coastal Engr., Reston, VA: ASCE.

Pawlowicz, R., Beardsley, R. and Lentz, S., 2002. Classical Tidal Harmonic Analysis including Error Estimates in MATLAB using T_Tide, *Computers and GeoSciences* 28, 929-937.

Pedlosky J., 2003. Waves in the ocean and atmosphere. Introduction to wave dynamics. Springer, New York, pp. 260. ISBN 3-540-00340-1.

Pugh,D., 2004. Changing Sea Levels. Effects of Tides, Weather and Climate. Cambridge: Cambridge University Press.

Rizal, S. and Sündermann, J., 1994. On the M2-tide of the Malacca Straits: a numerical investigation. Deutsche Hydrographische Zeitschrift 46: 61-80.

Rizal, S., Setiawan, I., Iskandar, T., Ilhamsyah, Y., Wahid, M. and Musman, M., 2010. Currents Simulation in the Malacca Straits by Using Three-Dimensional Numerical Model. Sains Malaysiana 39 (4) 519–524.

Rizal, S., Damm, P., Wahid, M.A., Sundermann, J., Ilhamsyah, Y., Iskandar, T. and Muhhammad, 2012. General Circulation in the Malacca Strait and Andaman Sea: A numerical model study. *American Journal of Environmental Science*, 2012, 8 (5), 479-488. doi:10.3844/ajessp.2012.479.488.

Fletcher, Sara Mikaloff, 2006. Lecture 3: Evaluating models: Skill scores, and Taylor diagrams. Princeton University. www.aos.princeton.edu/WWWPUBLIC/sara/statistics_course/Statistics_lecture3.pdf.

Stewart, R. H., 2008. Introduction to Physical Oceanography. Department of Oceanography, Texas A&M University.

Taylor, K.E., 2001. Summarizing multiple aspects of model performance in a single diagram, JGR, vol 106, no. D7, 7183-7192

Taylor, K.E., 2005. www-pcmdi.llnl.gov/about/staff/Taylor/CV/Taylor_diagram_primer.pdf. Taylor Diagram Primer.

Thia-Eng, C., Gorre I.R.L, Ross, S.A., Bernad, S.R., Gervacio, B. and Ebarvia, M.C., 2000. The Malacca Straits. Marine Pollution Bulletin 41 (Issues 1-6), pp. 160–178.

Tkalich P., Vethamony P., Luu, Q.-H. and Babu, M.T., 2013. Sea level trend and variability in the Singapore Strait, *Ocean Science*, pp. 9, 293–300, www.ocean-sci.net/9/293/2013/, doi: 10.5194/os-9-293-2013.

Tkalich, P., Vethamony, P., Babu, M.T. and Malanotte-Rizzoli, P., 2012a. Storm surges in the Singapore Strait due to winds in the South China Sea. *Natural Hazards* DOI: 10.1007/s11069-0211-8.

Tkalich, P., Babu, M.T. and Vethamony, P., 2012b. Technical Note: Mean sea level variation in the Singapore Strait from long-term tide data. *Ocean Sci. Discuss.*, 9, 2255–2271. doi:10.5194/osd-9-2255-2012.

Tong, J., Gan, Z., Qi, Y., and Mao Q., 2010. Predicted positions of tidal fronts in the continental shelf region of the South China Sea. *Journal of Marine Systems*, 82 (3), pp. 145–153.

Wei, J., Zeng, H., Ooi, B.H., Dao, M.H. and Cho, W., 2010. Multi-layer model simulation and data assimilation in the Serangoon Harbor of Singapore. Proceedings of the International Offshore (Ocean) and Polar Engineering Conference.

Wu, J., 1982. Wind-stress coefficients over sea surface from breeze to hurricane. *J Geophys Res* 87: 9704–9706.

Wyrtki K., 1961. Physical oceanography of the Southeast Asianwaters. Univ. Calif., NAGA Rept. no. 2, pp. 1 – 195.

Wyrtki K., 1991. On the slope of sea level along the west coast of Malaysia, unpublished paper, pp. 13.

Yang F. 2010. Misrepresentation of Model Performance by RMSE: From Mathematical Proof to Case Demonstration. Environmental Modeling Center National Centers for Environmental Prediction Camp Springs, Maryland, USA. www.docstoc.com/docs/112780933/RMSE_decomposition

Zervas, C. E., 1999. Tidal Current Analysis Procedures and Associated Computer Programs, NOAA Technical Report NOS CO-OPS 0021, Silver Spring, MD.

Zu, T., Gan, J., Erofeeva, SY., 2008. Numerical study of the tide and tidal dynamics in the South China Sea. *Deep-Sea Res* I 55, pp. 137 – 154.